Turnover and Localization of the Actin-Binding Protein Drebrin in Neurons

D i s s e r t a t i o n

zur Erlangung des akademischen Grades

d o c t o r r e r u m n a t u r a l i u m

(Dr. rer. nat.)

im Fach Biologie

eingereicht an der

Lebenswissenschaftlichen Fakultät

der Humboldt-Universität zu Berlin

von

Master of Science Eugenia Rojas Puente

Präsident der Humboldt-Universität zu Berlin

Prof. Dr. Sabine Kunst

Dekan der Lebenswissenschaftliche Fakultät

Prof. Dr. Richard Lucius

Gutachter/innen: 1. Prof. Hanspeter Herzel

2. Prof. Britta Eickholt

3. Prof. Matthew Larkum

Tag der mündlichen Prüfung: 24.08.2016

For my parents and Erik

Table of Contents

Summary

This thesis deals with the regulatory inputs modulating the abundance of the protein Drebrin (Developmentally Regulated Brain Protein) in neurons, which is an actin-binding protein capable of bundling actin filaments. Most excitatory synapses in the mammalian brain are formed on tiny protrusions, called dendritic spines that spread from the neuronal dendrite. It has been suggested that changes in dendritic spine morphology affect synaptic activity and plasticity, which are processes underlying memory formation, brain ageing, and some disorders, such as mental retardation. It is thought that Drebrin plays an important role in regulating dendritic spine morphology.
Drebrin levels are known to recede with age and could be associated with cognitive decline. Moreover, some neurodegenerative conditions have been shown to be linked with a decrease in Drebrin abundance. A weakening in the expression of this protein in dendritic spines is associated with the loss of synaptic connections, a common feature of ageing and various neurological disorders such as Alzheimer's disease. This evidence was the underlying motivation for studying the localization and turnover of Drebrin.
During the project reported in this thesis, I studied the effect of the site-specific S647 phosphorylation of Drebrin and found that such post-translational modification regulates protein stability and turnover. For the project, it was necessary to establish several novel techniques in our laboratory, including state-of-the-art methods such as FUNCAT-PLA and Puro-PLA for the visualization of de novo synthesized proteins in situ. Furthermore, my results show that Drebrin translation occurs not only in somata but also locally in the dendrites and dendritic spines of neurons. The same observation is true for Drebrin transcripts, which are present both in the soma and dendrites of neurons. I obtained this result using high-resolution fluorescence in situ hybridization. These observations suggest that Drebrin could play an important role during synaptic plasticity. My results allow the future investigation of the potential role of site-specific phosphorylation of Drebrin in spine morphology, in order to better understand the role of the protein in spines, as well as how its synthesis is controlled. Preliminary results in this direction are presented in this thesis. This PhD thesis represents a contribution to better understanding the regulation of Drebrin abundance. It also provides an experimental platform for additional investigation about the role of Drebrin in spine morphology, regarding its stability and its correlation with synaptic maintenance and function.

Zusammenfassung

Die vorliegende Arbeit erforscht die regulatorische Inputs, die die Expression von Drebrin (Developmentally Regulated Brain Protein) in Neuronen modulieren. Drebrin ist ein Protein das an Actin bindet und Actin-Filamente bündeln kann. Die meisten erregende Synapsen in Gehirnen von Säugetieren werden in kleinen Dendritenfortsätzen gebildet, die sogenannten Dendritendornen. Es ist postuliert worden, dass Änderungen in der Morphologie der Dendritendornen die synaptische Aktivität und Plastizität verändern können. Diese Prozesse spielen eine Rolle bei der Gedächtnisbildung und Alterung des Gehirns, sowie geistigen Störungen bzw. Behinderungen. Es wird angnommen, dass Drebrin eine wichtige Rolle bei der Regulierung der Morphologie der Dendritendornen spielt.

Es ist bekannt, dass die Drebrin-Präsenz im Alter zurückgeht – dies könnte kognitive Defizite erklären. Außerdem wurde gezeigt, dass einige neurodegenerative Krankheiten mit einer Reduzierung von Drebrin einhergehen. Eine Schwächung der Expression dieses Proteins in Dendritendornen ist mit einem Verlust an synaptischen Verbindungen gekoppelt, ein gemeinsames Merkmal von Alterung und neurologische Störungen, wie bei der Alzheimer Krankheit. Diese Befunde bildeten die Motivation und Grundlage für meine Erforschung der Produktion und Lokalisierung von Drebrin.

Während meines Projektes, habe ich den Effekt der sequenzspezifische S647-Phosphorylierung von Drebrin untersucht. Diese Arbeit zeigt, dass diese post-translatorische Änderung die Stabilität und Produktion des Proteins reguliert. Es war für das Projekt notwendig neuartige experimentelle Verfahren in unserem Labor zu etablieren, wie z.B. FUNCAT-PLA und Puro-PLA, Methoden die den neusten Stand der Technik auf diese, Gebiet darstellen, letzteres für die Visualisierung von de novo synthetisierten Proteinen in situ. Außerdem zeigen meine Resultate, dass Drebrin-Translation nicht nur im Zellkörper sondern auch lokal in den Dendritendornen stattfindet. Dasselbe gilt für Drebrin mRNA Transkripte, die sowohl im Zellkörper als auch in den Dendriten vorhanden sind. Diese Ergebnisse wurde durch den Einsatz von hochauflösender fluorizierender Hybridisierung in situ erreicht. Meine Resultate ermöglichen die zukünftige Erforschung der potentiellen Rolle der sequenz-spezifische Phosphorylierung von Drebrin für die Morphologie der Dendritendornen. Damit kann die Aktivität des Proteins in den Dendriten und die lokale Steuerung der Synthese dort

besser verstanden werden. Vorläufige Ergebnisse in diese Richtung werden in dieser Arbeit vorgestellt.

Diese Dissertation bietet eine Grundlage für das Verständnis der Regulierung der Drebrin-Konzentration in Zellen. Die Arbeit liefert eine experimentelle Plattform für zusätzliche Studien der Rolle von Drebrin bei der Bestimmung der Dornenmorphologie, sowohl in Bezug auf Stabilität als auch hinsichtlich der Korrelation mit der synaptischen Funktion und Erhaltung.

Motivation

This thesis addresses the role of the protein Drebrin (DBN) in neurons, and more specifically, the specific regulatory inputs that influence the expression and stability of DBN in dendritic spines. The effect of synaptic activity, oxidative stress, and post-translational modification is studied through the adaptation to our needs of state of the art laboratory techniques, which let us image the spatio-temporal patterns of expression of DBN within neurons. This thesis represents a contribution towards the elucidation of the role of DBN both during the development and ageing of the human brain.

DBN (**d**evelopmentally-**re**gulated **br**ain prote**in**) is an actin-binding protein present in cells of humans and other species. DBN was first identified in the chicken brain in 1985 applying two-dimensional electrophoresis -- it was later characterized in mammals (Shirao and Obata, 1985). Its role as an interaction partner of the phosphatase and tensin homolog protein (PTEN) has been and is being studied in the Eickholt Lab (Charite Universitätsmedizin Berlin). Both DBN and PTEN are present in brain tissue. PTEN is a protein that can act as tumor suppressor. It can function as a protein and a lipid phosphatase. As a lipid phosphatase, PTEN directly antagonizes the PI3K pathway, responsible for fundamental processes in the cell, such as cell growth, cell-cycle progression, metabolism, cell migration and protein synthesis.

PTEN mutations have been identified in cancer patients, and in neurological disorders such as Cowden syndrome, Bannayan-Riley-Ruvalcaba, and in autism spectrum disorders (Pilarski et al., 2011).

DBN was first identified as a developmentally regulated protein (hence the name) and is known to be important for neuronal development (Shirao and Obata, 1985). Using immunoelectron microscopy, it was shown shortly after its discovery that DBN is expressed in the dendrites of neurons from the cerebellar cortex of the chicken (Shirao et al., 1987). In 1989, DBN isoforms were first identified in rat brains by the Shirao group, and were first cloned and isolated from a human brain in 1993 (Toda M. et.al., 1993).

It was originally proposed that DBN affects neuronal morphogenesis because of its developmentally regulated expression and because of its actin-binding properties (Ishikawa et al., 1994). It has been shown to interact with other actin-binding proteins

and to modulate the morphology of dendritic spines in neurons – for example, it can induce the formation of filopodia-like structures in cells (Hayashi and Shirao, 1999; Jin et al., 2002; Mammoto et al., 1998; Sasaki et al., 1996). Furthermore, DBN-A, which is a brain-specific isoform, has been shown to alter synaptic activities of glutamatergic and GABAergic neurons in overexpression experiments (Ivanov et al., 2009a). DBN has also been linked to disease: for example, DBN levels are low in the brains of patients with Alzheimer's disease (AD) and Down syndrome (Shim and Lubec, 2002). However, the specific mechanisms behind the potential role of DBN in degenerative brain conditions remains unknown.

DBN is a phosphoprotein of which more than 13 phosphorylation sites have been identified. Post-translation modifications have been shown to regulate protein turnover in some cases. During the characterization of the PTEN-DBN protein-protein interaction (Kreis et al., 2013), it became clear that PTEN down regulation correlates with an increase in pDBN-S647 levels. Moreover, the interaction between DBN and PTEN was shown to partially occur in dendrites and to be synaptic activity dependent. However, the role of the S647 phosphorylation site remained unclear. Therefore, two main hypothesis were formulated regarding DBN function and control after those findings:

- First, that the site-specific phosphorylation of DBN is important for the control of DBN turnover.
- Second, that the spatial-temporal patterns of DBN could be relevant in the formation and maintenance of filopodia and dendritic spines.

In order to better understand how DBN is regulated and work towards proving or disproving these hypotheses, I pursued the following objectives during the realization of this thesis:

1. Find regulatory inputs for DBN stability in the context of oxidative stress
2. Study the effect of site-specific phosphorylation (S647/S601) on DBN stability and turnover.
3. Study the spatial-temporal patterns of DBN expression *in situ.*
4. Find regulatory inputs for DBN translation in the context of signaling cascades.

The results of this research agenda are detailed in this thesis which is organized as follows:

Chapter 1 is an introduction explaining the motivation for this project. It makes explicit the main hypothesis and objectives of this thesis. Moreover, it briefly describes what where the methodologies applied to produce the results. Chapter 2 walks the reader through the results of the thesis – it is organized in three sections: Section 2.1 deals with the identification of regulatory inputs relevant to the abundance of DBN, and with the study of different cellular models for studying DBN turnover. Several important control experiments are discussed. They constitute the basis for further trials explained in the following sections, which include testing different DBN antibodies in western blot and in immunostaining. In order to explore the stability of DBN and the potential molecular mechanisms contributing to cognitive decline during aging and disease, I applied compounds known to induce oxidative stress, such as the herbicide paraquat and Amyloid beta peptide (Aβ). The results of the experiment are described in this section.

Section 2.2 provides data showing the effect that site-specific phosphorylation has on DBN protein stability and turnover in overexpression models and in primary culture neurons. It describes state-of-the-art techniques for the visualization of *de novo* synthesis of DBN proteins in neurons, which I applied to study DBN turnover in primary neuronal cultures. Moreover, pulse-chase experiments in overexpression systems indicate that DBN degradation is inhibited when the proteasome itself is inhibited, suggesting a mechanism for degradation via the proteasome ubiquitin system (UPS). Together, these experiments indicate that C-terminal phosphorylation of DBN is an important regulatory input for the regulation of protein stability, and that DBN degradation might be at least partially controlled by the UPS.

Section 2.3 focuses on the regulation of DBN translation and the localization in neurons of DBN transcripts. Visualization *in situ* of both DBN transcripts and newly synthesized DBN, applying high-resolution fluorescence in situ hybridization and puromycilation-PLA, respectively, confirm the presence of DBN transcripts and its translation both in soma and in dendrites. This observation, suggests and important role of the protein for synaptic plasticity, as discussed in this chapter. Finally and based on the previous finding that PTEN indirectly controls DBN abundance, I explore the potential regulation of the PI3K-mTOR pathway during DBN synthesis. I found that acute inhibition of mTOR reduces DBN translation.

Chapter 3 discusses the main findings of this thesis. Chapter 4 ends with the conclusions and a discussion of future work. Finally, Chapter 5 contains a full description of the materials and methods that were used for obtaining the experimental data.

As is evident from the description above, this thesis provides new insights about the molecular mechanisms and cellular processes controlling DBN turnover, and is a contribution towards understanding DBN’s potential role in the regulation of spine morphology.

Abbreviations

AD	Alzheimer's Disease
AHA	azidohomoalanine
Akt	Protein kinase B
Aniso	Anisomycin
APS	Ammonium persulfate
CaMKII	α-subunit of $Ca2^{+}$/calmodulin- dependent protein kinase II
CNS	Central nervous system
CO_2	Carbon dioxide
COS-7	**C**V-1 (simian) in **O**rigin, and carrying the **S**V40 genetic material
DS	Down Syndrome
DBN	Drebrin
DIV	Days *in vitro*
DMEM	Dulbecco´s modified eagles medium
DMSO	Dimethylsulfoxide
DNA	Deoxyribonucleic acid
Drebrin	Developmentally regulated brain protein
E.	Embryonic day
EDTA	Ethylene diamine tetraacetic acid
ERK1/2	Extracellular signal regulated kinase ½
F-actin	Filamentous actin
FCS	Fetal calf serum
Fig.	Figure
FUNCAT	Fluorescence Non-Canonical Amino acid Tagging
GAPDH	Glycerin aldehyde-3-phosphate dehydrogenase
G-actin	Globular actin
h.	Hours
HBSS	Hank's balanced salt solution
HEK	Human embryonic kidney cells
HEK293T	Human Embryonic kidney cells expressing SV40 Large T-antigen
HRP	Horseradish peroxidase
kDa	Kilo Dalton
KO	Knock-out
LTD	Long-term depression

LTP	Long-term potentiation
MAP2	Microtubule-associated protein 2
Met	Methionine
min	Minutes
mL	Milliliter
mRNA	messenger Ribonucleic acid
mTOR	Mammalian target of rapamycin
P	Day postnatal
PBS	Phosphate buffered saline
PFA	Paraformaldehyde
PI3K	Phosphoinositide-3-kinase
PLA	Proximity Ligation Assay
PTEN	Phosphatase and tensin homologue deleted on chromosome ten
P/S	Penicillin/Streptavidin
RT	Room temperature
s	Seconds
SDS	Sodium dodecyl sulfate
SDS-PAGE	SDS- polyacrylamide gel electrophoresis
SILAC	Stable isotope labeling with amino acids in cell culture
TBS-T	Tris buffered saline with Tween20
WB	Western blot
w/o	without
µg	Microgram
µl	Microliter

Keywords

Neurons, drebrin, actin, cytoskeleton

Neuronen, drebrin, actin, cytoskelett

1 Introduction

1.1 Dendritic spines

Neurons develop two types of functionally and morphologically different cytoplasmic processes: axons and dendrites. Axons are usually long and produce terminal branches. Their growth cones transform into presynaptic terminals which then form synapses with the dendrites of other neurons. Dendrites are not as long as axons but branch extensively, giving rise to dendritic trees with thousands of synapses (see Figure 1. for a schematic representation of morphological changes in neurons) (Luo L, 2002). Most excitatory synapses extend directly from the dendrites. These are tiny postsynaptic protrusions called dendritic spines (Bourne and Harris, 2008). They are highly dynamic structures containing filamentous actin. This protein endows spines with dynamic properties -- it has been shown to be important for the morphogenesis and maintenance of dendritic spines.

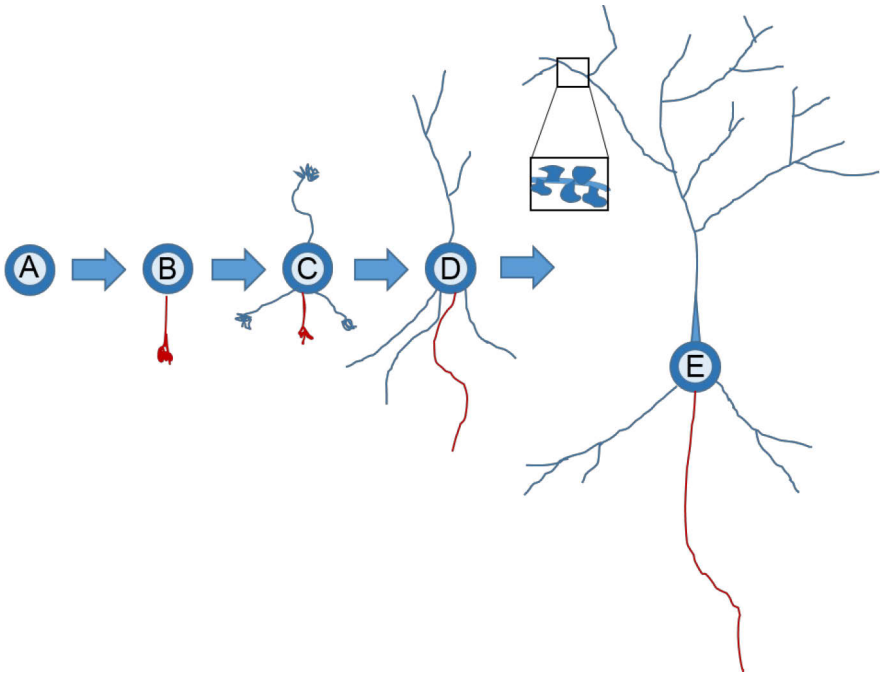

Figure 1| Schematic representation of morphological changes during neuronal development. Different stages in the life of a neuron (A-E) are visible. In E, the magnified inset represents dendritic spines, postsynaptic structures on dendrites. The long process growing on the bottom of the cell represents the axon, in this figure it is colored in red. Figure based on Luo L, 2002.

Different membrane morphologies can be observed during the development of spines. These include dendritic filopodia, which lack the postsynaptic compartment where scaffold proteins and synaptic receptors are found, and synaptic function. Dendritic filopodia have been proposed to function as precursor for dendritic spines. In addition to this, three further types of dendritic spines have been classified: the thin, stubby and mushroom shaped spines (see Figure 2 for a diagram) (Harris KM, 1992; Ziv NE & Smith SJ, 1996; Sekino Y et al., 2007). Thin spines have been strongly associated with plasticity -- it is believed that they play a role during the process of learning new information, whereas mushroom spines are thought to contribute to the formation of long-term memories and mediate strong synaptic currents (Morrison JH & Baxter MG, 2012). Moreover, mushroom spines are commonly recognized as mature, being characterized by the presence of neurotransmitter receptors, scaffold proteins anchoring the receptors, intracellular signaling molecules and different actin-binding proteins. Mushroom spines play a crucial role in synaptic activity (Harris KM, 1992; Shim KS & Lubec G, 2002; Toni N et al., 2007; Sekino Y et al., 2007). The role of stubby spines remains unclear (Morrison JH & Baxter MG, 2012). The main players involved in shaping the structure of dendritic spines are the actin-binding proteins, which are able to polymerize or de-polymerize filamentous (F) actin in response to internal and external signals. In Section 2.3, further down, a detailed description on the actin-binding proteins in dendritic spines is provided.

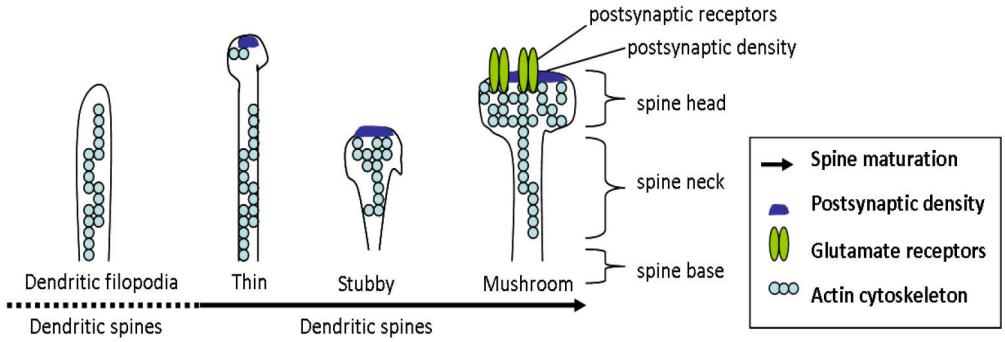

Figure 2| Schematic representation of the morphology of dendritic spines. Spine development starts with dendritic filopodia and continues with the formation of a head on top of them. It undergoes elongation, giving rise to different morphologies of dendritic spines, which correlate with synaptic activity and spine maturation. Mature spines are characterized by a widening of their head, containing postsynaptic machinery (PSD and receptors) and a branched actin cytoskeleton (mushroom shaped dendritic spines: see the text for details).

1.2 Actin cytoskeleton in dendritic spines

Actin is an evolutionary conserved protein. Three main actin isoforms are known in vertebrates, including the α-isoform expressed in different muscle cells, as well as the β- and γ- isoforms found together in almost all non-muscle cells (Dominguez R & Holmes KC, 2011). Actin in the cell is found as a monomer (globular or G-actin) and as a polymerized filament (filamentous or F-actin) (Sekino et al., 2007). G-actin contains a binding site for ATP and, when bound to ATP, it self-assembles spontaneously through weak non-covalent interactions into F-actin. F-actin contains two ends: a “minus” or pointed end, which is rather stable, and a “plus” or barbed end, where polymerization occurs. F-actin turnover is controlled by several actin-binding proteins responsible for the stabilization or destabilization of actin filaments. They do this by promoting actin nucleation, elongation, capping, severing or depolymerization. This process is essential for the reorganization of the actin cytoskeleton in cells (Campellone KG & Welch MD, 2010). Actin is one of the major components of the cytoskeleton, playing and important role in cell motility and shape dynamics, as well as contributing to other cellular functions such as cell division and intracellular protein trafficking.

In the central nervous system (CNS), the actin cytoskeleton is essential for the establishment of neuron morphogenesis and maturation, as well as for a number of dynamic changes in morphology. Changes in the morphology of spines as well as changes in spine density along dendrites are processes that require actin cytoskeleton rearrangements. These changes have been linked to synaptic plasticity (Cingolani and Goda, 2008; Engert and Bonhoeffer, 1999) Actin filaments are the major cytoskeletal component in dendritic spines, but actin in spines is found both in its monomeric structure and in its filamentous conformation (Landis DM & Reese TS, 1983). It is well known that the actin cytoskeleton contributes to regulate dendritic spines morphogenesis, maintenance and motility, as well as to support postsynaptic receptor anchoring (Cingolani LA & Goda Y, 2008; Hotulainen P & Hoogenraad CC, 2010). Actin filaments in the spine head are very dynamic and show a high turnover by continuous treadmilling (Star EN, et al., 2002; Cingolani LA & Goda Y, 2008). Polymerization of G-actin and disassembly of F-actin induce rapid changes in the cytoskeleton, enabling morphology and functional modifications of dendritic spines (Cingolani LA & Goda Y, 2008).

In cells, actin filaments are commonly assembled into extended structures such as branched networks and bundles. A study by Koroba & Svitkina 2010, characterized the molecular architecture of the synaptic actin cytoskeleton. In this study, using platinum replica electron microscopy, spine heads were observed to contain branched dense networks of cross-linked actin filaments, while spine necks were found to have loosely arranged actin filaments. The spine base presented long actin filaments (see Figure 3 for a model) (Koroba F & Svitkina T, 2010). This finding illustrates an essential role of the treadmilling of F-actin in regulating the morphology of dendritic spines as well as defining their different structures.

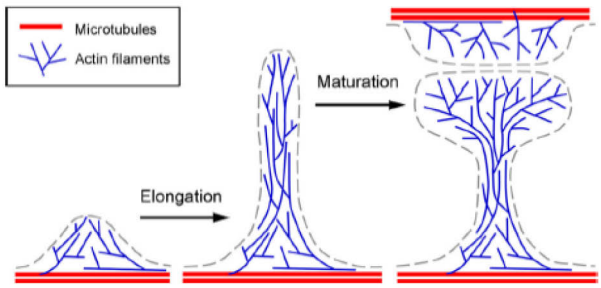

Figure 3| Model for F-actin organization in dendritic spines. Actin filaments (blue) are organized forming different networks: linear and branched anchored to microtubules (red) or actin filaments in the dendritic shaft (Figure from Koroba F & Svitkina T, 2010)

1.3 Actin-binding proteins

Actin-binding proteins have been identified as important modulators of spine morphogenesis and maintenance. They promote actin polymerization and depolymerization. Actin-binding proteins can be organized in three main groups with severing, stabilizing and modulating activity, respectively (Cingolani LA & Goda Y, 2008; Lin W & Webb DJ, 2009). Examples of severing proteins are cofilin (Andrianantoandro E, et al., 2006) and gelsolin (Coué M & Korn ED, 1985). They are molecules capable of binding F-actin and breaking it down into smaller pieces thus playing an important role in the maintenance of the G-actin pool required for new assembly (Star E et al., 2002). In contrast, the second group of stabilizing actin-binding proteins prevent F-actin to lose or add G-actin to already existing actin filaments, thus

stabilizing the actin cytoskeleton. This is the case, for example, for Eps8 (Menna E et al., 2009), that also functions as an actin-capping. Profilin is an example for proteins promoting actin polymerization (Ackermann and Matus, 2003). Finally, proteins such as α-actinin (Grazi E et al., 1992), CaMKII (Lin YC & Redmond L, 2008) and the developmentally regulated brain protein DBN modulate actin organization, affecting spine structure and function, by bundling or cross-linking actin filaments (Takahashi H et al., 2003; Lin W & Webb DJ, 2009). Numerous findings indicate that the actin signaling pathways in spines are regulated by many synaptic receptors including, for example, NMDA and AMPA receptors. They have been suggested to regulate the formation of the actin cytoskeleton mainly by mediating the influx of Ca^{2+} ions into postsynaptic neurons and by binding directly to actin-binding proteins (Hotulainen P & Hoogenraad CC, 2010). In addition to synaptic receptors, other actin-regulating proteins, such as receptor tyrosine kinases and synaptic adhesion molecules, have been described as important regulators of synapse function, but it is through multiple signaling pathways and tightly controlled regulation that actin-binding proteins modulate actin cytoskeleton dynamics in spines. GTPases of the Rho family and serine/threonine kinases regulate actin polymerization by targeting actin-binding proteins such as ProfilinII, CaMKII and ADF/Cofilin. Many of these proteins, which are modulating actin meshwork in dendritic spines, are regulated by phosphorylation (Da Silva JS & Dotti CG, 2002), a common post-translational modification.

1.4 Drebrin

Three DBN isoforms were first discovered in the chicken embryo brain by two-dimensional gel electrophoresis (Shirao T & Obata K, 1985). Later, two different DBN isoforms were described in mammals: an embryonic form or DBN-E (~115kDa) and an adult form or DBN-A (~125kDa) (Shirao et al., 1987). In the DBN proteins five domains have been identified: an N-terminal ADF homology domain, a coiled coil helical domain where an actin binding domain (Grintsevich E. Elena, 2010) is located, a proline-rich region suggested to regulate an interaction with profiling (Mammoto et al., 1998) and C-terminal Homer-binding domains (Shiraishi-Yamaguchi et al., 2009) (Figure 4). Moreover, the DBN gene is regulated in a developmental manner: Drebrin E is replaced by Drebrin A in the adult brain (Kojima et al., 1993).

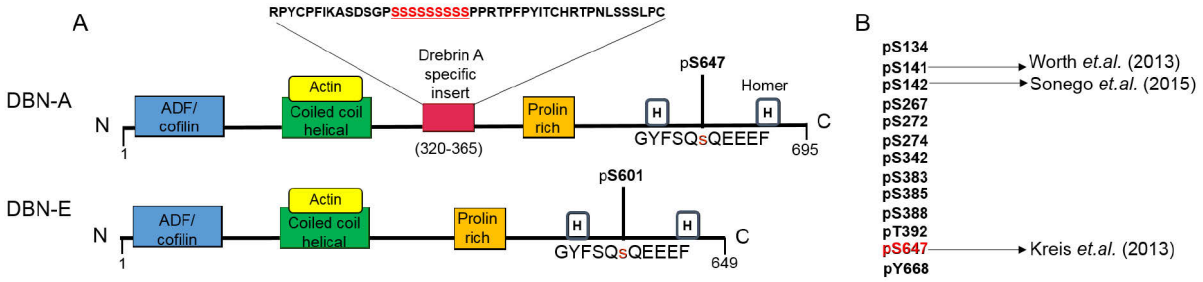

Figure 4| Diagram of Drebrin alternative splicing isoforms and domains. A) DBN is found in two isoforms produced by alternative splicing. DBN-A mRNA differs from DBN-E mRNA only by the presence of a 138-nucleotide sequence insert codifying for 46 amino acids depicted in the diagram. The protein domains of the two Drebrins are represented in this figure. By the N-terminus an ADF/cofilin domain (blue), a coiled coil region (green) where the actin binding domain (yellow) is located, a prolin rich region (orange) and two homer binding domains by the C-terminus region. B) 13 of the 17 phosphorylation sites that have been identified in the Drebrin protein are listed here.

1.5 Drebrin regulation

Post-translational modifications have been described to provide regulatory mechanisms for protein function. One common type of post-translational modification is phosphorylation involving the addition of a phosphoryl group. Phosphorylation of proteins can control different processes such as providing on and off switches of enzymatic activity, protein complex formation, protein localization, protein stability and turnover. DBN is a highly phosphorylated protein – to date 17 phosphorylation sites have been identified. These sites have been found by analysis of brain samples and cell lines using mass spectrometry (Ballif et al., 2004; Beausoleil et al., 2008; Chew et al., 2005; Molina et al., 2007; Olsen et al., 2006; Rush et al., 2005; Vosseller et al., 2005; Wollscheid et al., 2005; Zheng et al., 2005)

It has been shown that DBN is an actin-binding protein that modulates actin bundling and inhibits the interaction between F-actin and other actin-binding proteins such as α-actinin, fascin (Sasaki Y et al., 1996), tropomyosin and myosin (Ishikawa R et al., 2007; Hayashi K et al., 1996; Ivanov A et al., 2009). In adult neurons, DBN accumulates in spine heads enriched in actin that have formed long filamentous structures. It has been suggested that DBN modulates synaptic plasticity by affecting the morphology of dendritic spines and by regulating neuronal transmission (Hayashi K et al., 1996;

Hayashi K & Shirao T, 1999; Ivanov A et al., 2009; Aoki C et al., 2009). Additionally, it has been reported that DBN induces the synaptic clustering of the post-synaptic density scaffold protein (PSD-95), supporting its role in synaptic plasticity (Takahashi H et al., 2003). Interestingly, it has been shown that increasing the expression levels of DBN in neurons promotes spine elongation, whereas down-regulation of DBN reduces spine density (Mizui T et al., 2005; Takahashi H, et al., 2006).

Drebrin A (DBN-A) was described to be neuronal specific, therefore, in order to investigate the role of DBN-A in neuronal function, an overexpression model was generated by the Shirao group in Japan (Gunma University, Graduate School of Medicine). Morphological analysis of hippocampal neuronal cultures upon DBN-A overexpression, resulted in elongation of dendritic spines while the overexpression of a DBN-A mutant lacking the actin binding domain did not have this effect (Ivanov et al., 2009b). This study showed that the actin-binding domain was responsible for the morphological phenotype of DBN-A in spines. Moreover, in the same study it was reported that the overexpression of DBN-A in neurons did not interrupt spontaneous synaptic activities in synapses. However, measurements of cumulative probability plots for amplitude and frequency showed a shift in the neurons overexpressing DBN-A having significantly higher values than in control neurons (Ivanov et al., 2009).

In contrast to the overexpression effect of DBN on the morphology and function of neurons, downregulation of DBN-A with antisense oligonucleotides was reported to decrease the filopodia-spine density in comparison to the control but no changes in the elongation of the spines were detected (Takahashi et al., 2006). To further understand the functional role of DBN-A at the spines in neurons, a DBN-A knockout (KO) mouse model was generated. These animals presented deficits in homeostatic synaptic plasticity (Aoki et al., 2009). Further analysis of this mouse model showed that depletion of DBN-A impairs context-dependent fear learning (Kojima et al., 2010, 2016). While the KO model is specific for DBN-A, the other isoform DBN-E is still present in the KO, that could lead to misinterpretation of the data where the lack of DBN-A together with the potential substitution of DBN-E could be responsible for the changes that are reported in these studies. However, more recently, the group of Prof. Dr. Gert Lubec reported for the first time morphological and functional analyses of a full DBN knockout mice. These animals lack both DBN isoforms and morphological analyses of this animal model show a reduction in spine number on dendritic segments

of CA1 apical pyramidal cells and CA1 hippocampal neurons and electrophysiological analyses confirmed that memory related synaptic plasticity was affected in these mice (Jung et al., 2015).

Overall, the functional data for the role of DBN in neurons is still limited and further studies are required to clarify the function and regulation of DBN in the brain.

1.6 DBN in ageing and disease

The mammalian brain contains millions of specialized synapses -- interconnections between neurons generating neuronal networks. The first step in the formation of neuronal networks is the outgrowth of neuronal processes (i.e. presynaptic axonal terminals and postsynaptic dendritic regions, see Figure 1 for a schematic representation) which eventually enable the brain to perform complex tasks such as the formation of thoughts, memories, dreams, and learning (Shirao, 1995, Hotulainen P. & Casper C., 2010).

Electron microscopy and electrophysiological studies have shown that cognitive decline during ageing is accompanied by a loss of thin spines, while no loss of mushroom or stubby spines has been observed. Thin spines have been strongly associated with plasticity. It is believed that they play a key role in the task of learning new information, whereas mushroom spines are thought to contribute to long-term memories and mediate strong synaptic currents. The role of stubby spines remains unclear (Morrison JH & Baxter MG, 2012).

Proteins regulating spine morphology and maintenance are associated with cognitive impairment in ageing. This association was shown in a recent study where cognitively impaired by age or aged rats presented alterations in the expression of hippocampal proteins, which are normally responsible for synaptic-activity, signaling and structure. The proteins included MAP2, DBN, PSD-95 and CaMKIIα. Up-regulation of DBN significantly correlated with declining cognitive performance in aged impaired rats, indicating that a balance in the expression of the proteins, such as DBN, is essential for the maintenance of normal synaptic function during ageing (VanGuilder HD et al., 2011).

Neuronal dysfunction has been identified as hallmark in cognitive impairment and in neurodegenerative diseases, such as Alzheimer’s disease (AD) (Calon F et al., 2004).

Interestingly, an alteration in the expression levels of DBN has been observed in human hippocampal synapses in AD (Harigaya and Shoji, 1996). Other studies have shown that DBN levels decrease in brains of patients with AD and Down syndrome, thus supporting the hypothesis that DBN plays an important role in regulating synaptic activity in ageing and disease (Shim K S & Lubec G, 2002).

Since ageing and neurodegenerative conditions have been shown to correlate with an imbalance in the expression of DBN, this result may suggest that a decline of DBN in dendritic spines may weaken synaptic connections, a common feature observed in ageing and various neurodegenerative disorders (Harigaya and Shoji, 1996; Shim KS & Lubec, 2002; Kojima et al., 2010). Supporting this hypothesis, Kobayashi and colleagues found that a reduction of DBN induced by antisense knockdown in the brain of rats causes cognitive deficits (Kobayashi H et al., 2004). However, the molecular mechanisms involved still remain unclear.

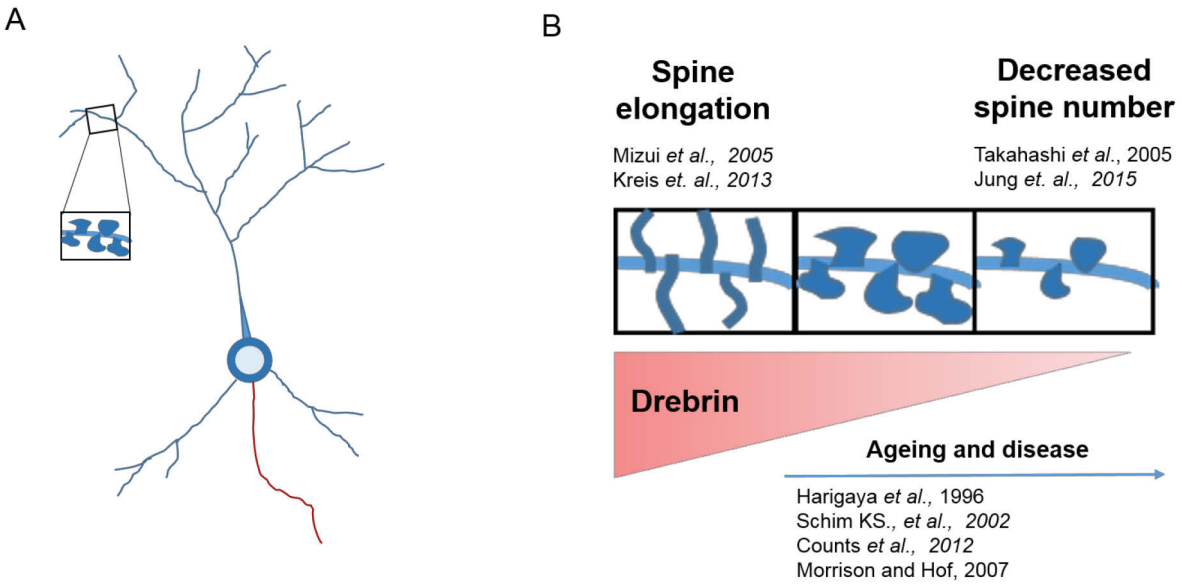

Figure 5| Spine morphology maintenance under DBN turnover. A) Schematic representation of a neuron. Magnification represents a fragment of a dendrite where dendritic spines grow. B) Model for spine morphology after overexpression, normal or downregulation of DBN. Different phenotypes for dendritic spines have been described where DBN abundance plays important roles. The same phenotypes correlate with ageing and disease when DBN is downregulated.

1.7 Protein Turnover in neurons

Protein turnover is the result of protein synthesis and protein degradation to maintain a steady-state protein abundance. This process is a key element for cell diversity and is regulated at different levels including: transcriptomics, metabolomics and proteomics (Doherty and Beynon, 2006).

Different protein pools and the abundance in which they are found in specific compartments control synaptogenesis and dendritic spine morphology. Protein composition and concentration provide individuality to synaptic boutons (axons) or spines (Schuman, 1999). The protein diversity pools found at the synapse are maintained by two mechanisms taking place in neurons: localized transport and localized translation of mRNAs in the spines and axons. Localized translation, is often observed in polarized cells such as neurons. However, the most classic and better characterized example for transcript localization is the drosophila oocyte where the spatial distribution of mRNAs directs the early patterning of the anterior-posterior poles (reviewed by Schuman, 1999). Electron microscopy images of synapses allowed the identification of polyribosomes –mRNA and ribosome complexes- in dendritic shafts and at the base of spines (Ostroff et al., 2002), supporting the paradigm of mRNA localization and local translation in neurons. Moreover, deep sequencing of the Neuropil and high resolution *in situ* hybridization of neuronal transcripts (see Figure 6) in neurons clearly show the presence of more than 2000 transcripts in dendrites (Cajigas et al., 2012). To date it is clear that mRNA translation in the soma of neurons is undoubtedly important, however increased evidence has been provided that support the functional significance of local protein synthesis. Local protein synthesis has been described to play a role in fundamental processes in neurons such as memory formation, dendrite and arbor branching, synapse formation, axon steering, cell survival and proteostasis (Tom Dieck et al., 2014).

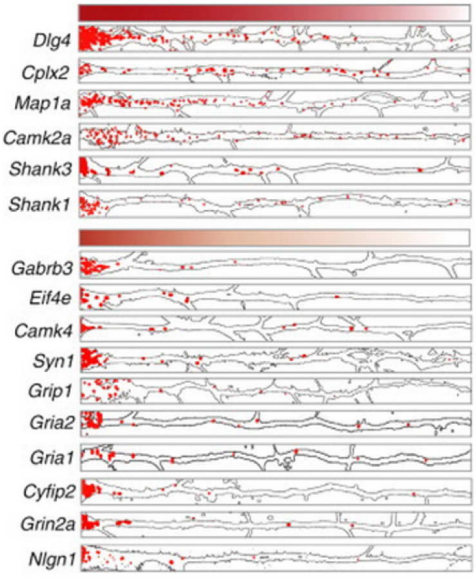

Figure 6I High-resolution fluorescent microscopy for detection of different mRNAs in primary neuronal cultures. This figure taken from Cajigas et.al, 2012 is an example for some of the evidence of localized transcripts in neurons. The red puncta represent the transcripts for the indicated genes found in dendrites and the panels are presented according to transcript abundance in dendritic shafts (top to bottom).

On the other hand, protein degradation has been shown to play an important role in neurons. The ubiquitin proteasome system (UPS) is the main mechanism for protein degradation in the cell and is highly conserved among species from yeast to human cells (Yi and Ehlers, 2005). Moreover, protein ubiquitination and subsequent degradation is a very specific process acting in a spatial-temporal manner (Yi and Ehlers, 2005). In the synapse, the UPS plays an important role in synaptogenesis and spine morphogenesis during activity-dependent spine outgrowth (Hamilton et al., 2012) and changes in spine morphology are known to underlie learning and memory (Engert and Bonhoeffer, 1999). These data provides evidence for the role of the proteasome regulating locally the growth of new dendritic spines.

We know from previous work from the Eickholt lab that PTEN a protein and lipid phosphatase antagonizing the PI3K pathway interacts with DBN and that this interaction affects pS647-DBN levels. PTEN knock down in primary neuronal cultures increased pS647-DBN levels suggesting DBN regulation to be indirectly controlled by PTEN (Kreis et al., 2013). This observation was the first hint to hypothesize that perhaps DBN stability could be mediated by phosphorylation. DBN abundance is particularly interesting in the context of spine maintenance and synaptic function and

currently very little is known about how is DBN regulated. Moreover, downregulation of DBN has been observed in disease. Therefore, DBN turnover and stability in neurons became the focus of our research for which the following hypotheses were formulated.

1.8 Hypotheses

The main hypotheses this thesis addresses are:

- Phosphorylation of DBN at S647 is important for the control of DBN turnover -- it is regulated by the phosphatase activity of PTEN.
- DBN synthesis could be controlled by the PI3K-mTOR pathway and DBN degradation by the protein phosphatase activity of PTEN.
- DBN turnover is likely to be controlled locally in dendrites and spines of neurons.
- Spatial-temporal patterns of pS647-DBN could be relevant in the formation and maintenance of filopodia and dendritic spines.

1.9 Phases and milestones of the project

During the first year of my PhD project, I generated and tested several expression plasmids (DBN full-length and different phosphorylation mutants) that allowed me to examine DBN protein turnover in well-defined experimental settings. I mastered the techniques for introducing the constructs into different cell lines, in order to analyze morphometric changes and also for performing evaluations by western blotting. This was an essential step for fully understanding the specificity of a set of commercially available and in-house generated DBN antibodies. I also tested different protocols for inducing oxidative stress in mature primary neuronal cultures under clear experimental conditions, this to simulate neurodegenerative conditions in an *in vitro* model. Through these experiments I determined that an Abeta peptide preparation and paraquat can be applied in studies that unambiguously reduce DBN abundance in neurons and likely in cell lines too.

In the second year of the project, I validated pulse-chase labeling protocols using metabolic labeling with the AHA, a methionine analog in order to study the stability of DBN depending on its post-translational modification. By the end of the year, the

relevant experiments were completed. They proved that one specific phosphorylation event at the DBN C-terminus (S647) is critical for controlling protein stability. Based on these findings, I continued my experiments in the laboratory of Prof. Erin Schuman of the Max-Planck Institute for Brain Research in Frankfurt. There, I acquired the expertise needed for applying a method that facilitates pulse-chase labeling of endogenous proteins and also the visualization of specific *de novo* synthesized proteins in cells. Initial characterization of the techniques validated them as a feasible approach for studying the spatial and temporal control of DBN turnover in neuronal primary cultures.

In January of 2014, I started setting up the FUNCAT-PLA experiments in Berlin and modified the conditions for mouse neurons. I also initiated a collaboration with Viktor Dinkel, a bioinformatics student, with whom I developed a software plugin for semi-automated analyses of PLA data. This plugin makes possible the systematic analysis of hundreds of confocal microscopy images. It was essential for obtaining the final quantifications and results for the different assays that I prepared applying PLA. The establishment of the technique, named FUNCAT-PLA, in the Eickholt Lab was accomplished at the end of the second and beginning of the third project years.

During the course of the third year of the project, I made and completed the FUNCAT-PLA experiments for studying DBN turnover in neurons. This assay provided information about the localization of the newly synthesized DBN proteins, showing that they could be translated locally in dendrites and spines. Therefore, in March of 2015, I went back to the Max-Planck Institute for Brain Research in Frankfurt and performed further experiments in neurons. By visualizing DBN transcripts in dendritic spines, I could confirm the presence of DBN mRNA in dendrites, providing additional support to the hypothesis that DBN is locally translated. While in Frankfurt, I also received training for applying Puro-PLA, an experimental technique that allows the visualization of specific proteins directly after translation with metabolic labeling using puromycin. During the course of my last project year, I established this technique in our lab and applied it to N1E neuroblastoma cells and primary neurons. The data obtained from the neurons confirms that DBN is not only translated in the soma of the neurons but also in dendrites, and possibly even in spines. I also applied this assay to study DBN translation after inhibition of the mTOR-PI3K pathway. I was able to show that mTOR inhibition reduces DBN translation in comparison to respective controls in

neuroblastoma cells under serum deprived conditions. Chapter 3 of this thesis provides the necessary experimental data and a discussion of these results.

1.10 Organization of the experiments and methodology applied

The main goal of this thesis project has been understanding the turnover and localization of the actin-binding protein DBN in neurons, and also determining the regulatory inputs for its stability. With these objectives in mind, some key experiments and the technology to be used were defined. The results of the thesis (in the next chapter) have been organized in three main sections that also present the methodology used in each experiment.

Section 1: Regulatory inputs of DBN abundance in cell lines and neurons

I started by investigating the expression levels for endogenous DBN in four different cell lines, as described in the first section of results. This was done with SDS-PAGE and western blot (WB) analyses. In the next step, I tested multiple antibodies against DBN, for their specificity in WB. Then, in order to test different plasmids for DBN, I performed transfection in cell lines and analyzed the expression levels using SDS-PAGE and western blotting (sections 2.1.1 and 2.2.2).

In order to test the specificity of our DBN antibodies in immunocytochemistry, I cultured hippocampal neurons from *DBN-KO* embryos. I transduced these neurons with either YFP-DBN or only with YFP. This enabled me to determine the specificity of multiple DBN antibodies and to compare with the labelling in wild-type neurons (section 2.1.3).

I applied the proximity ligation assay in order to obtain a direct visualization of the DBN-PTEN interaction in neurons. This assay is an antibody based technology (first described in Söderberg, 2006) that allows the direct visualization of interacting proteins as close as 30-40 nm in fixed cells (section 2.1.4).

In order to elucidate whether the phosphorylation site S647 of DBN plays a role in the formation of filopodia-like structures, I overexpressed YFP-DBN$_{wild\text{-}type}$ or the phospho-mutants: YFP-DBN$_{S647A}$ or YFP-DBN$_{S647D}$ in multiple cell lines. These experiments are discussed in section 2.1.5.

I also explored possible mechanisms that control the abundance of DBN in neurons by analyzing DBN expression levels using western blotting, after the induction of oxidative stress with different compounds (section 2.2.2). With the same objective, I stimulated neurons with the antagonist for GABA A receptors and followed the expression of DBN over time using SDS-PAGE and western blotting (section 2.2.4)

Section 2: DBN turnover

Additionally, this thesis examines the characterization of the phosphorylation site S647 and its potential role in the control of DBN turnover. In order to address this question, I developed pulse-chase experiments using metabolic labeling in cells overexpressing either Flag-DBN$_{wild\text{-}type}$, Flag-DBN$_{S647A}$ (phospho-dead), or FlagDBN$_{S647D}$ (phospho-mimetic). This allowed me to mark *de novo* synthesized proteins using pulse-labeling with AHA; a methionine analog. Their decay could be followed by chasing in complete medium. Click-chemistry allowed me to post-label with biotin the metabolically labeled proteins and their detection was then possible using streptavidin-HRP on a blot (section 2.2.1).

The next project goal was to investigate the turnover of DBN in neurons and the resulting spatial-temporal patterns. To do so, I performed pulse-chase experiments with FUNCAT-PLA (Fluorescence Non-Canonical Amino acid Tagging and Proximity Ligation Assay) as described in Tom Dieck et al., 2015. This assay, allows the direct visualization of specific proteins after metabolic labeling in cells and it can be combined with chase in complete medium. These experiments are discussed in sections 2.2.2 and 2.2.5. The FUNCAT-PLA provides microscopy images for quantitative analyses. Quantification required, the development of a semi-automated FIJI plugin with its description provided in section 2.2.4

I also employed metabolic labeling with puromycin in order to address the question: how is DBN translation controlled? To answer this, I studied the regulation of DBN translation upon inhibition of the PI3K-mTOR pathway in combination with puromycilation and Proximity Ligation Assay or Puro-PLA as described in (Tom Dieck et al., 2015). These results are discussed in section 2.2.6 and 2.2.7.

Section 3: Visualization of DBN mRNA in neurons and abundance after neuronal stimulation

The last section in the results chapter deals with the following questions: Where is DBN mRNA localized in neurons? Can its abundance and localization change when synaptic activity is blocked or enhanced? Finally, I investigated the localization of DBN transcripts in neurons by *in situ* fluorescence hybridization (FISH) at basal conditions and upon stimulation with bicuculline (for enhancing synaptic activity), or TTX + APV (silencing synaptic networks). These results are discussed in section 2.3.

2 Results

2.1 Analyzing regulatory inputs of DBN abundance in cell lines and neurons

This section describes the different treatments applied in experiments performed for establishing endogenous DBN presence in various cell lines and neurons. The overexpression of various DBN constructs was also tested. The main goal of these experiments was establishing models for studying DBN turnover, but also discovering regulatory inputs controlling the stability of DBN. Optimizing the parameters of this set of experiments turned out to be essential for the development of the more complex assays explained in the later sections.

2.1.1 Analyses of endogenous and exogenous DBN expression by western blotting

In order to investigate the endogenous expression of DBN, I prepared cell lysates from the following four cell lines that were continuously kept in culture:

- HEK293T: human embryonic kidney cells expressing the SV40 Large T-antigen,
- COS-7: fibroblast-like cell line derived from monkey kidney tissue,
- N1E-115 (N1E): mouse neuroblastoma cell line, and
- SH-SY5Y: human neuroblastoma cell line.

The samples were analyzed using western blotting and were probed for DBN with two different antibodies (mouse monoclonal and guinea pig serum), with pS647-DBN and with GAPDH as loading control. I identified endogenous DBN expression in all four cell lines (Figure 7) to approximately similar levels. I also used our custom antibody for detecting pS647-DBN levels, and in fact in all four cell lines different levels were identified. Out of the four cell lines, HEK293T cells show the highest levels of pS647, while the SH-SY5Y cells have the lowest levels.

The GAPDH bands have different sizes among four different cell lines shown in Figure 7, which might be due to the differences in the species of different cells lines

Following overexpression experiments were pursued in HEK293T, chosen for being cells easy to transfect. N1E-115 cells were used for imaging experiments as good neuroblastoma model and for immunocytochemistry purposes.

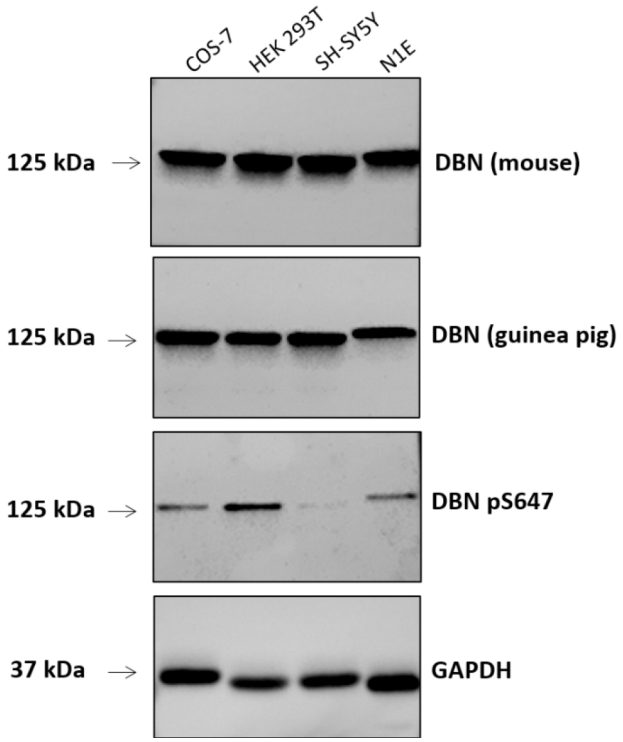

Figure 7| Endogenous DBN expression in cell lines. Cell lysates from HEK 293T, COS-7, N1E and SH-SY5Y were collected and analyzed using western blotting. DBN was identified in all of the analyzed cell lines at similar levels, using two different pan-DBN antibodies (M2F6 mouse monoclonal and polyclonal guinea pig). In contrast, levels of pS647-DBN varied between the different cell lines. GAPDH was used as loading control**.**

In the DBN literature little is known concerning the differences between the two DBN isoforms found in mammals. DBN-A and DBN-E are two different splicing isoforms of DBN. Whilst the overall amino acid sequence is almost identical, DBN-A (when compared to DBN-E) contains an extra sequence of 46 amino acids as shown in Figure 4. At the protein expression level, it has been reported that DBN-E is replaced by DBN-A in the brain tissue during development (Hayashi et al., 1998). Yet, no functional differences have been described to date. In order to gain some insights into the potential functional differences between DBN-A and DBN-E isoforms, I transfected HEK293T cells with tagged DBN constructs, and explored morphological changes by

microscopy and imaging analysis. First of all, I confirmed their expression at the protein level using western blotting after transfections (Figure 8). Secondly, I searched for differences in the phenotypes induced after DBN overexpression (Figure 14).

Transfection of DBN-E and DBN-A, Myc-DBN-E, YFP-DBN-E, YFP-DBN-A, YFP, Flag-DBN-E or Flag was performed and the expression was analyzed by western blotting using DBN and tag specific antibodies, as shown in Figure 8. all the different constructs were successfully transfected and were identified at the expected molecular weights. No band was found in non-transfected cells. The corresponding bands for those transfected with only YFP or Flag were not detected in these blots due to their small molecular weights. However, no band for DBN-tagged was found in the lysates from those cells transfected only with YFP and flag. Providing good controls for these experiments. Although we know that DBN is indeed express in HEK293T cells (see Figure 7), endogenous DBN was not always detected in the conditions where cells were not transfected with any construct or transfected with YFP, Flag. The reason for this is rather technical, the exposure time for detection of bands should be increased in order to visualize DBN endogenous levels.

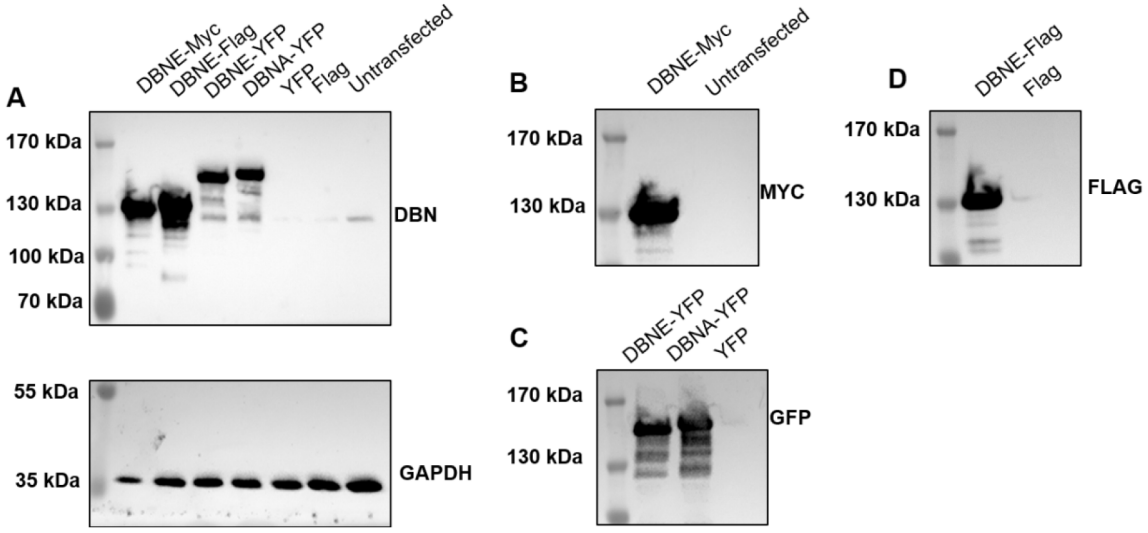

Figure 8| DBN overexpression with different plasmids. Cell lysates were analyzed by western blotting and blots were probed with DBN, GFP, MYC and FLAG specific antibodies, respectively, to identify exogenous DBN expression. Anti-GAPDH antibody was used as internal loading control. A) Transfected HEK293T cells with tagged DBN-E and DBN-A constructs as indicated. B) Transfected HEK293T cells with Myc-DBN-E or untransfected control cells. C) Transfected HEK293T cells with YFP-DBN-E, YFP-DBN-A or YFP. D) Transfected HEK293T cells with Flag-DBN-E or Flag.

2.1.2 Determining the Specificity of DBN Antibodies in Immunocytochemistry

Published DBN antibodies are commercially available, but specificity in immunofluorescence assays was nonetheless tested. This is especially important whenever the effect of the application of those antibodies is the main read-out of a particular assay. This is the case for example in techniques like immunocytochemistry (IC) and the proximity ligation assay (PLA). In the next section a detailed description of the PLA is provided.

During my thesis project, I performed many antibody-based assays. Therefore, it was important to control for the specificity of the two pan-DBN antibodies that were applied for IC and PLA in this project. Those antibodies were the M2F6 DBN antibody (mouse monoclonal) and our custom made DBN antibody (rabbit polyclonal Eickholt lab). The DBN (Eickholt lab) is an antibody that is collected after serum purification of our pS647-DBN antibody, and has been established to recognize total DBN. I tested the specificity

of these two DBN antibodies by performing immunocytochemistry in DBN-Knockout (DBN-KO) hippocampal neurons, using the DBN antibodies mentioned above.

In our lab, Dr. Till Mack has generated a DBN-KO mouse model missing the exons 1-6 of DBN, as described in the material and methods section. Cultured neurons from these animals should not produce any positive labeling for DBN when performing immunocytochemistry (IC) unless the DBN antibody being unspecific.

To confirm the specificity of these antibodies I performed IC in cultured DBN-KO hippocampal neurons transduced with either YFP-DBN (Figure 9 A and B) or YFP lentiviruses (Figure 9 C and D). After 22 DIV the neurons were fixed and immunocytochemistry for the detection of DBN and MAP2; a somato dendritic marker was performed. Transduced neurons were identified by the expression of YFP. For those neurons transduced with YFP-DBN a co-localization between YFP and DBN staining was observed (Figure 9 A and B). In contrast, neurons missing DBN and transduced only with the YFP lentivirus control have no expression and staining of DBN, proving the specificity of the antibodies (Figure 9 C and D).

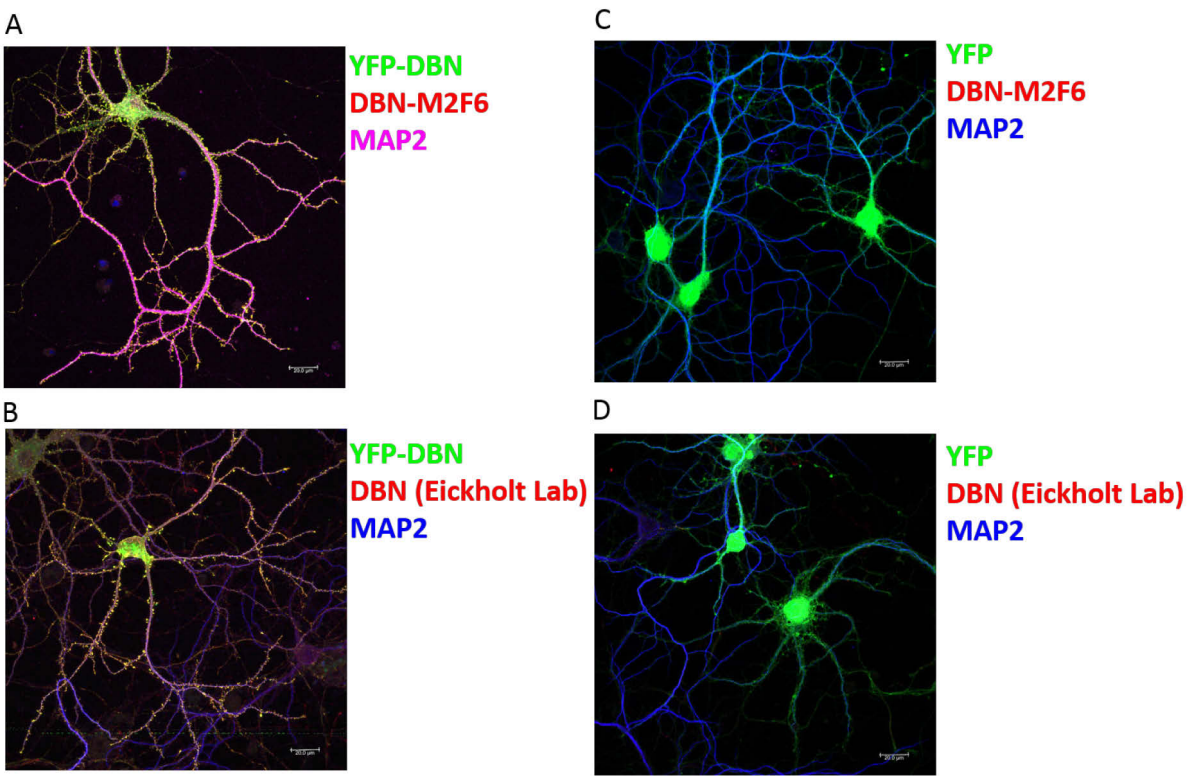

Figure 9| Control immunostaining for DBN antibodies in DBN-KO neurons. Cultured hippocampal neurons from DBN-KO mice were infected with YFP-DBN (A and B) or YFP (C and D) lentiviruses as indicated after 14 DIV and fixed at 22 DIV. Immunocytochemistry was performed using DBN (M2F6), or our homemade DBN rabbit antibody DBN (Eickholt lab) for DBN staining and MAP2 as a neuronal marker. The images are maximal projections; brightness and contrast has been manually modified for visualization purposes. Scale bar: 20 µm.

Moreover, DBN localization is known to be enriched in dendritic spines and to co-localize with F-actin. Therefore, it can be used as a postsynaptic spine marker. F-actin forms the actin cytoskeleton in neurons and it is usually complex and enriched in dendritic spines. In order to visualize the localization of DBN, using both of the antibodies tested above, I performed IC for DBN and MAP2 in wild-type neurons (Figure 10 A and B). In these pictures it is evident that DBN decorates the dendrites as synapses would do. In order to confirm this localization, I performed IC for DBN and F-actin wild-type neurons, using both DBN antibodies (Figure 10 C and E). DBN has been shown to be enriched in dendritic spines and to accumulate in areas where F-actin is highly abundant. As shown in Figure 10 C and E, DBN is indeed found in dendritic spines and it highly co-localizes with F-actin in these neuronal compartments.

This is evident by the presence of the yellow color; consequence of the merge between green (F-actin) and red (DBN).

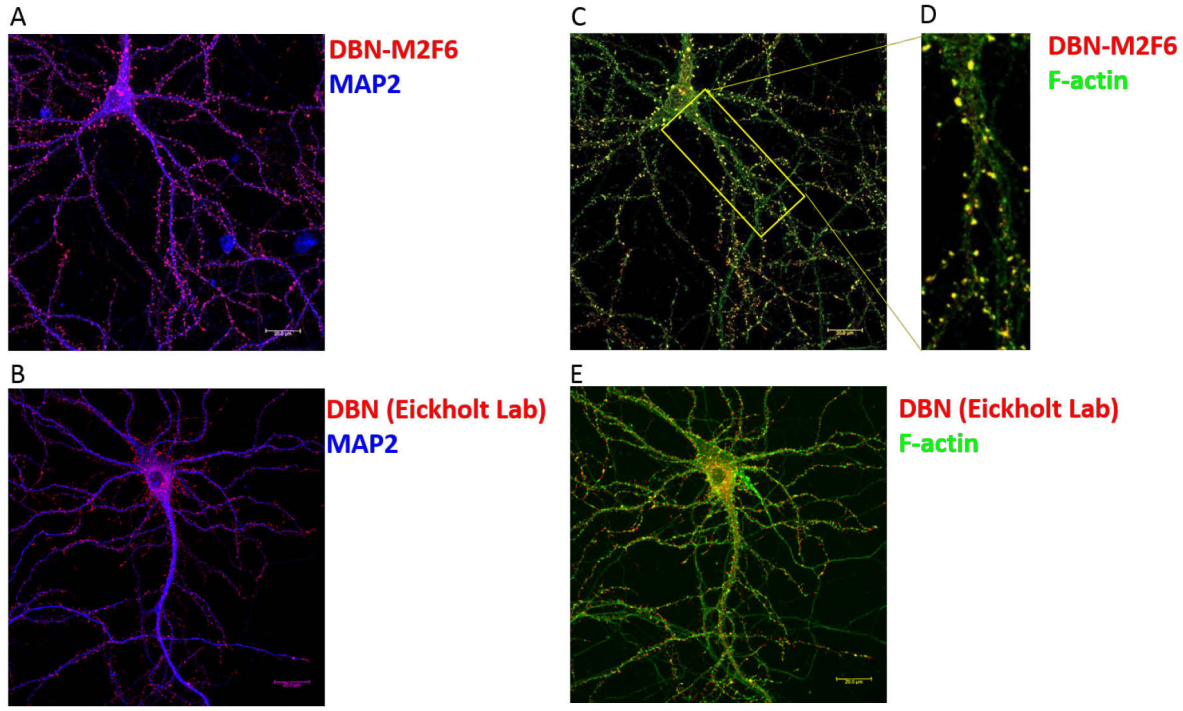

Figure 10| Localization of DBN in neurons from wild-type mice. Cultured hippocampal neurons from wild-type mice were fixed after 22 DIV and stained with DBN (M2F6) (A and C) or DBN (Eickholt Lab) (B and E) antibodies (red). An antibody against MAP2 was used as a neuronal marker to distinguish neurons from non-neuronal cells (blue) in A and B and phalloidin was used to label F-actin in C, D and E. The images are maximal projections; brightness and contrast has been manually modified for visualization purposes. Scale bar: 20 µm.

2.1.3 Visualization of DBN and PTEN interaction in neurons

Kreis et.al. (2013) identified DBN as an interaction partner of PTEN. The interaction was detected in the rat brain by mass spectrometry analysis and it was confirmed by co-immunoprecipitation. The interaction was further characterized in overexpression systems in PC12 cells using multiphoton fluorescence-lifetime imaging microscopy. Moreover, experiments with hippocampal rat neurons cultured for 18 DIV and stained with anti-pS647-DBN and PTEN antibodies, showed that PTEN is mainly found in dendrites and only occasionally in spines, while pS647-DBN is highly concentrated in spines. In this paper, anti-DBN antibody labelling, as well as labelling using the anti-pS647-DBN antibody, demonstrated some co-labelling with anti-PTEN antibody in cultured neurons. One of the main observations was that whenever PTEN was

detected in spines, pS647-DBN was missing. These results suggested that PTEN and pS647-DBN segregate into complimentary compartments, supporting the idea that PTEN can negatively regulate pS647-DBN in neurons (Kreis et al., 2013).

In order to further explore the localization of the PTEN-DBN interaction in neurons, as well as to establish a new platform in which we can test if the interaction is of direct nature, I performed a proximity ligation assay in cultured hippocampal neurons as shown in Figure 12 A for PTEN and DBN.

Several methods for visualizing protein interactions *in situ* have been developed during the last decades. In order to visualize direct protein-protein interaction in cells, most approaches rely on the overexpression of genetic constructs, and they have been successfully used in assays of living cell maintained in tissue culture as well as in fixed cells (Hu et al., 2002; Jares-Erijman and Jovin, 2003). However, most of these assays involve the introduction of exogenous proteins.

I wanted to investigate the interaction between DBN and PTEN at endogenous levels in normal conditions. To do so, I applied the proximity ligation assay or PLA; an assay that offers the possibility for the direct visualization of specific protein-protein interactions that are in the proximity of 30 nm (Söderberg et al., 2006). The PLA is an antibody based assay, combining proximity ligation with rolling circular amplification (RCA). The PLA probes consist of species-specific antibodies coupled to linear oligonucleotide sequences that in the proximity and the presence of a ligase will catalyzed the ligation between the two ends in proximity. RCA is directed by a polymerase and the addition of fluorescence labeled oligonucleotides complementary to the PLA probes. A schematic representation of this assay in depicted in Figure 11.

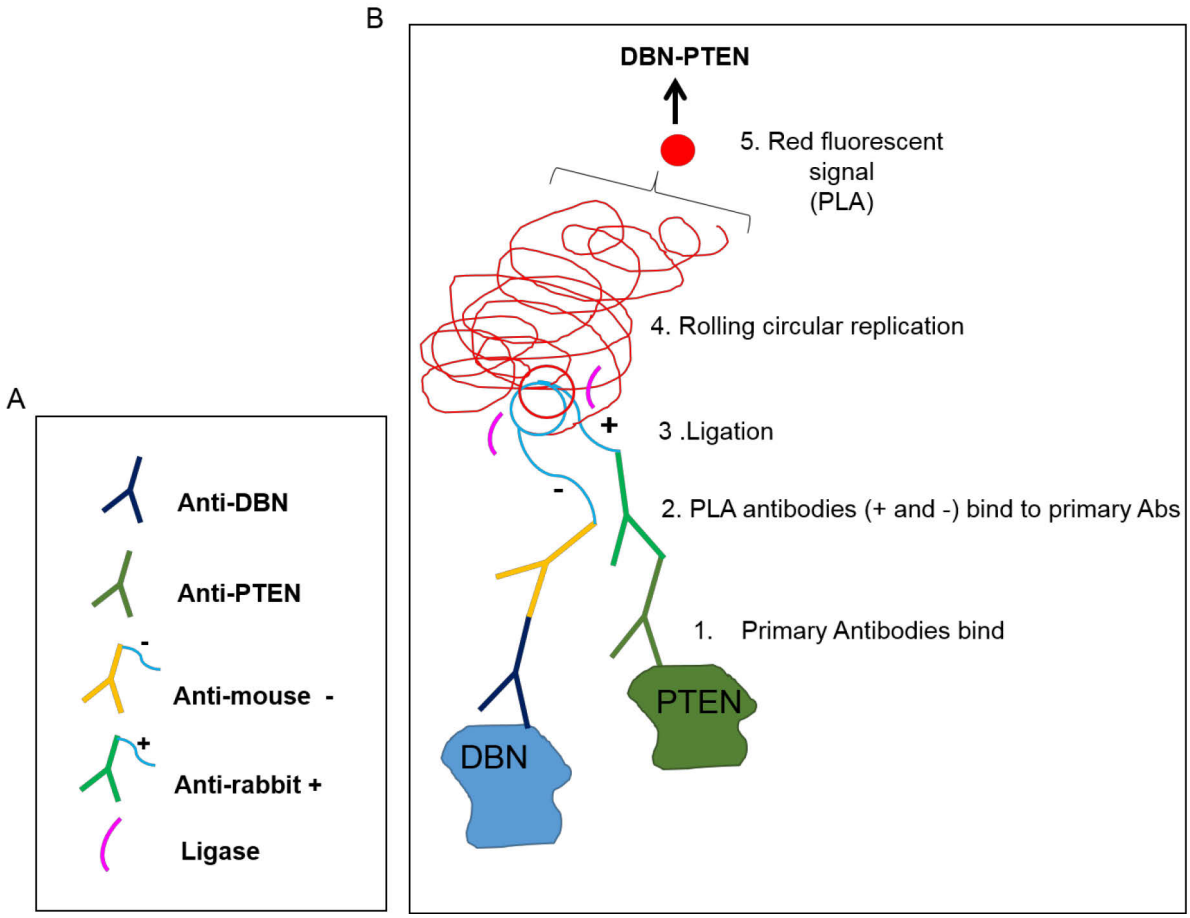

Figure 11| Schematic representation of the PLA for DBN and PTEN. A) The PLA assay is an antibody based assay. In order to visualize the interaction between DBN and PTEN antibodies specific to these proteins as well PLA^{-}-mouse and PLA^{+}-rabbit probes were applied. B) In this diagram 1-5 provides a guide to the general procedure conducted for the detection of the DBN-PLA complex in neurons using PLA.

In order to detect and visualize the endogenous interaction between DBN and PTEN, the PLA in 18-21 DIV cultured hippocampal neurons using anti-DBN and anti-PTEN antibodies was performed, according to the manufacturer's manual. Following the amplification reaction, cells were then stained with an anti-MAP2 antibody to establish the general outline of the soma and dendrites, and to exclusively label neurons (Figure 12). These experiments resulted in puncta from the PLA reaction that were found in close proximity to MAP2 positive dendrites. In order to control for the specificity of this approach, I undertook three sets of control experiments. In the first, both primary antibodies were omitted, whilst in the second and third, neuronal cultures were labeled with the PTEN antibody only or the DBN antibody only. In all experiments, the secondary antibodies were used. The PLA in these experiments resulted in no puncta,

indicating the specificity of the approach in detecting PTEN-DBN interaction. This is the first time that PTEN-DBN interactions have been visualized at endogenous levels in neurons.

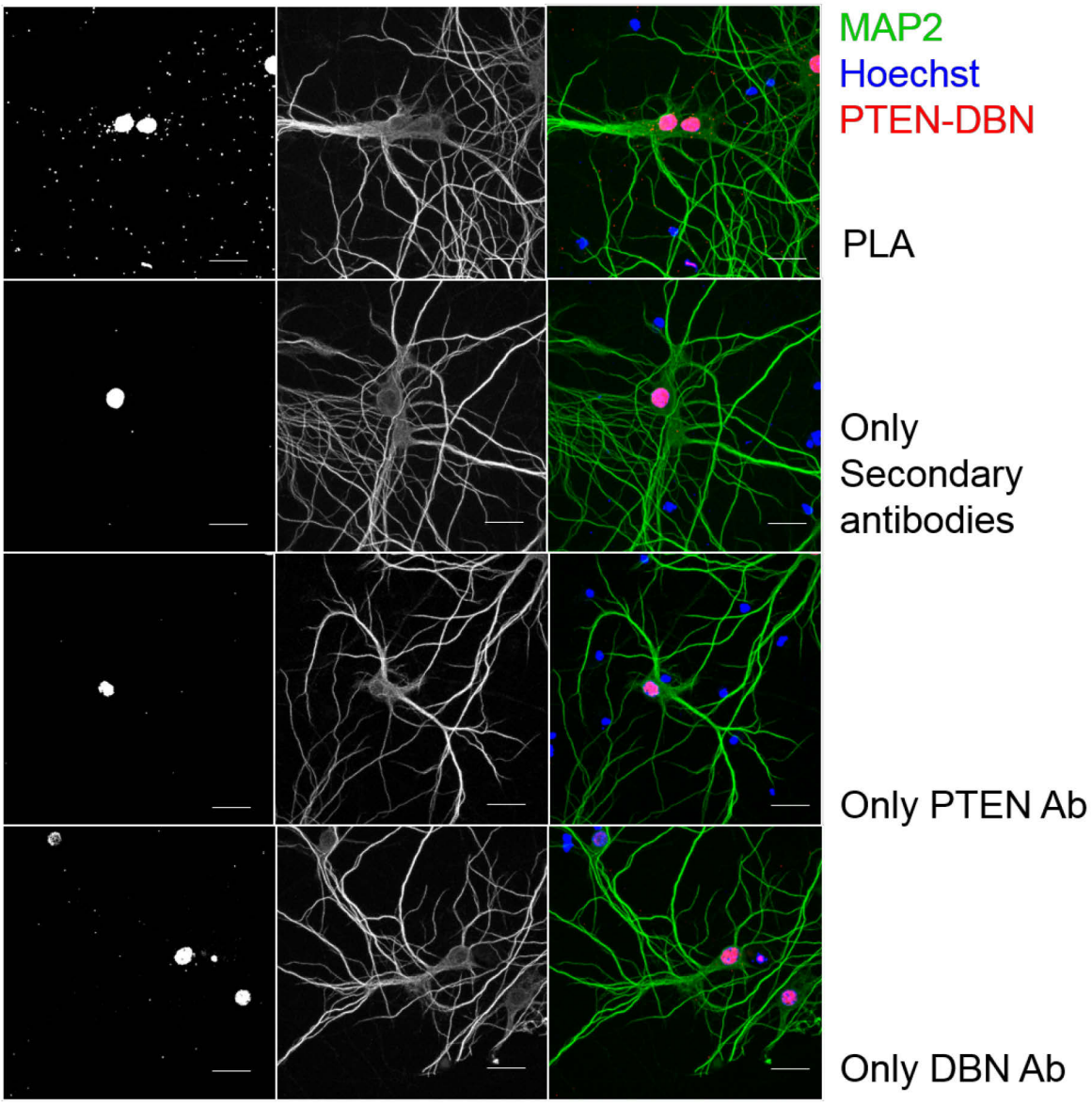

Figure 12| PTEN-DBN interaction in neurons. PLA for DBN and PTEN was performed in fixed 18-21 DIV mouse neurons. A) PLA controls for the visualization of the PTEN-DBN interaction in neurons applying PLA. The first row of images shows the interaction between PTEN-DBN (red) in neurons. The second, third and fourth rows, show that in the absence of one or both of the antibodies in the PLA assay, the interaction is not detected, proving the specificity of the signal in the assay. The neuronal marker MAP2 is shown in green, the PTEN-DBN interaction in red and Hoechst in blue. Scale bar: 20 µm

In order to unequivocally localize the obtained PLA signals to dendritic spines, I also performed the assay and co-labelled with F-actin. As demonstrated in Figure 13, some puncta co-localize to F-actin rich dendritic spines. However, only a minority of spines show evidences of PTEN-DBN PLA signals, suggesting this complex to be a rare incidence.

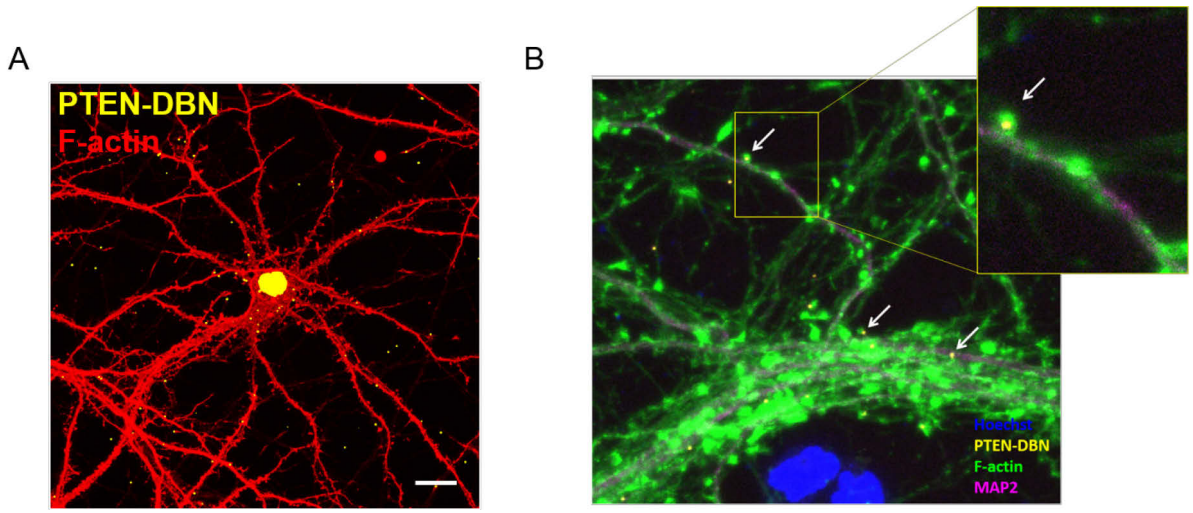

Figure 13| Visualization of PTEN-DBN interaction in neurons with PLA. A) PLA for DBN and PTEN (yellow) in co-localization with F-actin (red) in neurons. B) Visualization of the presence of the PTEN-DBN complex in spines (PLA). F-actin is stained in green, MAP2 in magenta, Hoechst in blue, and the PTEN-PLA complex in yellow. This staining shows the presence of the PTEN-DBN complex in dendrites and base/neck of spines. Scale bar: 20 µm

2.1.4 DBN biological role in the formation of filopodia-like structures when overexpressed in cell lines.

As an F-actin binding protein, DBN overexpression has been reported to induce filopodia-like structures in a number of different cell types and cultured neurons (Hayashi and Shirao, 1999; Mizui et al., 2005). In order gain first insights into the potential effect of the phosphorylation site of DBN in cells, I exploited a cell line based assay to monitor filopodia formation using YFP-tagged wild-type isoforms DBN A and E as well as of amino acid substitutions mimicking a dephosphorylated state (DBN S647A for the adult form and in the site **S601A** for the embryonic form). COS-7 cells (Figure 14-A) or SH-SY5Y (Figure 14-B) cells were transfected with the individual constructs and were then fixed after 24 h, before stained for microtubules with anti-

tubulin and nuclei with Hoechst. Representative confocal microscope images are shown in Figure 14.

In cells overexpressing DBN-A, there was a clear induction of a prominent filopodia phenotype, similar to the results reported by Hayashi and Shirao (1999) in CHO cells. Here, overexpression of DBN-E, as well as the mutant DBN S647A/S601A constructs induced filopodia to the same extend as DBN-A. Therefore, S647/601 is not likely to influence DBN activity toward influencing actin dynamics during filopodia induction, at least not in this assay.

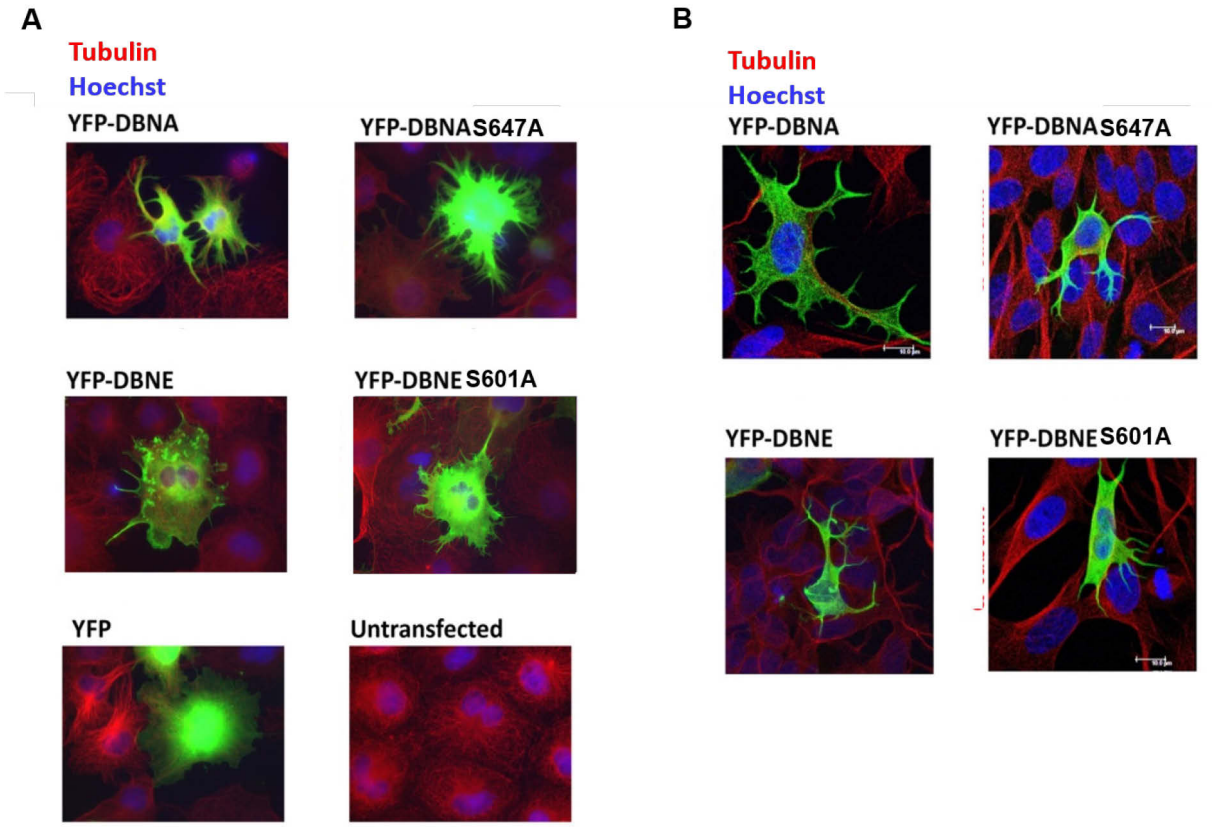

Figure 14| Overexpression of DBN induces the formation of filopodia-like structures. A) COS-7 and B) SH-SY5Y cells were transfected with either YFP-DBN-E, YFP-DBN-E-S601A, YFP-DBN-A, YFP-DBN-A-S647A or an YFP control, as indicated and labeled in green for 24 h. As an extra control non-transfected cells are included. After transfection, cells were fixed and stained for tubulin in red and Hoechst in blue. The images were captured using a confocal microscope.

2.1.5 Induction of oxidative stress by paraquat reduces DBN expression levels in cortical neurons

The production of reactive oxygen species (ROS) is consequence of the metabolism of the cell, however when the ROS present un-pair electrons they are known as free radicals. Free radicals are highly reactive molecules that can affect important processes in the cell leading to cell dead (Ramalingam and Kim, 2011). An increase in the production of ROS has been described to contribute in the pathogenesis of some diseases including AD (Ramalingam and Kim, 2011). In connection to this, multiple studies have reported a decrease on DBN protein levels in the brains from AD patients suggesting a possible correlation between DBN levels and cognitive impairment (Counts et al., 2012; Harigaya and Shoji, 1996; Shim and Lubec, 2002). However, clear evidence about how DBN influences AD disease remains to be elucidated.

I hypothesized that DBN may be modified by oxidative stress. Therefore, I investigated whether DBN levels decrease during oxidative stress by challenging matured cortical neurons testing three compounds commonly used for the induction of oxidative stress in cells: H_2O_2 and the herbicide paraquat (Wang et al., 2009; Doré et al., 1999; Ramalingam and Kim, 2011). In addition to those compounds, Aβ the Alzheimer's disease related protein was also tested.

In order to assess DBN stability during conditions that may resemble aged or disease-like insults and to find the right experimental conditions, H_2O_2, paraquat and Aβ were applied at different concentrations. I observed that H_2O_2 at the tested concentrations (1-10 μM) had no effect on DBN protein levels in 14 DIV cortical neurons. Treatments with Aβ applied (0.25μM-2μM) were rather difficult since occasionally the effect was very toxic leading to neuronal death. However, the herbicide paraquat significantly reduced DBN protein levels in a 20 μM concentration with no cytotoxic effects (Figure 15), providing a good platform for future experiments targeting the regulation of DBN abundance during oxidative stress. These data demonstrate that levels of DBN are vulnerable to increased oxidative stress providing a good experimental setup for future investigations.

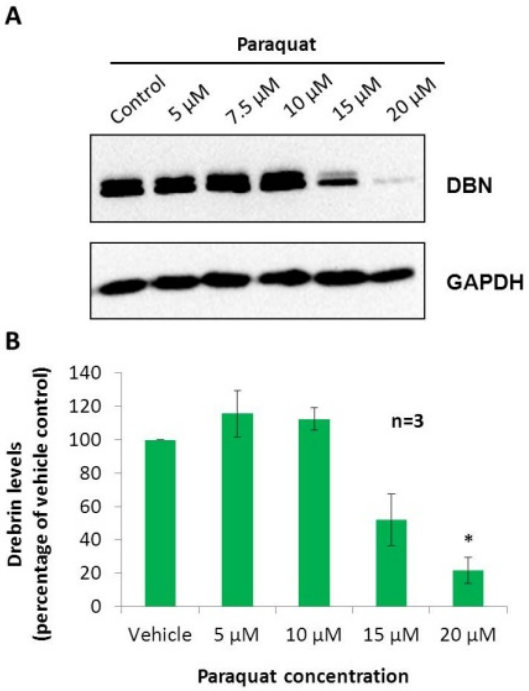

Figure 15| Induction of oxidative stress by paraquat reduces DBN levels in 14 DIV cortical neurons. Mouse embryonic day 16.5 (E16.5) cortical neurons were cultured for 14 days in vitro and were treated with different concentrations of paraquat. Twenty-four hours after treatment, the cells were lysed and analyzed for DBN levels (A). Equal amounts of lysates were loaded on 8% poly-acylamide gels and were probed for DBN and GAPDH. B) The relative levels of DBN were quantified and normalized to vehicle control levels. These values are plotted for three independent experiments, where the error bars represent +/- SEM and *p=0.010

2.2 Regulation of DBN turnover

This section describes the experiments I performed in order to study the potential role of DBN phosphorylation at (S601) in the stability of the protein. I designed and established pulse-chase experiments using metabolic labeling with AHA. These experiments allowed me to study the degradation and turnover profiles of Flag-DBN$_{wild-type}$ and two Ser-substituted mutant forms, mimicking either a dephosphorylated (Flag-DBNS601A) or a phosphorylated state (Flag-DBNS601D) of the protein.

2.2.1 Pulse-chase experiments using L-Azidohomoalanine in a cell culture system show that pS647 regulates DBN stability

Cell homeostasis is a process highly dependent on the proteome. The proteome is very dynamic and it is regulated by protein synthesis and protein degradation. This regulation is implicated in several biological processes such as cell proliferation, cell growth, cell differentiation, cell metabolism, memory and learning (Dieterich et al., 2006). Therefore, understanding the means for proteostasis can provide insights into the regulation of such processes. DBN is a protein which has been described to play a role in synaptic plasticity (Jung et al., 2015) and which protein levels seem to be important in the regulation of filopodia formation and spine maintenance (Hayashi and Shirao, 1999; Kreis et al., 2013).

DBN is a highly phosphorylated protein and site-specific phosphorylation is speculated to regulate localization and stability of DBN. Therefore, I explored DBN turnover in dependence of S647/S601 phosphorylation, a phosho-site shown by Eickholt and colleagues to be regulated by PTEN levels (Kreis et al., 2013). To do so, I applied bioortogonal noncanonical amino acid tagging (BONCAT) (Dieterich et al., 2006).

BONCAT was developed by Schuman and colleagues (2006) for the identification of newly synthesized proteins in mammalian cells using metabolic labeling with AHA. Application of assays such as isotope labeling amino acid, 2D gel electrophoresis, radioactive isotope labeling amino acid and others had been applied before for this purpose (Dieterich et al., 2006). However, BONCAT opened the possibility of enriching labeled *de novo* synthesized proteins. This is possible with AHA and ‘click-chemistry’ for the alkyne-biotin cycloaddition.

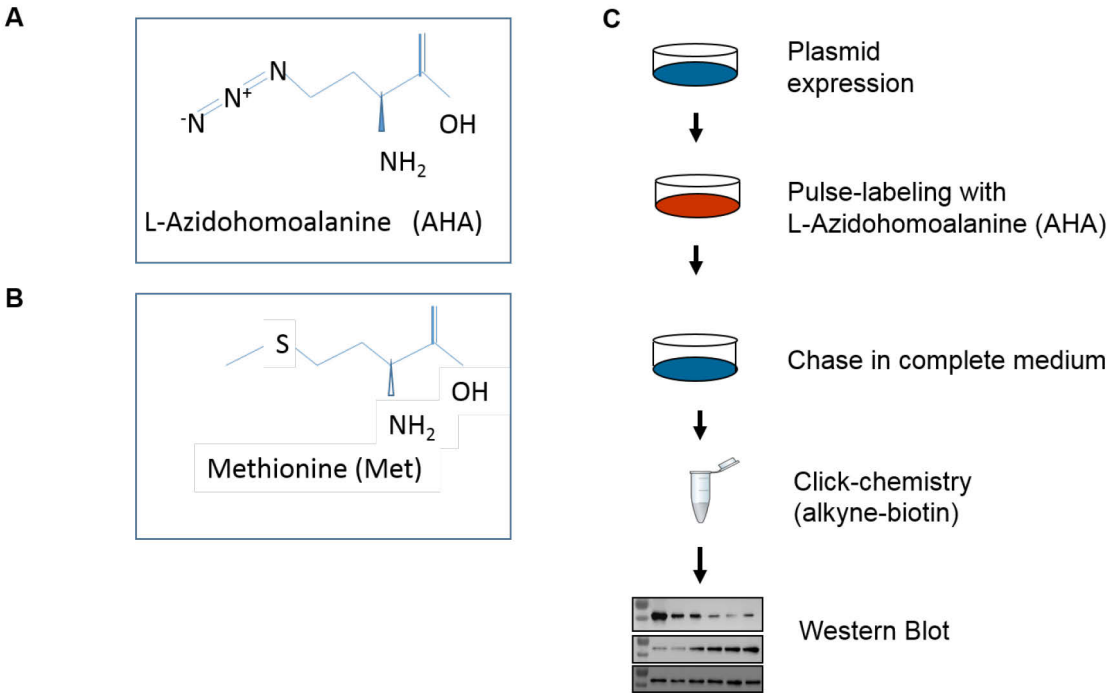

Figure 16| Overview of the experimental setup for pulse-chase experiments using metabolic labeling. A) Chemical structure of the methionine analog L-azidohomoalanine. B) Chemical structure of the aminoacid methionine. C) Flow chart of the protocol for pulse-chase experiments. 293T cells were transfected and later pulse-labeled with AHA. Cells were lysed and click-chemistry was performed. Detection of AHA-labeled proteins was performed with streptavidin-HRP in western blot.

AHA is an unnatural amino acid that is incorporated into newly synthesized proteins instead of Methionine (Met) during pulse-labeling. This principle was used to label expressed protein over defined periods of time, chasing them with complete medium for studying the labelled protein's stability. As shown in Figure 16, HEK293T cells were transfected and, after 24 h, Met starved for 1 h and pulse-labeled with 1 mM AHA for 1 h. Then, cells were lysed and click-chemistry was performed. Samples were analyzed by WB, whereby the detection of the AHA-labeled proteins was performed with streptavidin-HRP.

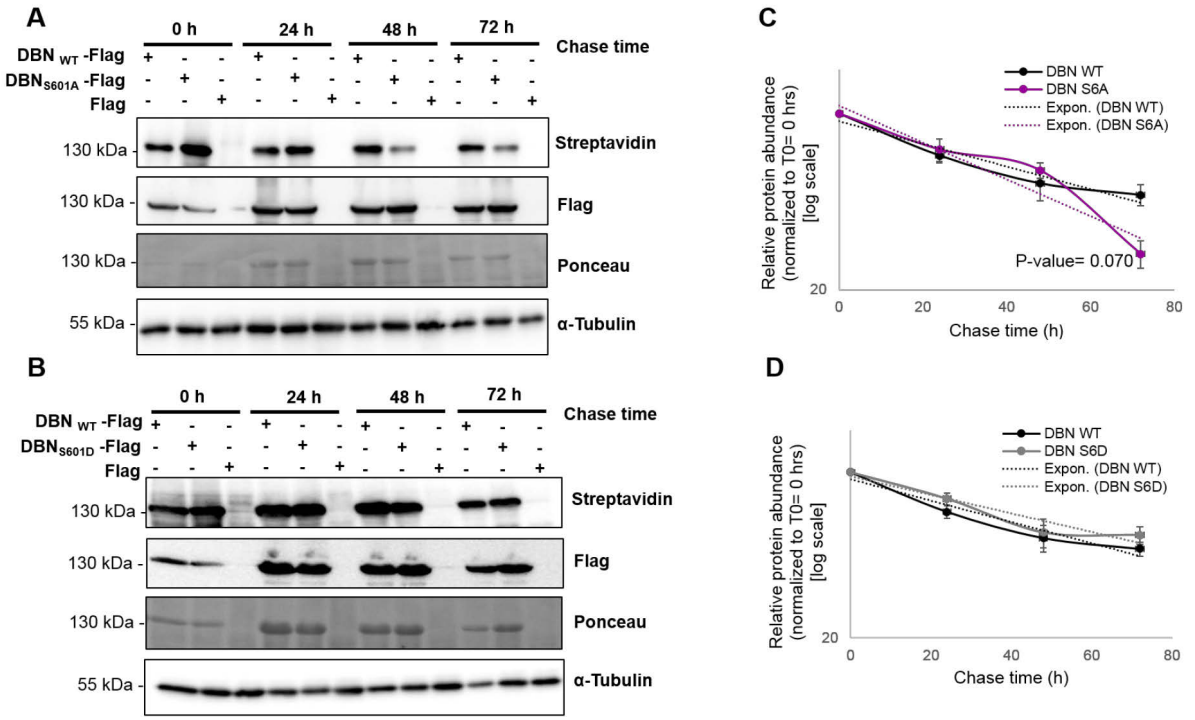

Figure 17| DBN protein stability is pS647 dependent. HEK293T cells were transfected 24 h after platting with DBN_{WT}-Flag, DBN_{S647A}-Flag, DBN_{S647D}-Flag or Flag. 24 h after transfection cells were methionine starved for 1 h followed by pulse-labeling with L-azidohomoalanine (AHA) for 1 h and chased in complete medium for 0, 24, 48 or 72 hrs. Cell lysates were collected and used for click-chemistry (alkyne-biotin cycloaddition). Pellets were resuspended in sample buffer and analyzed by western blotting using streptavidin for the detection of AHA labeled proteins or the indicated antibodies. A) Pulse-chase experiments comparing DBN_{WT}-Flag and DBN_{S647A}-Flag protein stability or B) DBN_{WT}-Flag and DBN_{S647D}-Flag protein stability by western blotting. C-D) Western blots were quantified and relative protein abundance after normalizing to loading control (tubulin) and to time point 0 h is plotted. Pointed lines indicate the respective exponential decay curves and error bars show the SEMs.*P-value= 0.070

These experiments show that DBN_{S601A} is degraded faster than the $DBN_{wild\text{-}type}$ isoform (Figure 17). This observation suggests that the stability of DBN is S601 phosphorylation dependent. In contrast, DBN mutant isoform mimicking a phosphorylated state (S601D) is as stable as the wild-type DBN-E isoform after 72 h chase (Figure 17). In addition, I estimated protein half-lives for all the DBN proteins: wild-type and mutants (Figure 18). The protein half-lives indicate that DBN is a long-lived protein and that ablating DBN S601 phosphorylation increase its turnover (half-live=39 +/-3 hours). Moreover, the half live of $DBN_{wild\text{-}type}$ does not differ significantly from the half live of DBN_{ES601D} (75 ± 8 hours and 97± 16 hours, respectively), indicating

that DBN is highly phosphorylated under normal conditions. These results suggest that DBN stability is dependent on S647 phosphorylation.

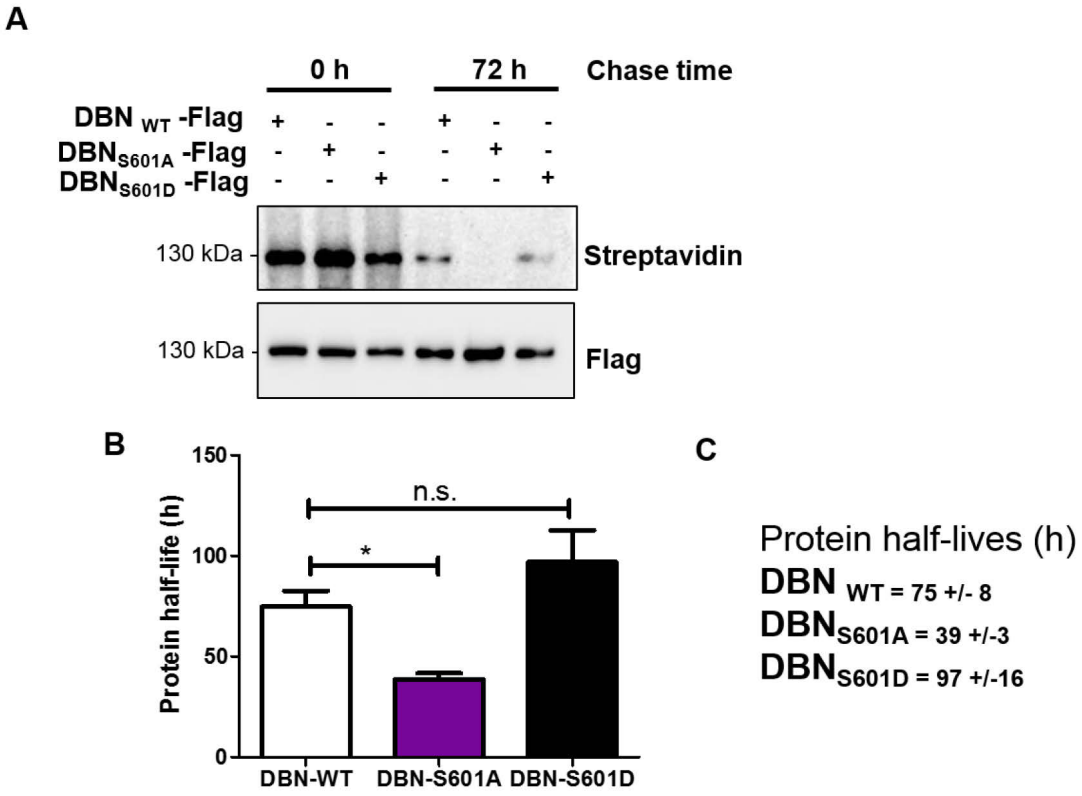

Figure 18| DBN protein stability is pS647 dependent. A) HEK293T cells were transfected 24 h after platting with DBNWT-Flag, DBNS647A-Flag or DBNS647D-Flag. 24 h after transfection cells were methionine starved for 1 h followed by pulse-labeling with L-azidohomoalanine (AHA) for 1 h. Cells where then chased in complete medium for 0 and 72 h. Cell lysates were collected and used for click-chemistry (alkyne-biotin cycloaddition). Pellets were resuspended in sample buffer and analyzed by western blotting using streptavidin-HRP for the detection of AHA labeled proteins or Flag-specific antibody to detect total exogenous gene product. A) Representative western blot showing time points 0 and 72 h chase. DBN AHA-labeled proteins are detected with streptavidin-HRP. Less AHA-labelled DBNS647A-Flag is present after 72 h chase compared to DBNWT-Flag and DBNS647D-Flag. B) and C) Protein half-lives were calculated from quantification of three independent experiments and are plotted in this bar plot C) The half-lives indicate that DBN is a long-lived protein and that ablating DBN S647 phosphorylation increases its turnover. Error bars indicate SEMs and * indicates P-value < 0.01.

2.2.2 Proteasome inhibition in pulse-chase experiments reveals that DBN is degraded via the Ubiquitin Proteasome System

Cellular control of protein degradation involves a number of different mechanisms. For example, membrane proteins are proteolytically cleaved in the lysosome compartment whilst most cytosolic proteins are degraded by the proteasome. Since I was studying the degradation profiles of DBN and the regulation of its stability, the connected question arose: how is DBN degraded in the cell?

At the time of this investigation there was no data in the literature providing any evidence about the mechanisms for DBN degradation. Therefore, a viable first approach was to apply a proteasome inhibitor, MG132, in the already developed pulse-chase system and follow DBN degradation in the presence or absence of such inhibitor. Later, Chimura et.al. (2015) published that DBN degradation is calpain mediated during cytotoxicity with NMDA.

Pulse-chase experiments in which MG132 was applied during the chase resulted in a change in the turnover of DBN. As shown in Figure 19, DBN was stabilized when the proteasome was inhibited during the 24 and 48 h chases. Quantification of 2 independent experiments was performed and relative protein abundances for DBN-wild-type and DBNS647A are plotted in the bar plot of Figure 19. These analysis show that both isoforms are stabilized when the proteasome is inhibited, suggesting a degradation via UPS.

In order to further investigate the degradation of DBN, ubiquitin assays for DBN were performed in collaboration with Dr. Patricia Kreis (Postdoc in the Eickholt lab). The results support the idea that DBN is degraded, at least partially, via UPS (these experiments are not reported in this thesis).

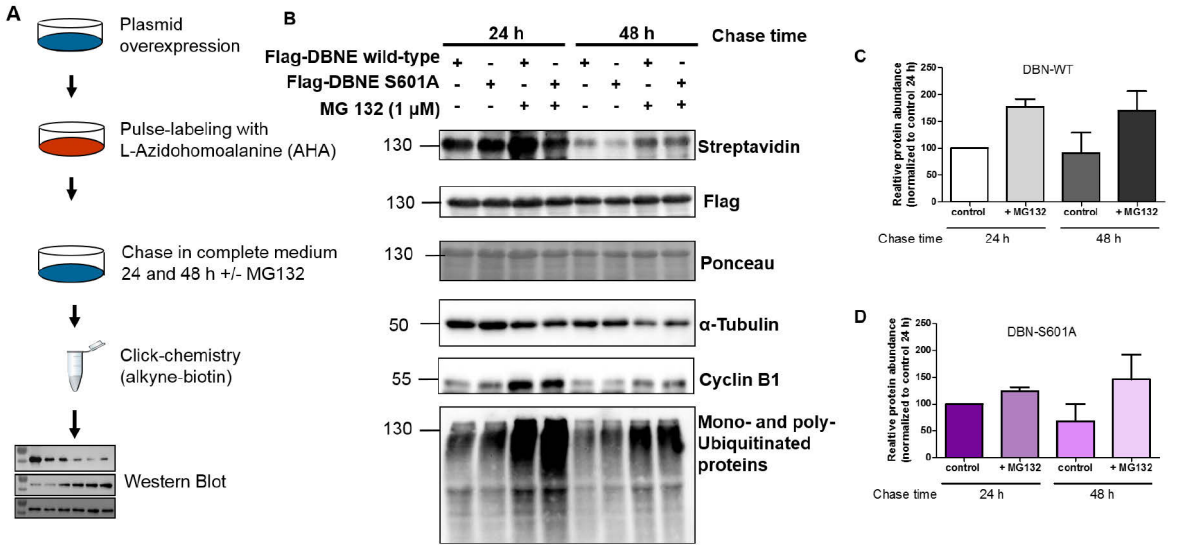

Figure 19| DBN degradation is proteasome dependent. A) HEK293T cells were transfected 24 h after platting with DBNWT-Flag, DBNS601A-Flag or Flag. 24 h after transfection, cells were methionine starved for a period of 1 h followed by a pulse-labeling with AHA for 1 h and chase in complete medium for 24 or 72 h in the absence (control) or presence of 1 µM MG132. B) Cell lysates were collected and used for click-chemistry (alkyne-biotin). Samples were analyzed by western blotting using streptavidin-HRP and the specified antibodies. C) Western blot quantification representing two independent experiments of streptavidin normalized first to loading control (α-tubulin) and 24 h chase DBN-WT control, which equals maximum labelling. D) Western blot quantification representing two independent experiments of streptavidin normalized first to loading control (α-tubulin) and 24 h chase DBN-S601 control, which equals maximum labelling. Data from two independent experiments is shown.

2.2.3 Studying DBN turnover in neurons.

We asked how DBN abundance is regulated. To answer this question, we studied DBN turnover in pulse-chase experiments. These experiments suggest that DBN is a long lived protein with an estimated half-live of 3 days. Moreover, we were able to show that the stability of DBN is controlled by the phosphorylation of S647 (S601), located at the C-terminus of the protein. To further confirm these results we searched for an experimental approach that could allow us studying DBN turnover at the endogenous level in neurons. We collaborated with Prof. Dr. Erin Schuman (Max Planck Institute for Brain Research, Frankfurt am Main) to perform FUNCAT-PLA (Fluorescence Non-Canonical Amino acid Tagging- Proximity Ligation Assay) in neurons in order to get more insight into DBN stability in neurons. In this section the results for these analyses are presented.

2.2.3.1 Visualization of de novo synthesized proteins in vitro with FUNCAT-PLA in neurons

FUNCAT-PLA (Tom Dieck et al., 2015) combines two different techniques – FUNCAT: Fluorescence non-canonical amino acid tagging (Dieterich et al., 2010) and PLA: proximity ligation assay (Söderberg et al., 2006). Combined they help to visualize the synthesis of specific proteins at the single molecule level in fixed cells. FUNCAT is a method that allows the visualization of newly synthesized proteins after metabolic labeling with AHA. This assay was introduced by Schuman and collaborators (Dieterich et al., 2010).

Using FUNCAT-PLA, the abundance and localization of newly synthesized individual proteins can be quantified. In addition, it can be combined with variable chase periods, making it possible to study the turnover of specific proteins. Our focus is on DBN; therefore I applied FUNCAT-PLA to study the spatial-temporal localization of newly synthesized DBN in neurons (Figure 22). As exemplified in Figure 20, Click-chemistry is performed on fixed cells, covalently linking the newly synthesized AHA bearing proteins to biotin. The nascent proteins can later be detected using a fluorophore–coupled antibody against biotin. PLA, which traditionally has been used for the visualization of individual protein-protein interactions by proximity ligation at various subcellular structures, can be used to label specific proteins that have incorporated AHA during a pulse of 2 h. This is achieved, using the anti-biotin antibody in combination with an antibody against the protein of interest (e.g. anti-DBN).

The diagram in Figure 20 shows the seven general steps of the protocol:

1. Pulse-labeling with AHA.
2. Click-chemistry (alkyne-biotin).
3. Incubation with primary antibodies (E.g. DBN and Biotin).
4. Incubation with PLA probes (anti-mouse- and anti-rabbit+).
5. Ligation.
6. Rolling circular replication.
7. Microscopy imaging for detection of red fluorescent signal.

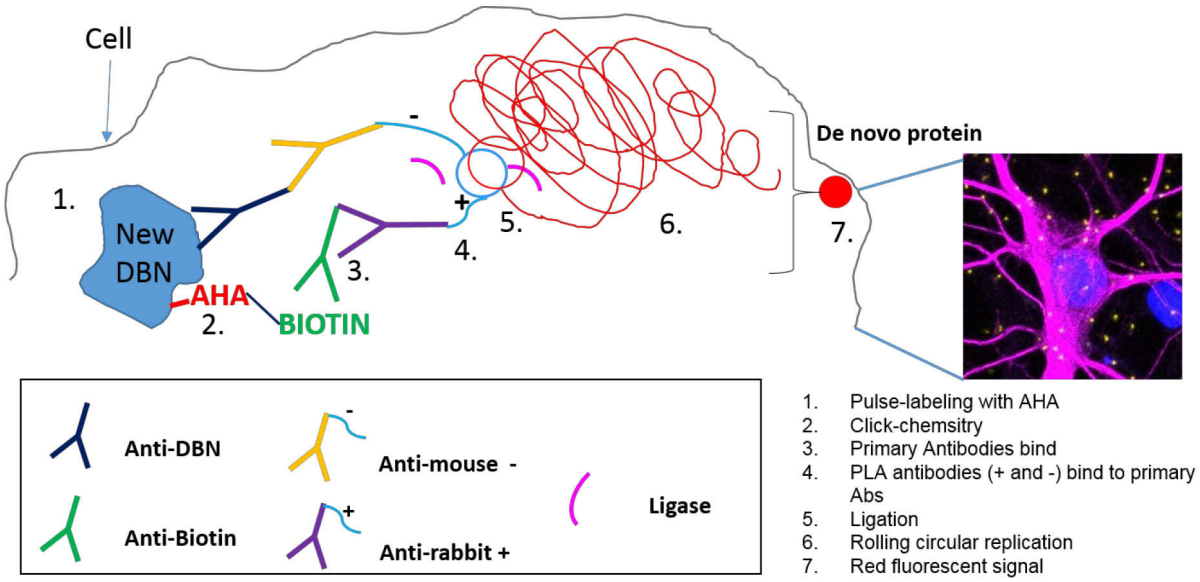

Figure 20| FUNCAT-PLA Scheme. This scheme shows the principle behind the technique that was applied for the direct visualization of DBN in neurons. Using metabolic labeling, cells were pulse-labeled with the non-canonical amino acid AHA (1). AHA intercalates into newly synthesized proteins instead of methionine labeling nascent proteins. Click-chemistry for alkyne-biotin cycloaddition is then performed on the fixed cells, covalently linking the newly synthesized AHA bearing proteins to biotin (2). Anti-DBN (mouse) and anti-biotin (rabbit) antibodies are applied (3), followed by the incubation with the anti-mouse MINUS and the anti-rabbit PLUS PLA probes (4) Secondary antibodies coupled to a short and unique oligonucleotide sequence. Upon close proximity (<40nm) the PLA probes will come together in a ligation step (5). This interaction between the two DNA strands can then be amplified by performing a rolling circular replication in the presence of a polymerase and fluorescent-coupled deoxyribonucleotides (6). In the end the signal is observed as red puncta representing the novo protein synthesis (7).

2.2.3.2 Development of automatic FUNCAT-PLA analysis

For quantitative evaluations of PLA signal systematic analyses of multiple confocal microscope images became apparent. Therefore, we developed a JAVA program for the quantitative analysis of the PLA signal in confocal images, in a semi-automated way. This program was developed under my supervision with Viktor Dinkel, which formed essential part of his BSc project (thesis advisor: Prof. Raul Rojas, Department of Mathematics and Computer Science, Freie Universität Berlin).

The original sequence for the analysis of the PLA distribution in cells was created by Lisa Kochen (Department of Synaptic Plasticity, Max Planck Institute for Brain Research). Using her sequence, we further optimized the analysis in order to increase its rigor. We developed a systematic approach for quantifying our results. The program is optimized to process multiple images from a given folder with an approximate processing time of 10-20 seconds per image. At the end of the analysis, the program provides a summary report for individual images that includes the following data:

a. Raw image file.

b. Images for individual channels.

c. Mask for cell volume marker (e.g.MAP2, tyr-tub or GFP).

d. Values for the thresholds used. Thresholds can be chosen automatically or can be set manually.

e. Values for total area occupied by the cell volume marker (e.g. MAP2 in neurons).

f. Number of PLA puncta for each image and total area occupied.

g. Fluorescent intensity for PLA signal.

The image is further filtered to exclude puncta that are either non-overlapping with the cell volume marker, or are in close proximity (< 1 μm) to cover the area of the dendritic spines that are not label by MAP2. Finally, the ratio of the specific PLA signal area over the cell volume marker area are calculated and presented as a percentage of total cell area. This pipeline of image processing and data acquisition is repeated for individual images. The analysis is performed on maximal projections for one group of images with the same experimental condition and contains a summary table with the values for the thresholds used, the total number of images analyzed, the mean values for PLA and MAP2 areas, as well as the PLA/MAP2 mean ratio (as a percentage) for the group of images analyzed. In addition, the summary report allows us to return to the previous step during the evaluation process, for each image. All images, including masks, are individually stored for manual control in the analyses folder, if needed. An example of a summary report is presented in Figure 21.

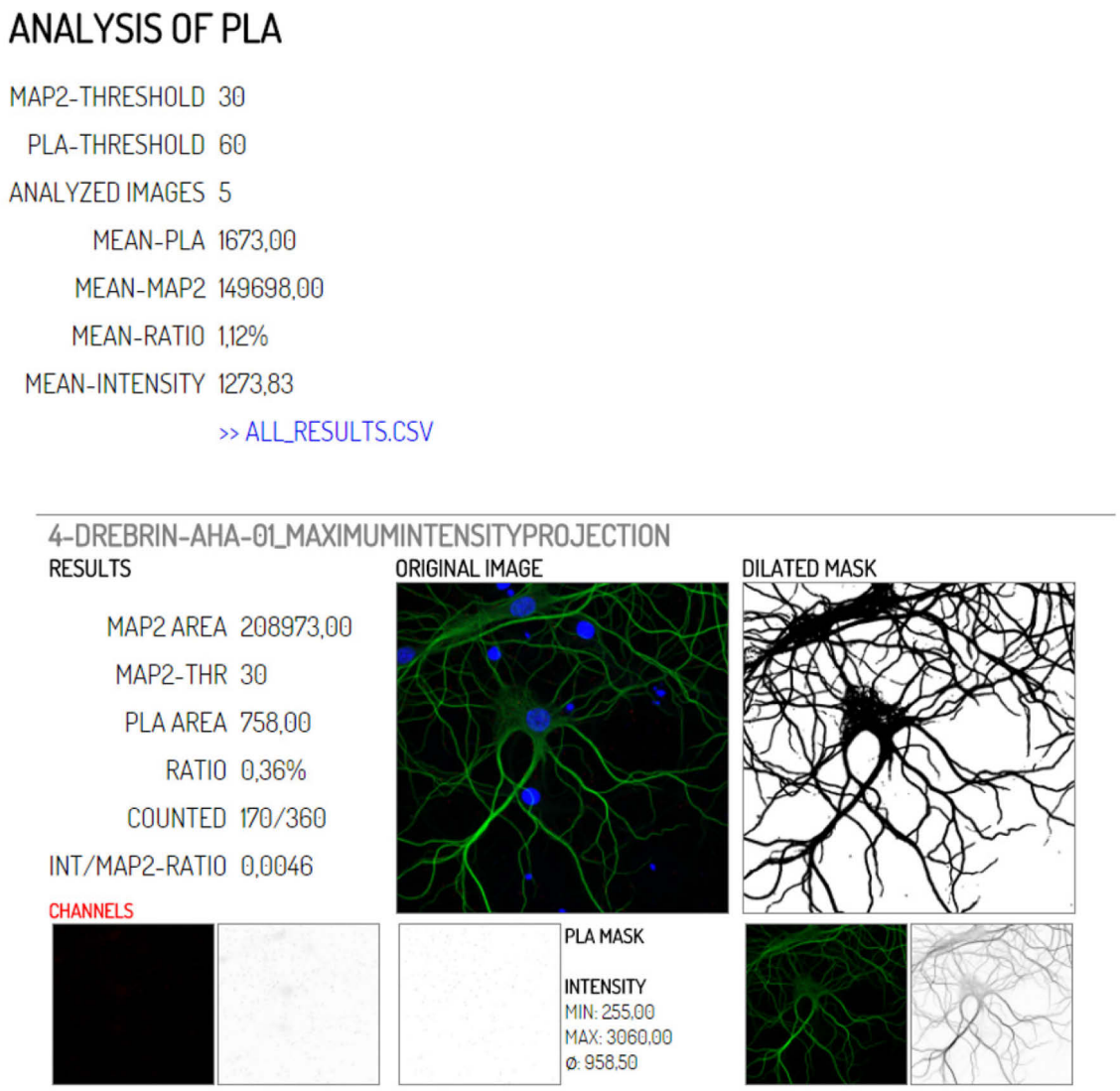

Figure 21| Report for PLA analysis of confocal images. The report for a folder containing multiple images includes the complete analysis of the group, and also provides individual results for each image, as shown in this figure. The top panel is the report for the entire group, which in this case contains 5 images. The next panel is an example for one image, where the original image, the image for the MAP2 mask (cell volume marker) and the splitting of the channels is included. The report also contains the quantification for the total area occupied by MAP2 and by the number of puncta that have been counted. It gives the ratio PLA area over MAP2 area as a percentage, and shows the total number of puncta, both filtered and total. The blue letters are a link to an Excel file containing the quantification for all the images, where the complete data is organized in a table facilitating data analyses.

2.2.3.3 Visualization of *de novo* synthesized DBN *in situ* with FUNCAT-PLA in neurons

DBN overexpression studies in HEK293T cells revealed that DBN stability is phosphorylation (S601) dependent. However, I wanted to know whether this also holds true for endogenous DBN in neurons. To study the turnover of DBN in neurons, I performed pulse-chase experiments with FUNCAT-PLA for DBN.

To do so, rat hippocampal dissociated neurons (18-20 DIV) were pulsed-label with AHA for 2 h and chased for 15 min before fixation, as indicated in the schematic representation (Figure 22). PLA for biotin and DBN was followed on the fixed cells after click-chemistry. To evaluate the specificity of the labeling, two negative controls were prepared: a methionine control (met), whereby the complete medium contains methionine but no AHA, and an anisomycin control (aniso) where protein synthesis was blocked. Finally, staining of MAP2, a neuronal somato-dendritic marker was applied.

These experiments indicated that the DBN pool, labeled for 2 h with AHA, is present both in soma and dendrite and that this signal is specific (Figure 22). The specificity was confirmed by quantitative analyses of the two control conditions: Met or AHA-aniso and compared to AHA. The signal in Met and AHA-aniso is 80 fold lower therefore considered as a background signal. These experiments were the bases for performing pulse-chase experiments applying FUNCAT-PLA for studying DBN turnover in neurons.

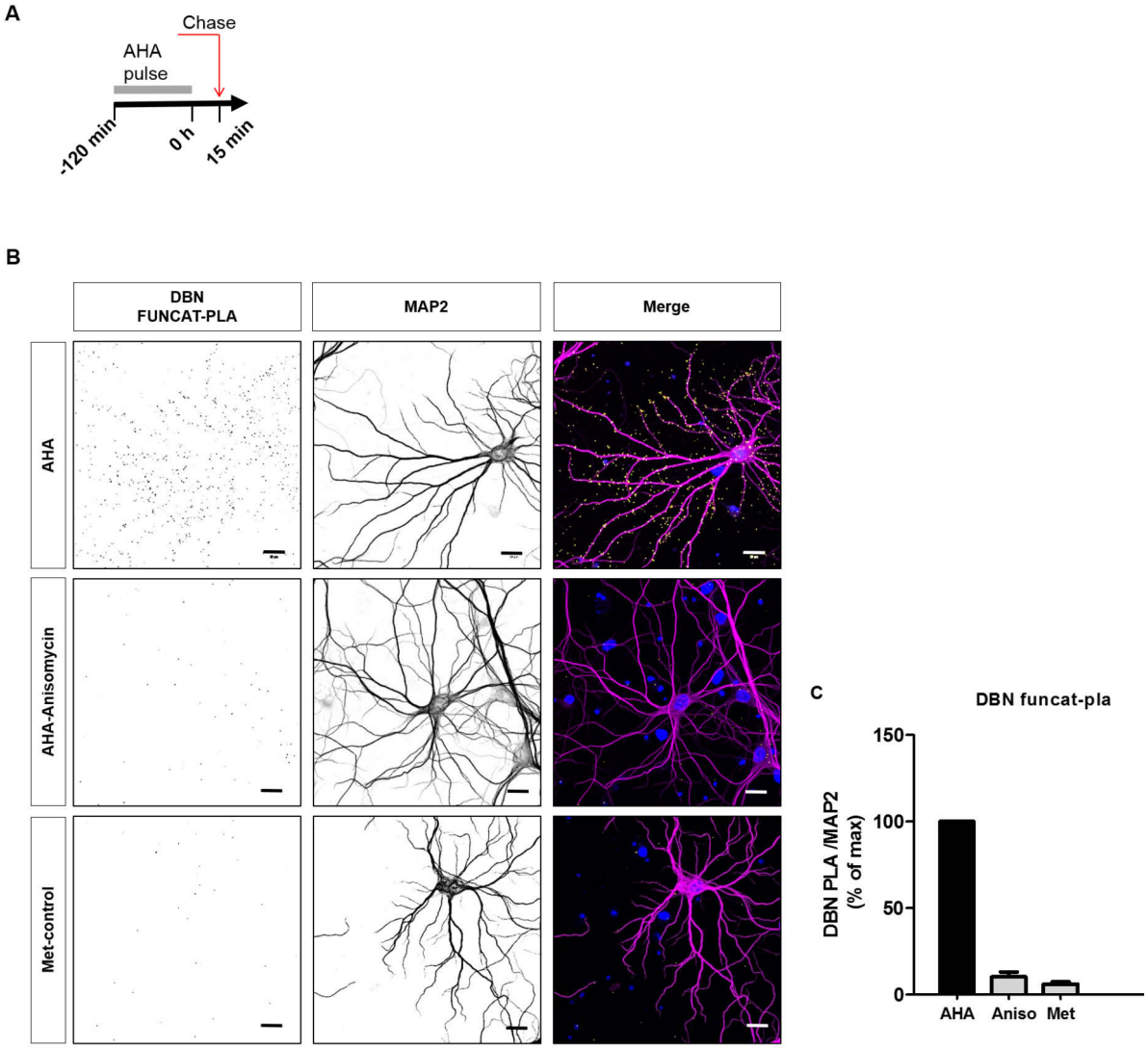

Figure 22| FUNCAT-PLA for visualization of DBN synthesis in situ. A) 18-20 DIV primary neurons were pulse-labelled for 2 h with AHA and were fixed after a 15 min chase in complete conditioned medium. B) To follow DBN synthesis in situ click-chemistry (alkyne-biotin cycloadition) and PLA using antibodies against DBN and Biotin was performed on the fixed neurons. This was performed for the three FUNCAT-PLA control conditions: AHA-control, Met-control and AHA-anisomycin. MAP2 is shown in magenta, PLA in yellow and DAPI in blue. C) Quantification of the PLA signal after MAP2 normalization as percentage of AHA-control (error bars indicate SEM from three independent experiments. Images were modified for visualization purposes. Scale bar: 20µm

2.2.3.4 DBN turnover and pS647-DBN kinetics in rat hippocampal neurons

I performed pulse-chase and FUNCAT-PLA experiments in rat hippocampal neurons with the objective of studying DBN turnover in neurons. The degradation of DBN was followed for 24 h and 68 h after pulse-labeling as shown in the schematic representation in Figure 23. Representative images of the experiments for 0 h, 24 h and 68 h chase are displayed on Figure 23. Quantification of these images from three independent pulse-chase experiments shown in Figure 23-C indicate that approximately 50% of the DBN protein is degraded after ~70 h, while no degradation occurs during the first 24 h. This is in line with my previous experiments performed in the lab using biochemical assays, which determined the half-life of DBN to be 75 ± 8 h in pulse-chase experiments.

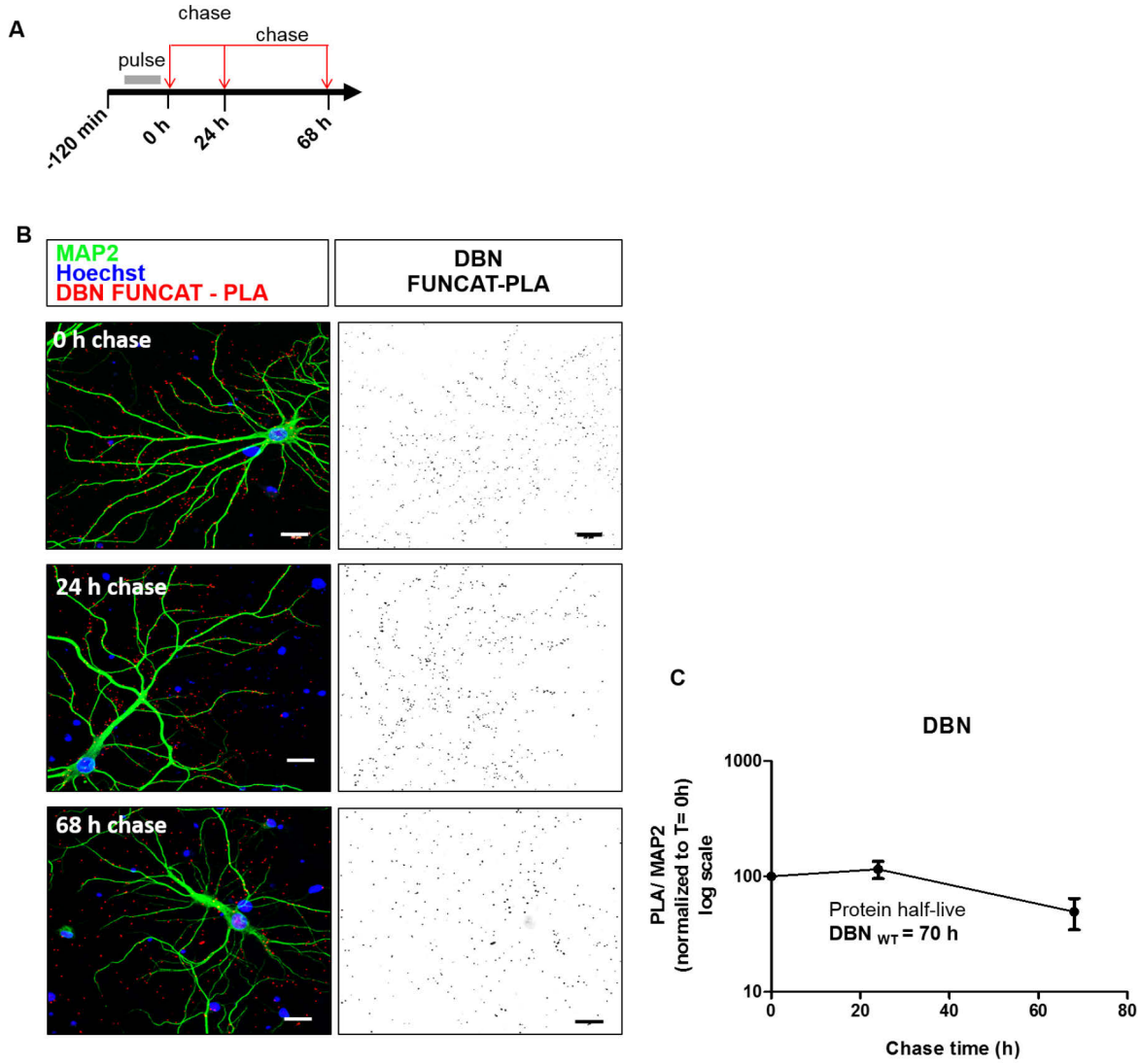

Figure 23| Pulse-chase experiments with FUNCAT-PLA to follow the spatio-temporal pattern of de novo synthesized DBN A) 18-20 DIV primary neurons were pulse-labelled with AHA for 2 h and fixed after 0, 24 or 68 h chase in complete conditioned medium. B) To follow the spatio-temporal patterns for newly synthesized DBN click-chemistry (alkyne-biotin) and PLA using antibodies against DBN and Biotin was performed on the fixed neurons. These was performed for the three FUNCAT-PLA control conditions: AHA-control, Met-control or AHA-anisomycin. (MAP2 is shown in green, PLA in red and DAPI in blue. C) Quantification of the PLA signal after MAP2 normalization as percentage of AHA-control (error bars indicate SEM of three independent experiments). Images were modified for visualization purposes. Protein half-live was calculated assuming an exponential decay degradation. Scale bar: 20 µm.

2.2.4 Deciphering DBN translation control and localization *in sit*u in neurons

It has become clear that several synaptic proteins are locally translated in dendrites and synapses (Tom Dieck et al., 2014). Moreover, polyribosomes have been identified in the dendritic shafts and spines, which suggests a role of local protein synthesis in the regulation of synapses (Ostroff et al., 2002). Furthermore, it has been proposed that synaptic plasticity requires synthesis of proteins and that this occurs locally for the long-term synaptic plasticity underlying memory formation (Tom Dieck et al., 2014 and Santini et al., 2014). These results together with others reported in the literature lead us to the next question. How is DBN translation controlled in neurons and where are DBN transcripts localized? Therefore, it became relevant to study whether DBN is synthesized locally or if it is transported to the dendrites. To address these questions, I made use of two technologies. Firstly, I applied metabolic labeling with puromycin in combination with PLA (Puro-PLA) for the investigation of DBN translation control. These experiments are described in section 2.2.4.1. And secondly, I performed high-resolution fluorescence in situ hybridization (FISH) for the visualization of DBN mRNA transcripts as shown in section 3.

2.2.4.1 Visualization of *in situ* DBN translation in neurons applying metabolic labeling with puromycin in combination of the proximity ligation assay.

Puromycin is an antibiotic that acts as a protein synthesis inhibitor by truncating the nascent chain of a peptide. It is also structurally an aminoacyl tRNAs analog (see Figure 24) and can be used for metabolic labeling of translated proteins. It has been used successfully as a nonradioactive method to measure protein synthesis rates (Schmidt et al., 2009), as well as to visualize de novo proteins in situ in combination of PLA as reported in and named Puro-PLA (Tom Dieck et al., 2015).

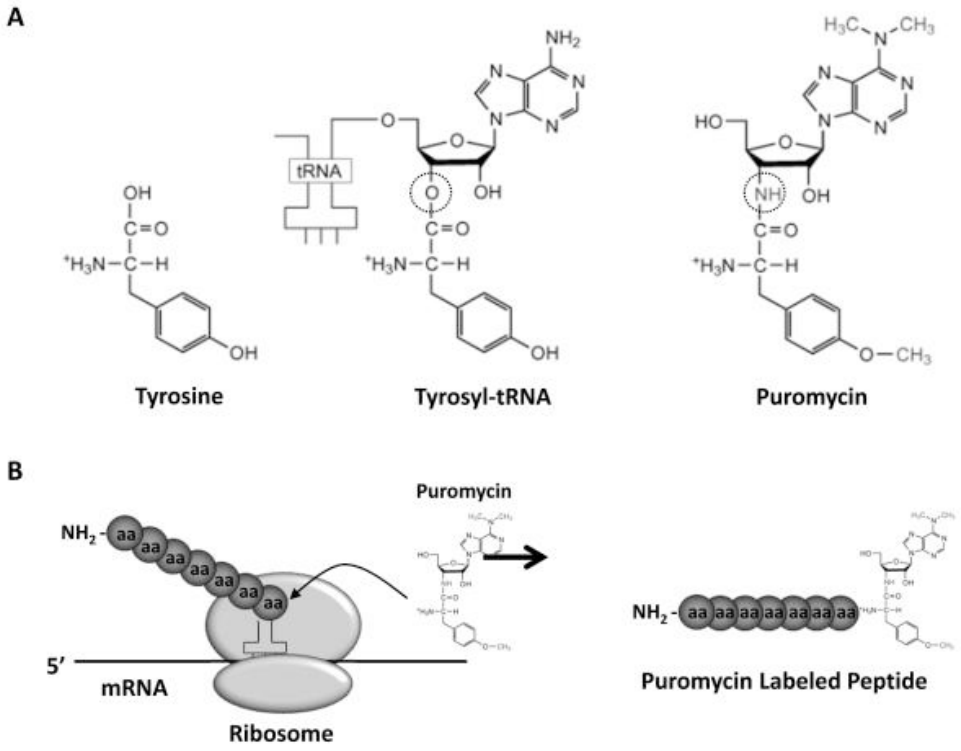

Figure 24| Metabolic labeling with puromycin. A) Chemical structures of the amino acid tyrosine, the tRNA Tyrosyl and the protein synthesis inhibitor puromycin. Puromycin is a tRNA analog and can covalently bind into nascent peptide chains. B) Schematic representation of the process of protein synthesis in the presence of puromycin which inhibits the process of synthesis inducing the release of the synthesized peptide when binding to the nascent chain. (Figure adapted from Goodman and Hornberger (2015).

In addition to studying the turnover of DBN in neurons, I also explored the localization of newly synthesized DBN. To do so, I visualized newly synthesized DBN combining puromycilation applying Puro-PLA in neurons.

For this, cells are briefly treated with puromycin to label proteins in the process of translation, then PLA for DBN and puromycin is performed. Finally, microscopy imaging is used to capture multiple images for the analyses of PLA (see Figure 25 for diagram). The resulting signal provides a quantitative read-out for DBN synthesis rates as well a quantitative result for the localization of the protein synthesis in the cell.

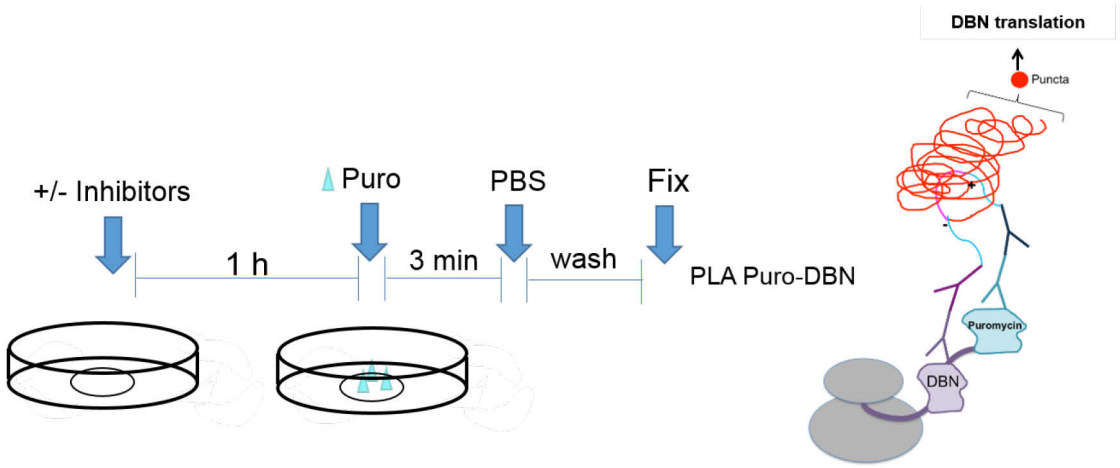

Figure 25| Puro-PLA. N1E cells or primary mouse neurons are treated with different inhibitors for 1 h followed by a 3 min incubation with 1 µM puromycin with or without the respective inhibitors. Cells are fixed and PLA with antibodies against puromycin and DBN is performed.

These experiments demonstrate than a pool of DBN is translated in dendrites and spines, implying that DBN is locally translated in dendritic shafts. This can be observed in the upper panel of Figure 26. The arrow indicates *de novo* synthesized DBN puncta found in dendrites. This observation is in line with the previously shown distribution of DBN detected in neurons when applying FUNCAT-PLA (see Figure 22). In contrast to FUNCAT-PLA where pulse-labeling with AHA was performed for 2 h, allowing enough time for protein transport, in Puro-PLA the pulses with Puro were performed for only 3 min, excluding long-range protein transport. However, short-range protein diffusion cannot be completely excluded during the delay between labelling and fixation. Nevertheless, to further confirm this observation I explored the localization of DBN transcripts in neurons as shown in the last section of results.

To evaluate the specificity of the labeling, two negative controls for the Puro-PLA assay were included: anisomycin to block protein synthesis with a pre-treatment of 30 min and a condition without puromycin. As shown in Figure 26 , no signal comparable to the control can be detected, proving the specificity of the antibodies in this assay and the specificity of the puromycin labeling.

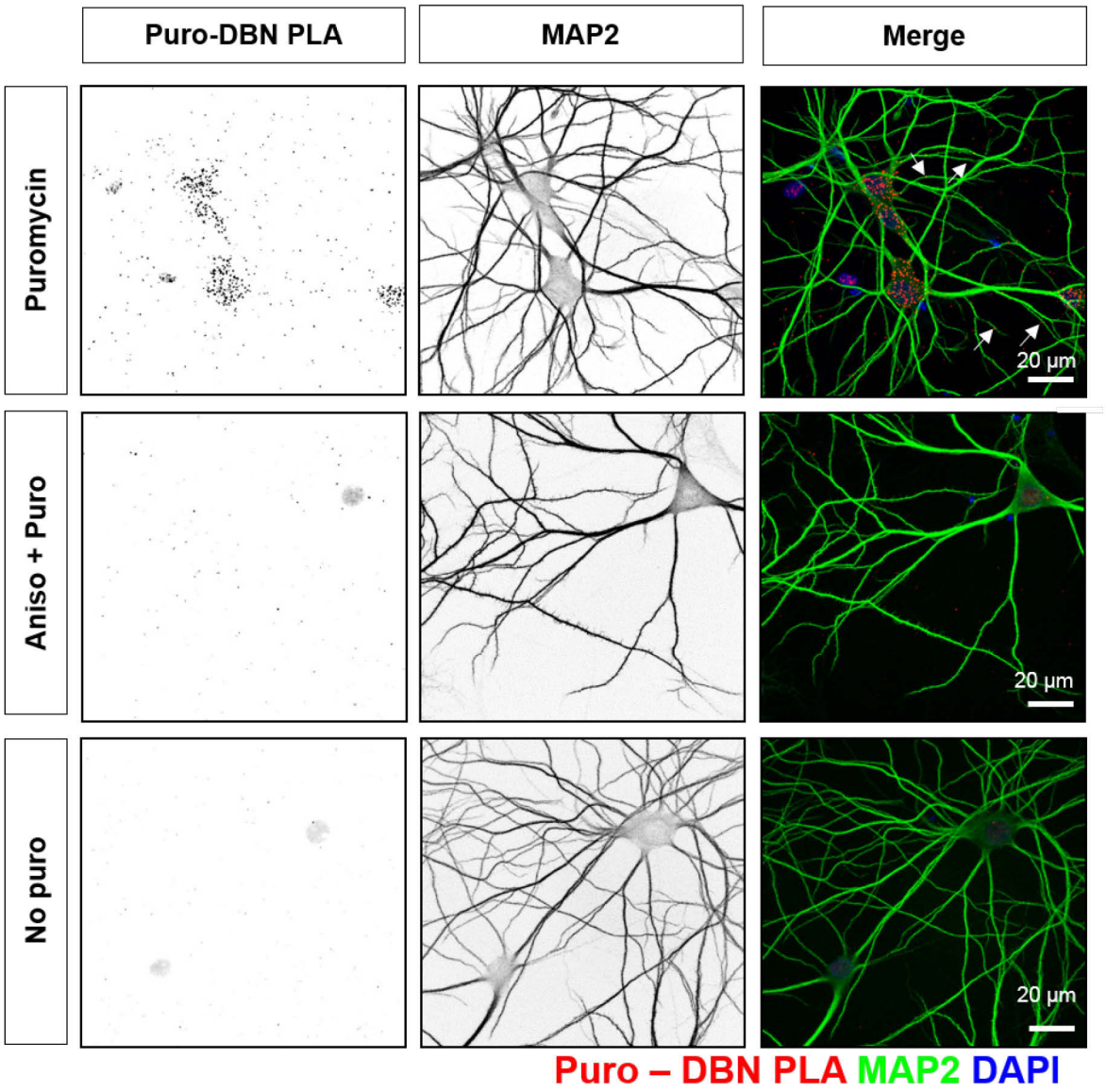

Figure 26| DBN is locally synthesized. Cultured hippocampal neurons from E16.5 mice were grown for 14 DIV and incubated for 3 min with 1 µM puromycin, washed and fixed. PLA with antibodies against puromycin and DBN was then performed on the fixed cells. Puromycin (puro) shows DBN synthesis in situ and anisomycin (aniso + puro) or No puromycin (no puro) are negative controls. Arrows in top right image indicate PLA signal found in distal dendrites. Scale bar: 20 µm.

2.2.4.2 DBN protein synthesis is affected by the PI3K-mTOR pathway

One of the main objectives of this thesis was to find regulatory inputs for the turnover of DBN. Therefore, I wanted to explore whether the Phosphatidylinositol 3-kinase – mammalian target of rapamycin (PI3K-mTOR) pathway (see Figure 27 for schematic representation) plays a role in the regulation of DBN translation. The PI3K-mTOR pathway is known to control the translation of some proteins, therefore we explored whether DBN was one of those.

The PI3K pathway controls essential processes of the cell such as cell proliferation and cell growth. PTEN antagonizes this pathway while PI3K activates it. In neurons, the kinase activity of mTOR is involved in translation regulation and long-lasting synaptic plasticity. The PI3K pathway starts with the activation of PI3 kinase which occurs after growth factor stimulation. Phosphoinositol-3-Kinase (PI3K) catalyzes the conversion of phosphatidylinositol 4-5 diphosphate (PIP2) into phosphatidylinositol 3,4,5 triphosphate (PIP3). This reaction is antagonized by phosphatase and tensin homolog (PTEN). PIP3 activates Protein kinase B (AKT) which subsequently can activate the mammalian target of rapamycin (mTOR). mTOR activates ribosomal protein S6 kinase beta-1 (S6K1), this activation has an effect in protein synthesis. 4EBP, in contrast, if activated has a translation repression activity. A schematic representation of a simplified version of this pathway as well as the target proteins for some inhibitors of the pathway are shown in Figure 27.

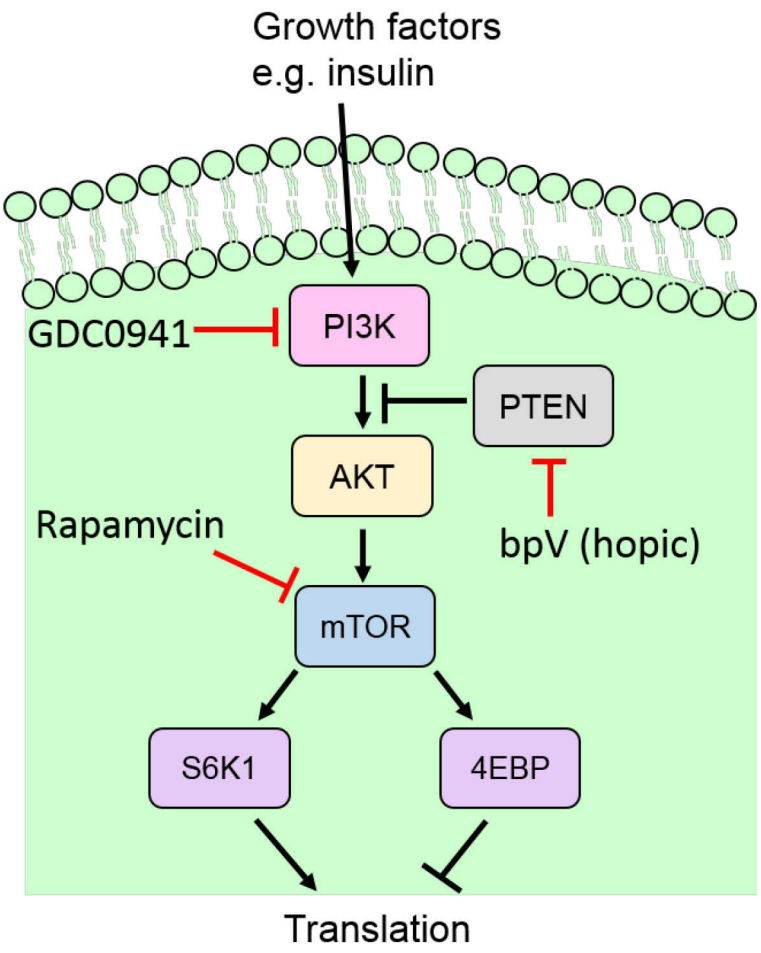

Figure 27| Simplified schematic representation of the PI3K-mTOR pathway. Phosphoinositol-3-Kinase (PI3K), Protein kinase B (AKT), phosphatase and tensin homolog (PTEN) mammalian target of rapamycin (mTOR), ribosomal protein S6 kinase beta-1 (S6K1). Inhibitors for PI3K, PTEN and mTOR are indicated in the pathway.

In order to gain insights into the regulation of DBN translation in dependence of the PI3K-mTOR pathway, I first tested the mTOR inhibitor rapamycin, the PI3K inhibitor GDC0941 and the PTEN inhibitor bpV(hopic) in cells and analyzed their activity by western blotting (Figure 28). Inhibition of mTOR with rapamycin resulted in the reduction of downstream pS6 levels, inhibition of PI3K decreased the levels of pS473AKT and inhibition of PTEN with increased pS6 levels. These results proved that all inhibitors were working and acting as anticipated in this cellular model.

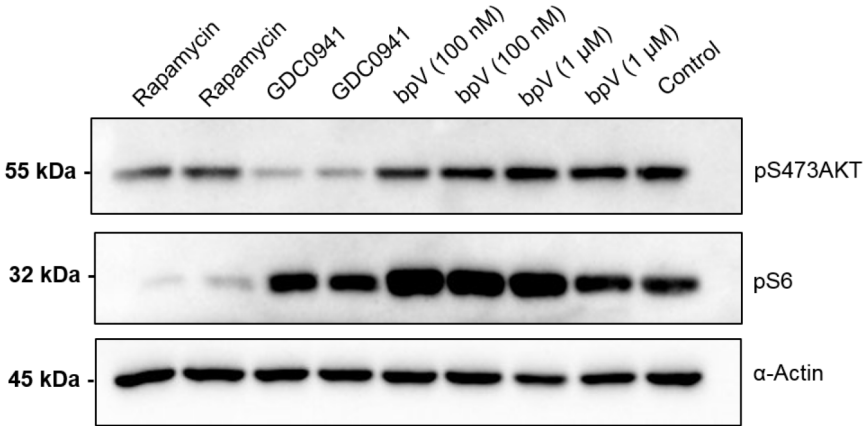

Figure 28| Different inhibitors induce inhibition or over-activation of the PI3K-mTOR pathway. N1E cells were treated for 1 h with 100 nM rapamycin, 0.25 µM GDC0941, 100 nM or 1 µM bpV (hopic) in duplicates or DMSO as a control. Cell lysates were collected and analyzed by western blotting to evaluate the inhibitors activity using AKT-pS473, pS6 and α-actin as a loading control.

The next step was to control for the efficiency of puromycin in western blot and to confirm that the presence of puromycin does not affect the activity of the tested inhibitors. To do so, puromycilation for 5 min was analyzed by western blotting. A schematic representation of the experimental design is depicted in Figure 29.

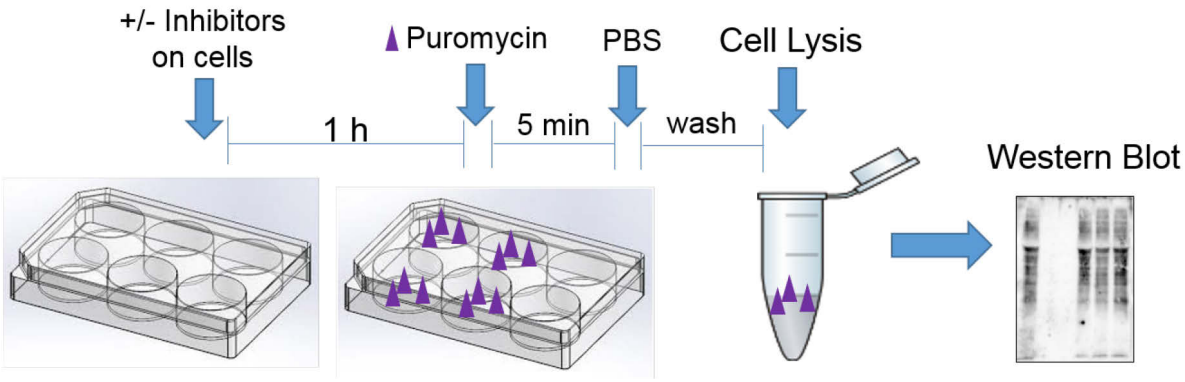

Figure 29| Puromycilation protocol. A) N1E cells are treated with different inhibitors for 1 h followed by a 5 min incubation with 4 µM puromycin with or without the respective inhibitors. Cells are lysed and lysates are analyzed by western blotting. To detect puromycilation a puromycin antibody is applied in Western blots.

Results on Figure 30-A show a reduction on pS6 upon treatments with rapamycin, an increase in pS6 after PTEN inhibition and a reduction of pS473 after PI3K inhibition.

These results prove that co-treatment with puromycin does not interfere with the activity of the applied inhibitors. In parallel, in Figure 30-B, it can be observed that puromycin efficiently labeled newly synthesized proteins and that this labeling can be completely abolished with a pre-treatment with anisomycin (aniso) to block protein synthesis. Additionally, absence of puromycin (no-puro) does not provide any signal, confirming the specificity and efficiency of the labeling of *de novo* synthesized proteins in N1E cells without detectable background.

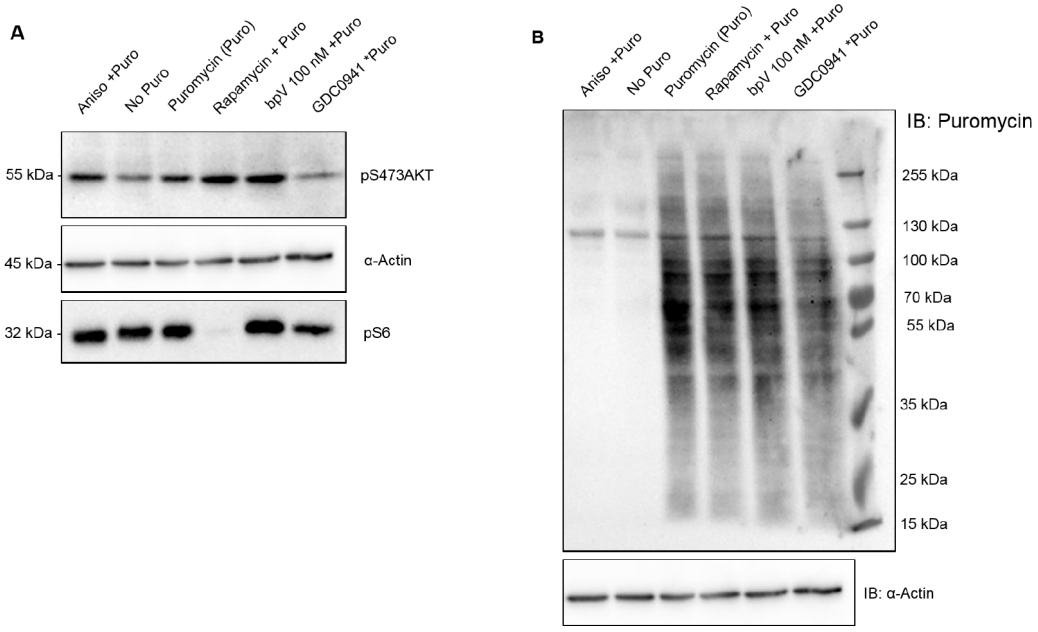

Figure 30| Controls for PI3K-mTOR pathway inhibitors in combination of puromycin. A) In order to confirm that our different inhibitors are active in combination of puromycin, N1E cells were grown in DMEM 1 % FCS for 24 h and then treated for 1 h with 40 µM anisomycin, 100 nM rapamycin, 0.25 µM GDC0941,100 nM or 1 µM bpV (hopic), or DMSO as a control and directly incubated for 5 min with 4 µM Puromycin +/- inhibitors. Cells were washed with PBS and cell lysates were collected and analysed by western blotting to evaluate the activity of the inhibitors in the presence of puromycin; a tRNA analog that causes protein truncation, probing for AKT-pS473, pS6 and α-actin as a loading control. In line with what is reported in the literature, pS6 levels are massively reduced when rapamycin is applied and in contrast increased when PTEN is inhibited with bpV, pS473AKT levels are downregulated when PI3K inhibitor GDC0941 is applied and anisomycin blocks protein synthesis. B) Samples were analyzed using a Puromycin antibody to detect the total newly synthesized proteins or the puromycilated fraction and α-actin as a loading control. Importantly, the respective inhibitors do not seem to affect global protein synthesis while we observe that some of them affect DBN protein synthesis specifically in our Puro-PLA experiments.

To further investigate the potential role of the PI3K-mTOR pathway in the regulation of DBN translation, I performed PURO-PLA experiments in combination with acute inhibitions of PTEN, PI3K or mTOR. Quantification of the PLA signal for all the different conditions proves that the inhibition of PTEN and PI3K do not affect the translation rate of DBN in comparison to the control. However, inhibition of mTOR significantly reduces DBN synthesis in N1E cells. These results are shown in Figure 31.

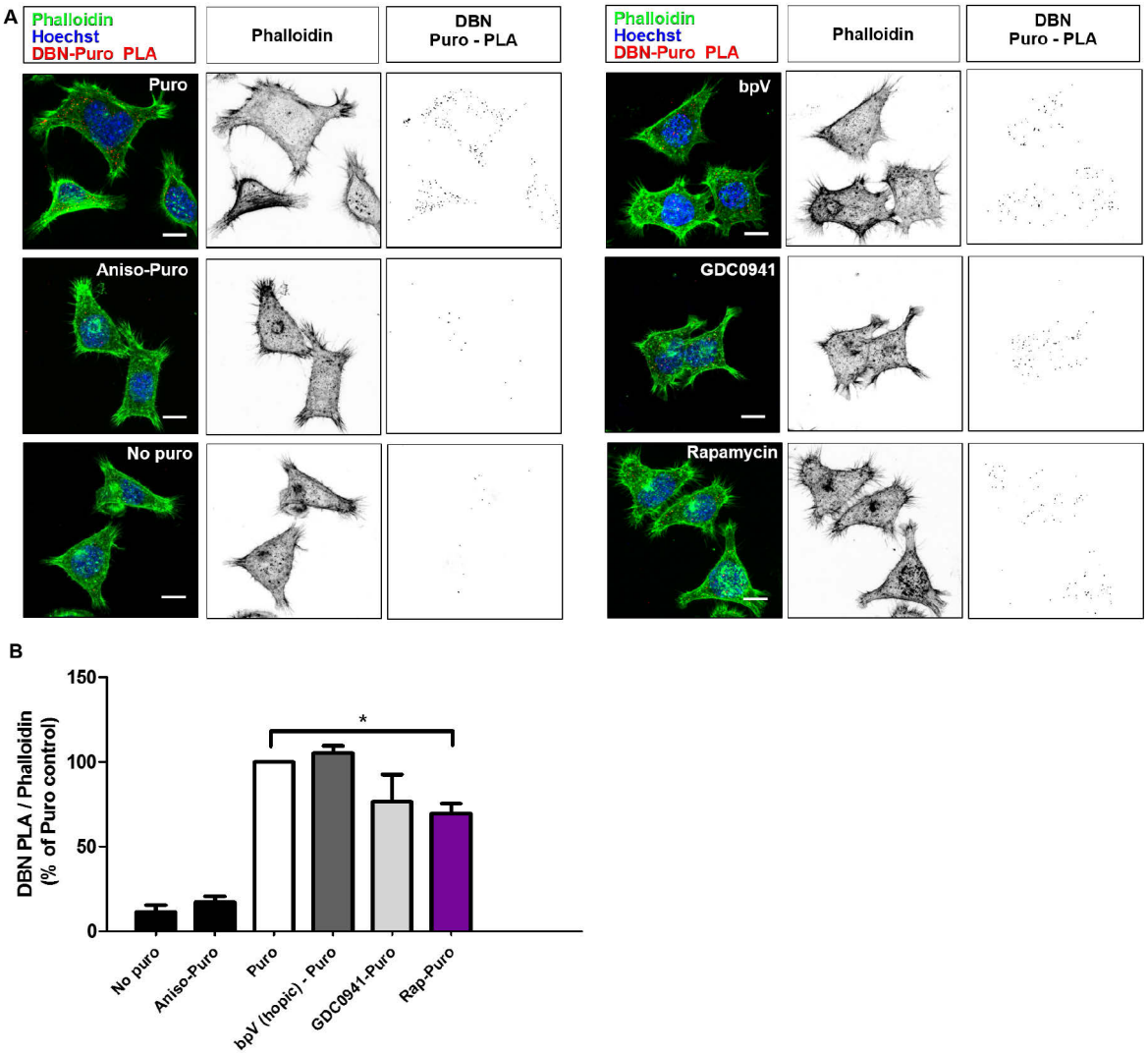

Figure 31| Treatment with rapamycin reduces DBN translation. A) N1E cells were grown in DMEM 1% FCS for 24 h and then treated for 1 h with 100 nM rapamycin, 0.25 µM GDC0941,100 nM or 1 µM bpV (hopic), 4 µM anisomycin, or DMSO as a control and directly incubated for 3 min with 1 µM Puromycin +/- inhibitors or without puromycin. Cells were washed and directly fixed. PLA with antibodies against puromycin and DBN was then performed on the fixed cells. B) DBN Puro-PLA quantification. (Error bars indicate SEM of three independent experiments and * pValue< 0.01). Scale bar: 10 µm.

2.3 Visualization of DBN mRNA in neurons and abundance upon neuronal stimulation

2.3.1 DBN mRNA transcripts are present in dendrites.

Experiment performed in neurons applying FUNCAT-PLA and Puro-PLA show that de novo synthesized DBN is present in dendrites and spines. This observation suggested that DBN could be a protein which local translation is needed during synaptic plasticity. To further characterize the localization of DBN translation I performed high-resolution FISH experiments for the visualization of DBN transcripts in neurons. Confocal microscopy images of these experiments show the presence of DBN mRNA in dendrites supporting the idea that DBN translation is localized (Figure 32). A negative control where no probe was added was included in the experiment and as shown in Figure 32 no signal can be detected.

A

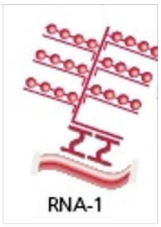

FISH: Fluorescence *in situ* hybridization (Panomics)

B

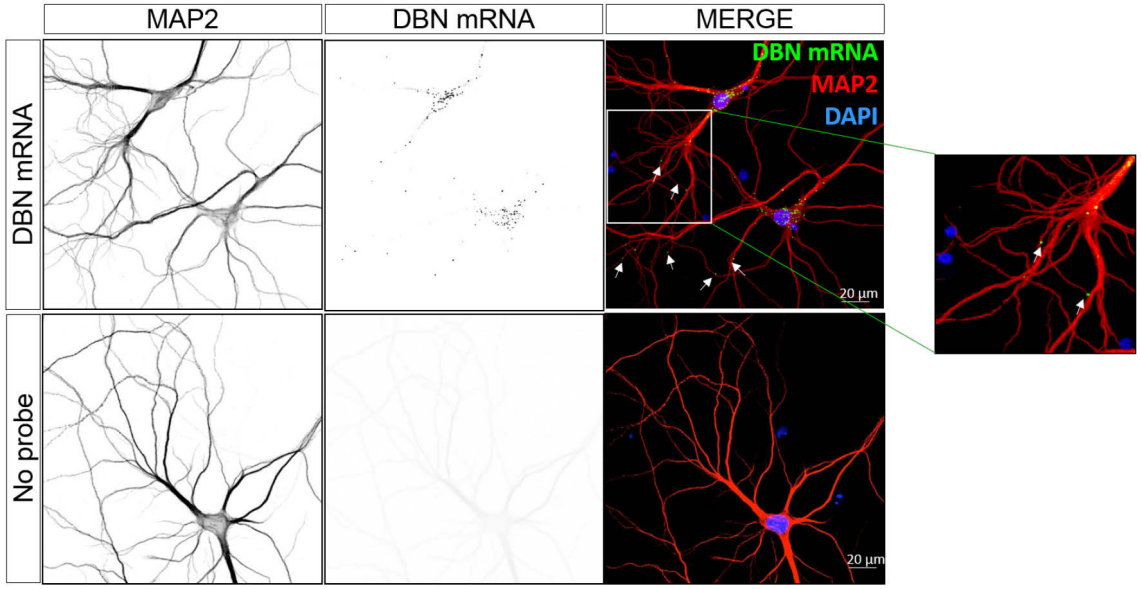

Figure 32| DBN transcripts are localized in dendrites. A) Schematic representation for the in situ hybridization amplification system for the fluorescence detection of mRNA (Panomics). B) RNA fluorescence in situ hybridization for DBN mRNA using Panomics probes. MAP2 staining was applied as a neuronal marker and DAPI as nuclear stain. Images were modified for visualization purposes. Scale bar: 20 µm

2.3.2 Visualization of DBN mRNA abundance in neurons with high-resolution FISH

Cajigas et al. 2012 reported over 2000 mRNAs to be present in the neuropil, including DBN. In addition, high-resolution FISH in cultured hippocampal neurons clearly showed the presence of diverse mRNA transcripts in dendrites and also different soma to dendrite ratios for the abundance of these (Cajigas et al., 2012). Therefore, I performed high-resolution FISH for DBN, beta-actin and CamKII. By observing representative images it is possible to compare their abundances in cultured neurons. CamKII is reported to be highly abundant in neurons, this can also be observed in my

experiments. When comparing these levels those of Beta-actin and DBN mRNA puncta it looks like they are in the lower range (Figure 33). However, more experiments should be performed for a clear conclusion on this matter.

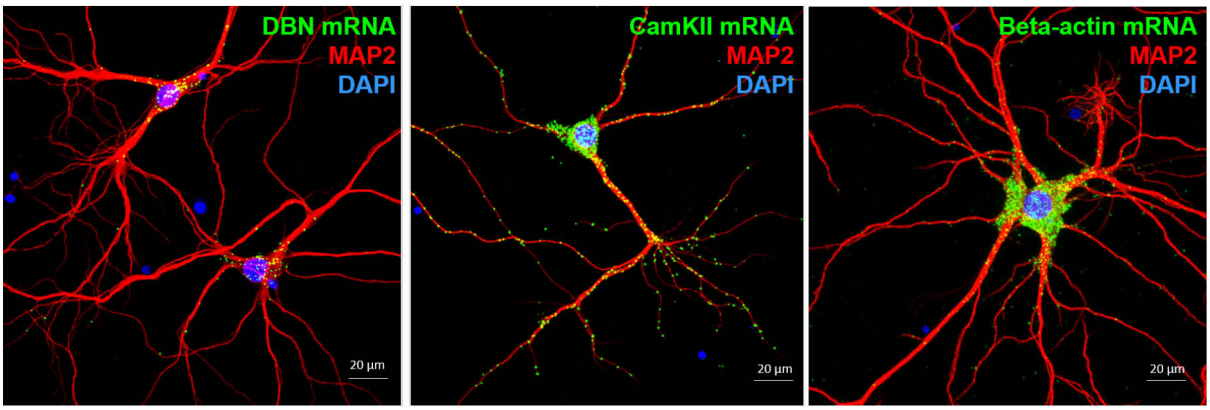

Figure 33| DBN, CamKII and Beta-actin mRNA abundance in neurons. RNA fluorescence in situ hybridization for detection of DBN mRNA (A), CamKII mRNA (B) and Beta-actin mRNA (C) was performed in primary hippocampal neurons using Panomics probes. MAP2 staining was applied as a neuronal marker and Dapi as a nuclear staining. Representative images show different transcript abundance for DBN and Beta-actin in comparison to CamKII known to be highly abundant in neurons.

2.3.3 Neuronal network silencing during homeostatic plasticity results in more DBN localized transcripts.

In order to investigate whether DBN is regulated at the transcriptional level upon synaptic activity stimulation or during homeostatic plasticity, I performed high-resolution FISH in cultured hippocampal neurons after treating 24-28 DIV neurons for 2 h with either bicuculline, TTX + APV or vehicle control. Using the PLA plugin for FIJI I quantified the total signal (Figure 34 -B), the signal in the soma (Figure 34-C) and calculated the signal in the periphery (Figure 34-D) for the different conditions. The results are shown in Figure 34. No significant differences are observed after enhancing synaptic activity with biccuculline in comparison with the control. However, silencing of the network and spontaneous activities with TTX + APV changes the total mRNA abundance of DBN. No changes are observed in the soma whereas an increase in the abundance in dendrites is evident.

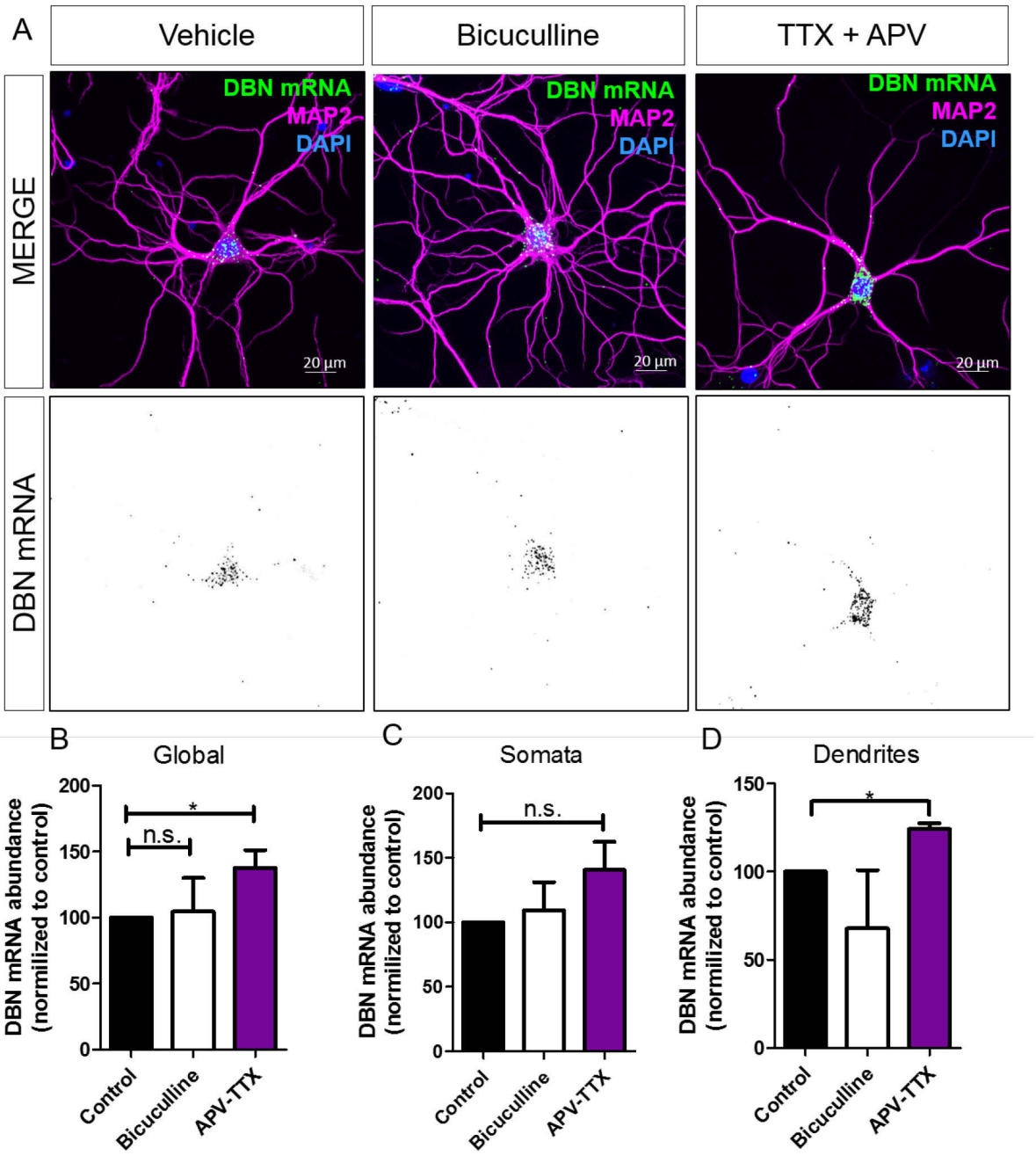

Figure 34|Neuronal network silencing results in more DBN transcripts. A) RNA fluorescence in situ hybridization for DBN mRNA using Panomics probes was performed in primary hippocampal neurons treated for 2 h with Bicuculline (30 µM), TTX (1µM) + APV (20 µM) or vehicle control. MAP2 staining was applied as a neuronal marker and DAPI as a nuclear stain. Images were modified for visualization purposes. B) Global mRNA signal was quantified after MAP2 normalization as percentage of Vehicle-control C) Signal in somata and D) Signal in dendrites.

3 Discussion

Experimental evidence in neurons for DBN overexpression (Kreis et al., 2013; Mizui et al., 2005), DBN downregulation (Takahashi et al., 2006) and complete depletion of DBN in a DBN-KO model (Jung et al., 2015) have shown that DBN levels - too high or too low - can affect spine morphology as well as synaptic function. These results suggested that DBN abundance is essential for the modulation and stability of spine morphology. Moreover loss of DBN in the brain is linked to cognitive impairment as well as Alzheimer's disease and Down's syndrome. Therefore, studying the inputs that control the turnover and stability of DBN is of great interest not only to understand how DBN is regulated but also to understand how DBN affects synaptic plasticity and how it contributes to aging.

Protein damage and oxidative stress are thought to contribute to age-related pathology. Thus, in the first section of my discussion I analyze the decrease of DBN abundance during oxidative stress conditions using oxidizing agents in neurons. The second part of the discussion is dedicated to understanding how DBN stability is regulated and how DBN is degraded.

In the last two sections I will discuss the regulation of DBN translation and the presence of DBN transcripts in dendrites.

3.1 Effect of oxidative stress on DBN abundance and its link to neurodegeneration

During aging, the entire proteome is affected by oxidative stress, however the consequences may differ from one protein to another. Considering the decrease of DBN during aging, I hypothesized that DBN may be modified by oxidative stress. To assess DBN stability during oxidative stress, I challenged matured cortical neurons with H_2O_2 and Paraquat, compounds that are commonly used to induce oxidative stress (Wang et al., 2009; Doré et al., 1999; Ramalingam and Kim, 2011) as well as Aβ the Alzheimer's disease related protein. In order to find the right experimental conditions, H_2O_2, Paraquat and Aβ were tested at different concentrations and applied in cultured cortical neurons. I observed that H_2O_2 at the tested concentrations has no effect on DBN protein levels at 14 DIV cortical neurons. Treatments with Aβ were difficult to reproduce since occasionally the effect was very toxic leading to neuronal

death. However, the herbicide paraquat reduced DBN protein levels in a 15 µM concentration with no cytotoxic effects, providing a good platform for future experiments targeting the regulation of DBN abundance during oxidative stress

Towards finding new therapeutics for the treatment of neurodegenerative diseases where neuronal loss occurs, studying the effect of reactive oxygen species during synaptic plasticity is a very common approach (Guo et al., 2015; Santini et al., 2015). Moreover, oxidative stress has been described as one characteristic in neurodegeneration (Klein and Ackerman, 2003). Therefore, having an experimental system where DBN protein levels decrease is an important readout in the context of neurodegeneration. Future studies, could clarify the molecular mechanisms behind DBN and its described downregulation in AD (Counts et al., 2012; Harigaya and Shoji, 1996) and Down syndrome (Shim and Lubec, 2002).

Overall, these results provide insights into the potential regulation of DBN abundance during oxidative stress. However, to clarify the mechanisms modulating the effects on DBN decreasing levels, further investigation is necessary.

3.2 DBN turnover and stability in dependence of S647 phosphorylation

We have previously shown that DBN interacts with the phosphatase and tensin homolog (PTEN) protein. We found that DBN is highly phosphorylated at Serine 647 residue and that this phosphorylation is negatively regulated by the phosphatase PTEN (Kreis et al., 2013). A reduction in PTEN protein levels coincided with an increased in pS647-DBN levels (Kreis et al., 2013). Moreover, the PTEN-DBN interaction is destabilized upon neuronal activity. Therefore, we were interested in the understanding of the dynamics of DBN phosphorylation and dephosphorylation and its role in DBN stability during synaptic plasticity.

My PhD thesis had as one key objective to answer how DBN abundance is regulated. To address this question, I studied DBN turnover in pulse-chase experiments in HEK293T cells. These experiments suggest that DBN is a long lived protein with an estimated half-live of 3 days. Moreover I was able to show that the stability of DBN is controlled by the phosphorylation of the S647, located at the C-terminus of the protein and that the turnover of DBN is slower when inhibiting the UPS. To further confirm these results, I searched for an experimental approach that could allow me studying

DBN turnover at the endogenous level in neurons. I applied FUNCAT-PLA in cultured hippocampal neurons and followed the degradation profile of endogenous DBN for 24 and 68 h after pulse labeling with AHA. Analyses of these experiments confirmed that DBN is a long lived protein in neurons with a calculated half-life of ~ 70 h. This is in line with my previous experiments using biochemical pulse chase assays, which indicated the half-life of DBN to be ~ 75 h. Moreover, Cohen and colleagues have estimated the protein half-life of 150.48 h for DBN and suggested that the average turnover of synaptic proteins is of 99.6 h (Cohen et al., 2013). In contrast to my experimental approach for DBN turnover analysis, Cohen et.al, (2013) calculated protein half-lives mass spectrometry analyses. The analyzed data was generated by applying isotope labeling with amino acids in cell culture (SILAC) in 14 DIV rat cortical neurons, while our data was obtained from the analyses of HEK293T cells and 18-21 DIV rat hippocampal neurons labeled with AHA. Different cell systems as well as different techniques for labeling proteins could be the reason for finding a big difference between the calculated half-life for DBN by Cohen et.al. (2013) (~150 h) and the half-lives I calculated in both my assays (~ 75 h). Nevertheless, in both cases DBN results to be a long-lived protein.

Overall, my data provides new information on the turnover of DBN and confirms that DBN is a very stable protein which stability is controlled by phosphorylation.

3.3 DBN stabilization upon inhibition of the ubiquitin proteasome system

In order to study the possibility of DBN stabilization when inhibiting the most common path of degradation in the cell I applied MG132, an UPS inhibitor in my pulse-chase experiments. There was no data available in the literature concerning the mechanisms for DBN degradation. Our first hypothesis was that DBN could be ubiquitinated and degraded via the UPS. To address this, I performed pulse-chase experiments in HEK293T cells as shown in the result section (Figure 19) in the presence or absence of MG132, an UPS inhibitor. The addition of MG132 during the chase resulted in the stabilization of DBN, suggesting that DBN degradation could be directed by ubiquitination. To study this further, ubiquitination experiments (not shown in this thesis) were performed by Dr. Patricia Kreis. The results support the observation of DBN degradation by UPS. However, in 2015, Yoshida and colleagues reported DBN

degradation by calpain. In this work, they induced excitotoxicity in cultured hippocampal neurons by prolonged stimulation of NMDA-receptors (NMDA-R) (Chimura et al., 2015). Excitotoxicity is the pathological term for neuronal degeneration by long exposures to neurotransmitters or excessive depolarization of the cells. Such stimulation induced the degradation of DBN after only a few hours when treated acutely with NMDA. The NMDR-R overstimulation induced degradation of DBN was rescued when applying a chelating agent or a calpain inhibitor suggesting DBN degradation by calpain (Chimura et al., 2015).

Two ways of degradation for DBN are presented here. DBN degradation by calpain is suggested to occur by NMDA induced excitotoxicity in neurons while inhibition of the UPS with MG132 stabilizes DBN in pulse-chase experiments. Further investigation would be needed to clarify how exactly DBN degradation is targeted and whether different conditions activate different pathways for the degradation of the protein. Specific degradation of proteins can be context dependent regulated. This is the case for exampled for PTEN. PTEN has been described to be ubiquitinated and degraded by the UPS (Lee et al., 2015) in cancer cell lines. However it has also been suggested that PTEN degradation is mediated by calpain-2 after neuronal stimulation with BDNF (Briz et al., 2013). This example, supports the idea that DBN degradation can be controlled by different mechanisms during different responses.

3.4 Regulation of DBN translation by the PI3K-mTOR pathway

Protein turnover is the result of protein synthesis and protein degradation. In order to get insights into the regulation of DBN turnover I first addressed DBN degradation in dependence of phosphorylation as discussed in previous sections. However, it was important to explore potential regulators of DBN translation. Therefore, as a first approach I targeted several candidates of the PI3K-mTOR pathway, a pathway known to regulate protein synthesis. The mammalian target of rapamycin (mTOR) is an evolutionary conserved kinase known to play a role in controlling protein synthesis during synaptic plasticity and memory (Blenis, 2009; Santini et al., 2014). There are multiple stimuli controlling mTOR activity in neurons. Neurotransmitters and metabolic changes can activate mTOR through upstream activation of AMPA-receptors, NMDA-receptors, dopamine receptors, mGluRs and BDNF receptors. It has been suggested that mTOR signaling contributes to short-term (minutes) and long term (hours)

activation of translation. *De novo* protein synthesis that occurs after neuronal stimulation has been observed to happen locally in the active synapses providing evidence to the idea that localized translation is associated and needed for memory formation during synaptic plasticity (Costa-Mattioli et al., 2009; Santini et al., 2014).

In order to elucidate signaling mechanisms responsible for DBN regulation as well as what events during synaptic plasticity induce or block DBN synthesis or degradation, I studied DBN synthesis in the presence of PI3K, mTOR and PTEN inhibitors applying PURO-PLA in N1E cells. The results show that DBN translation is controlled by mTOR since inhibition of mTOR with rapamycin decreased DBN translation rates.

It is well known that the mTOR signaling pathway is essential for synaptic plasticity and memory consolidation. The evidence indicates that late long-term potentiation (L-LTP induces the phosphorylation of mTOR downstream proteins. Moreover, application of rapamycin inhibits long-lasting synaptic changes and memory formation in mammals during certain behavioral tasks (reviewed in Costa-Mattioli et al., 2009).

My results together with the literature lead to the hypothesis that DBN translation during L-LTP, which underlies synaptic plasticity and mimics memory, may be regulated by mTOR downstream targets. In order to study whether DBN translation is controlled by mTOR during synaptic plasticity, examination of DBN translation upon short treatments with rapamycin during L-LTP in neurons would clarify this point. This could be performed applying PURO-PLA in neurons combining BDNF and Rapamycin treatments.

3.5 DBN localized translation in dendrites

Applying FUNCAT-PLA in neurons I have been able to visualize the pool of DBN protein that is synthesized within two hours in neurons. Newly synthesized DBN is enriched in the dendritic shaft and localizes at the base of the spines. Whether DBN was locally translated or transported after synthesis remained an open question after performance of the pulse-chase experiments with AHA where the pulse lasted 2 h, enough time for protein transport to occur. However, application of PURO-PLA demonstrates that a pool of DBN is translated in dendrites supporting the idea that DBN is locally translated in neurons. This observation may emphasize the role of DBN in synapse maintenance. It has become clear that in neurons several synaptic proteins

are locally translated in dendrites and synapses (Tom Dieck et al., 2014). Polyribosomes have been identified in the dendritic shafts and spines, which suggested a role of local protein synthesis in the regulation of synapses (Ostroff et al., 2002) Furthermore, it has been proposed that synaptic plasticity requires synthesis of proteins and that this occurs locally during long-lasting synaptic plasticity; underlying memory formation (Costa-Mattioli et al., 2009; Kang et al., 1996; Santini et al., 2014; Tom Dieck et al., 2014). In order to further characterize the regulation of localized DBN translation in dendritic shaft other experiments need to be performed. For example induction of neuronal stimulation by applying BNDF together with rapamycin, shown to control DBN translation in my experiments with N1E cells, could provide interesting data. Nevertheless, the general consensus indicates that late phase of LTP depends on transcription since it has been shown to be blocked when applying inhibitors for transcription and for translation (Costa-Mattioli et al., 2009).

3.6 Dendritic localization of DBN mRNA

My data generated with FUNCAT-PLA and PURO-PLA suggests that DBN is locally translated in neurons. However, to further support this observation I examined the localization of DBN transcripts in neurons. Interestingly, I found DBN transcripts in the dendrites of cultured hippocampal neurons. This observation was performed by applying high-resolution *in situ* hybridization. DBN is not the first transcript to be found in dendrites, in fact several mRNAs have been shown to be transported into dendrites in cultured hippocampal neurons (reviewed by Martin and Zukin, 2006). Some of the first mRNAs that were identified to be localized in dendrites include the microtubule associated protein MAP2 (Garner et al., 1988), the activity-regulated cytoskeleton-associated proteins Arc (Lyford et al., 1995) and the brain-derived neurotrophic factor BDNF (Tongiorgi et al., 1997). However, more recently applying deep sequencing analyses and high-resolution *in situ* hybridization, Schuman and colleagues generated a library with more than 2000 transcripts identified in the neuropil of the hippocampus (Cajigas et al., 2012). In this study DBN was identified as one of the localized mRNAs in dendrites. However, I am the first to show the visualization of localized DBN mRNAs in the dendrites of cultured hippocampal neurons.

Localized transcripts are transported into dendrites in large granules where they remain latent until activation by specific stimuli. The granules contain mRNAs, RNA

binding proteins, ribosomes and translational factors. The mRNA trafficking is a quick process with an average speed of 0.1 μm/s, is bidirectional and it is directed by microtubules (reviewed by Martin and Zukin, 2006).

Dendritic mRNA localization has been described to play a role in neuronal development and synaptic plasticity. Moreover, several studies have reported examples for dendritic mRNAs pools which turnover or show trafficking changes upon neuronal stimulation. Tongiorgi *et.al*. (1997) demonstrated that the dendritic localization of mRNAs coding for BDNF and its receptor TrkB increases after neuronal stimulation with high potassium (Tongiorgi et al., 1997).

Towards finding potential inputs regulating DBN mRNA trafficking into dendrites, I applied biccuculline to enhance synaptic activity and Tetrodoxin (TTX) together with APV to silence the neuronal network onto cultured neurons. Use of both TTX and APV results in complete blockage of synaptic activity. TTX blocks neurotransmitter release by action potentials and APV, an NMDA antagonist, inhibits miniature excitatory synaptic events. Application of bicuculline had no effect on DBN mRNA abundance or localization. However, after simultaneous application of TTX and APV in cultured hippocampal neurons I observe an increase in the total abundance of DBN transcripts and this increase is observed to be significantly different in the dendrites but not in the soma in comparison to the vehicle-control, after the inhibition of active and spontaneous synaptic events. One possible explanation for this, is that this kind of stimulation induces both transcription and trafficking of DBN transcripts into dendrites. However, to fully understand what the reason for this change in the dendritic DBN mRNA pool is, other experiments need to be performed. In general, changes in the abundance and localization of DBN transcripts could be due to an increase in mRNA synthesis (1), changes in the turnover of DBN mRNA (2) or due to unmasking of mRNA granules (3) permitting the targeting of the transcripts and their visualization.

4 Conclusions and Outlook

Changes in dendritic spine morphology alter synaptic activity and plasticity, a phenomena important in memory formation, ageing and disorders such as mental retardation. One key protein in these processes is DBN, which is fundamentally important in regulating dendritic spine morphology. During my PhD, I studied the effect of site-specific phosphorylation of DBN and found that this post-translational modification regulates protein stability and turnover. In this context, my work identifies that DBN is locally translated in the dendritic spines in cultured hippocampal neurons.

The overall aim of my PhD project was to understand regulatory inputs relevant to the protein abundance of DBN. DBN abundance declines with age and this is correlated with cognitive decline during ageing. I have identified a phosphorylation site (S647) controlling DBN stability and found that oxidative stress induced by treatments with the herbicide paraquat reduce DBN protein levels in neurons in a concentration dependent manner.

During my PhD work, I also investigated the control of DBN synthesis. This was assessed with the PURO-PLA assay by application of different PI3K and mTOR inhibitors in neurons and N1E-115 cells. I could demonstrate that DBN translation is regulated by mTOR pathway. These results are very interesting since rapamycin is known to block long term synaptic plasticity and L-LTP is known to involve the transcription and synthesis of new proteins in dendrites and synapses. Performing experiments in neurons during L-LTP and simultaneously adding rapamycin could provide new information clarifying the mechanisms behind DBN turnover in neurons and its role in the modulation of spine maintenance.

Furthermore, my experiments for the visualization of DBN mRNA in neurons demonstrate their dendritic localization. Treatments in neurons for the blockage of synaptic activity with TTX and APV resulted in an increase in the dendritic localization and abundance of DBN mRNA. These results indicate that local translation of DBN might be indirectly regulated by spontaneous activity.

Overall my work provides new insights into the regulation of DBN turnover and stability. In addition, I show that DBN translation is controlled by mTOR and my data also

suggests that DBN degradation occurs via the UPS. This thesis also delivers data demonstrating the dendritic localization of both DBN transcripts and DBN translation. A working model summarizes all these findings and postulates that DBN turnover in neurons is locally controlled. Several inputs mentioned previously contribute towards the regulation of DBN turnover and are shown in Figure 35. However, further work needs to be performed to better correlate DBN protein abundance with synaptic function, spine maintenance and synaptic plasticity.

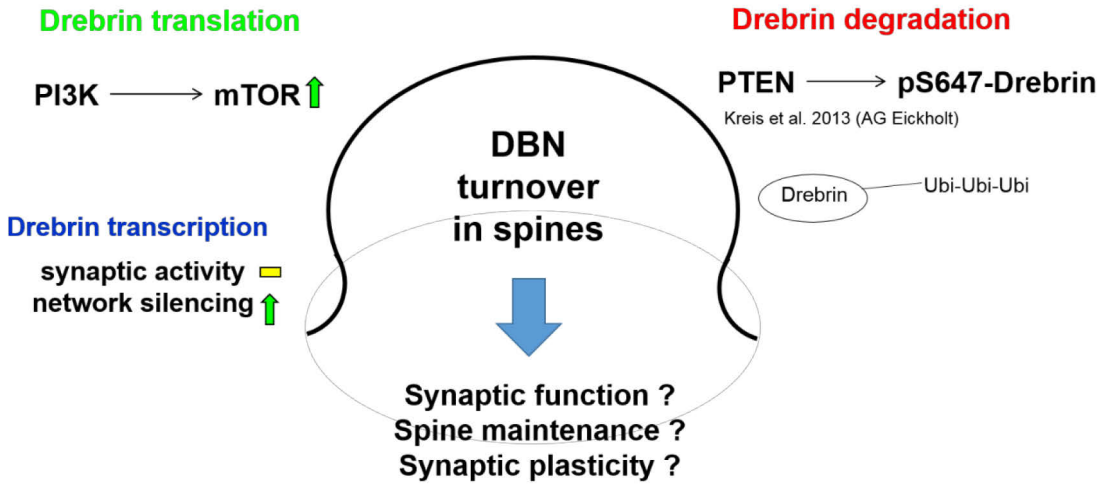

Figure 35| Working model for the control and regulation of DBN turnover in dendritic spines. This thesis show that DBN translation is controlled by mTOR pathway. Data in this thesis suggest that DBN mRNA trafficking and transcription are indirectly regulated by spontaneous synaptic activity. On the other hand, DBN stability dependent of phosphorylation of S647, and as shown before in the Eickholt Lab PTEN depletion increases pS647-DBN levels therefore indirectly regulating DBN turnover in a PI3K-independent manner. Last, this thesis shows that DBN translation occurs locally in dendrites and in proximity of the spines. We propose that DBN turnover is controlled locally in spines and that this regulation contributes to synaptic function, spine maintenance and synaptic plasticity.

5 Materials and Methods

This chapter explains how the experimental work was conducted. It should enable the reader to fully understand the results reported in Chapter 3. It provides all the necessary details for successful replication. All experimental techniques used, as well as the preparation of the experimental samples, are covered.

This chapter is organized as follows: Sections 5.1 to 5.10 contain the lists of laboratory consumables, protocols and detailed information used in the realization of the experimental work presented in this thesis. The topics include: experimental models, treatments and manipulations, assays, imaging-acquisition, molecular biology, solutions and buffers, culture medium and chemicals and kits.

1.1 Molecular biology

Transfections in this work were performed using lipofectamine and the following plasmids were available in the Eickholt Lab. All these constructs have the CMV promoter. All YFP- and Flag-DBN constructs were generated in the Eickholt lab and are based on the human cDNA sequence. DBN constructs with serine to alanine/aspartic acid substitutions were generated by site directed mutagenesis, and then validated by sequencing. The Myc-DBN E construct originated from the lab of T. Shirao (Gunma University, Japan).

1.1.1 Plasmids

YFP-DBNA, YFP-DBNE, YFP-DBNAS647A, YFP-DBNAS647D, YFP-DBNES601A, YFP-DBNES601D, YFP-empty, Flag-DBNE, Flag-DBNES601A, Flag-DBNES601D, Flag-empty and Myc-DBNE.

1.2 Consumables

All consumables are enlisted in five tables presented in this section.

Table 1: Primary antibodies

Table 2: Secondary antibodies and HRP-reagents

Table 3: Buffers

Table 4: Culture medium

Table 5: Chemicals and kits

Table 1 lists the primary antibodies, the assays in which they were applied, and their dilutions. Company and catalog number are indicated to facilitate their acquisition when commercially available.

Table 1- Primary antibodies

Antibody name	Antibody specie	Assay	Dilution	Company	Catalog.No
Debrin M2F6	mouse	FUNCAT-PLA WB	1:300	GenTex	GTX12350
DBN (Eickholt Lab)	rabbit	Puro-PLA Immuno.	1: 1000	In house made	Collected after pS647-DBN purification by Dr. Till Mack)
DBN	Guinea pig	WB	1:1000	Progen	GP823
pDBN (S647)	rabbit	WB Immuno.	1:1000 1:500	In house made	
Biotin	rabbit	PLA	1:5000	Cell signaling	5597
Biotin	mouse	PLA		Sigma-Aldrich	B7653
PTEN (138G6)	rabbit	WB PLA	1:100	Cell signaling	9559
pS6 (Ser235/236)	rabbit	WB	1:1000	Cell signaling	2211
P44/42 MAPK (Erk1/2)	rabbit	WB	1:1000	Cell signaling	4370
Probe Anti-Rabbit PLUS	rabbit	PLA	1:10	Duolink Sigma-Aldrich	DUO92002
Probe Anti-Mouse MINUS	mouse	PLA	1:10	Sigma-Aldrich	DUO92004
Puromycin [3RH11]	mouse	Puro-PLA WB	1: 4000 1:1000	Kerafast	EQ0001
MAP2	guinea pig	Immuno.	1:1000	Synaptic Systems	188004
Alpha-Tubulin	mouse	WB	1:3000	SRM	T6199-200UL
Flag	mouse	WB or WB AHA labeling (pulse-chase)	1:1000 or 1:100000	Sigma	F3165
GAPDH [6C5]	mouse		1:5000	Calbiochem	CB1001
Tubulin [YL1/2]	rat	immuno	1:500	Abcam	ab6160
anti-Ubiquitin	rabbit		1:1000	DAKO	00051128)
pAKT(Ser 473)	rabbit	WB	1:2000	Cell signaling	4060L
AKT (pan)	rabbit	WB	1:2000	Cell signaling	4691
Cyclin B1	mouse	WB	1:1000	Santa Cruz	sc70898

Table 2 lists the secondary antibodies, assays in which they were applied, and the corresponding dilutions. Company name and catalog number are indicated to facilitate their acquisition when commercially available.

Table 2- Secondary antibodies and HRP-reagents

Antibody name	**Assay**	**Dilution**	**Company**	**Catalog.No**
Streptavidin-HRP	WB	1:500	Cell signaling	
Anti-mouse	WB	1:3000	VECTOR	PI-2000
Anti-rabbit	WB		VECTOR	PI-1000
Anti-mouse alexa 568	Immuno	1:500	Invitrogen	A-11004
Anti-mouse alexa 488	Immuno	1:500	Jackson Immuno Reseach	715-545-150
Anti-rabbit alexa 568	Immuno	1:500	Invitrogen	A-11011
Anti-rabbit alexa 488	Immuno	1:500	Jackson Immuno Reseach	711-545-152
Anti-rat alexa 568	Immuno	1:500	Invitrogen	A-11077
Anti-guinea pig Cy5	Immuno	1:500	Jackson Immuno Reseach	706-175-148
donkey anti-guinea pig IgG Cy2			Jackson Immuno Reseach	706-225-148
Alexa Fluor 488 phalloidin	Immuno	1:50	Life Technologies	A12379
Phalloidin 647 Alexa Flour	Immuno	1:25	Life Technologies	A22287

1.3 Solutions and buffers

Table 3 lists the name and recipes of buffers and solutions prepared and used for conducting all experiments.

Table 3- Buffers

Buffer name	Concentration	Assay	Chemicals	Company	Catalog.No.
Buffer A Buffer B	Ready made	PLA	In situ Wash Buffers, fluorescence	Sigma-Aldrich	DUO82049
Stacking buffer	0.5 M Tris-HCl 0.4% SDS pH 6.8	WB	Tris-HCl SDS	homemade	
Trypsin	10 mg/ml in HBSS	Primary culture	Trypsin HBSS	SRM	14170146
10x TBS-T	50 mM Tris-HCl 150 mM NaCl 0.05% Tween 20 detergent	WB	Tris-HCl NaCl Tween 20 detergent	Roth Roth Calbiochem	9090.3 9265.1 655205
10x Transfer-buffer	Rothiphorese SDS-Page	WB		Roth	3060.2
Roti-Load sample buffer	Ready made	WB		Roth	K929.2
APS 10%	100 µg/ml Ammoniumperoxo disulfat	WB	Ammoniumperoxodisulfat	Roth	9592.3
Stripping buffer I	Ready made	WB		AppliChem	A7140, 0125
Temed	≥99 %	WB		Roth	2367.1
RIPA buffer	50 mM Tris-HCL pH 7.4 150 mM NaCl 0.5% sodium deoxycholate 1% NP40 0.1% SDS	WB	Tris-HCL NaCl sodium deoxycholate NP40 SDS	homemade	
PBS 1x	Tablets for preparation of 500 ml PBS in water	All assays	phosphate buffered saline	AppliChem	A9191.0012
Blocking and antibodies solution for western blot	5% Milk in TBS-T	WB	Low fat powder milk	Roth	T145.2
Mowiol 4-88	5 g Mowiol 20 ml PBS 10 ml glycerine	Immuno		Calbiochem	
PBS-MC	1 x PBS PH 7.4 1mM $MgCl_2$ (Stock: 1M in H_2O) 0,1mM $CaCl_2$ (Stock: 0.1M in H_2O)	FUNCAT-PLA	$MgCl_2$ $CaCl_2$		
4% PFA, 4% Sucrose in PBS-MC pH= 7.4	20 g PFA 400 mL PBS-MC 5 µl $MgCl_2$- Stock (1M in H_2O) 5 µl $CaCl_2$- Stock (0,1M in H_2O) 20 g Sucrose	Immuno. FUNCAT-PLA Puro-PLA			
Poly-DL-Ornithine	1.5-mg/mL (100X)			Sigma Aldrich	P8638

1.4 Culture medium

Table 4 lists the different medium cultures used for growing the cell lines and primary neurons.

Table 4- Culture medium

Medium	**Cell type**	**Company**
DMEM + GlutaMax	Cell lines	Gibco – 31966021
MEM	Glial cells (rat)	Gibco – 31095029
Neurobasal-A	Primary cultures	Gibco- 10888022
DMEM Met-Free (custom made)	293T cells for metabolic labeling	Gibco
Neurobasal-A Met- free (custom made)	Neurons for metabolic labeling	Gibco

1.5 Chemicals and kits

Table 5 shows the list of chemicals and kits used during this project.

Table 5- Chemicals and kits

Chemical	**Assay**	**Company**	**Catalog.No.**
Azidohomoalanine	BONCAT, FUNCAT-PLA	Anaspec	AS-63669
Puromycin (50mg/ml)	Puro-PLA Puro-WB	Sigma-Aldrich	P8833
Anisomycin	FUNCAT-PLA, Puro-PLA	Tocris	1290
Biotin-Alkyne (Acetylene-PEG4-Biotin)	FUNCAT-PLA	Jena Biosciene GmbH	CLK-TA105
ECL western blotting substrate	WB	Promega	REF W1001
$CuSO_4$-$5H_2O$	FUNCAT-PLA	Sigma-Aldrich	678937
TCEP-HCl	FUNCAT-PLA	Pierce	20490
Triazole ligand (TBTA)	FUNCAT-PLA	Sigma-Aldrich	678937
Duolink In situ detection reagent – Red	PLA	Duolink Sigma-Aldrich	DUO92008
Click-iT® Protein Reaction Buffer Kit	Click-chemistry (cell lysates)	Invitrogen	C10276
Hoechst	IC	Sigma-Aldrich	14530
Biotin-alkyne (4 mM stock)	Click-chemistry (cell lysates)	Invitrogen	B10185
protease inhibitor cocktail	WB	Calbiochem	539134
Lipofectamine 2000	Transfections	Life Technolog/SRM	11668019
1x phosphatase inhibitor cocktails 2 and 3	WB	Sigma-Aldrich	P5726 and P0044
Rapamycin	mTor inhibitor, puromycilation	Cell signaling	9904S

GDC0941	PI3K inhibitor, puromycilation	Selleckchem	S1065
bpV (hopic)	PTEN inhibitor, puromycilation	Calbiochem	203701
MG-132	Proteasome inhibitor, Pulse-chase 293T	SRM/Caymann	10012628
Papain dissociation System	Primary culture	Worthington	LK003150
Bicuculline	Competitive antagonist of $GABA_A$ receptors (enhances neuronal synaptic activity)	Tocris	0130
Tetrodoxin citrate (TTX)	Reversible, selective blocker of Na^+ channels, silencing of network activity	Tocris	1069
GlutaMax	Primary culture	Thermo Scientific	35050061
FCS	Primary culture	Biochrom	S 0615
B27 supplement	Primary culture	Life Technologies	17504-044
Penicillin/streptomycin	Primary culture	Life Technologies	15140122
D-AP5 (APV)	Neuronal stimulation	Tocris	0106

1.6 Experimental cell models

Different cell models were used in order to establish the most valuable systems to address the scientific questions reported in this thesis. To do so, cell lines and primary neuronal mix cultures were used. In this section, I characterize the conditions needed to maintain and grow cell lines and neurons isolated from mouse and rat in culture.

1.6.1 Cell models

COS-7, HEK293T and N1E-115 cells were grown and maintained for several passages in the incubator at 37°C and 5% CO_2 in Dulbecco's Modified Eagle Medium (DMEM) supplemented with 10 % fetal calf serum (FCS) and 1% penicillin/streptomycin (P/S).

1.6.2 Primary neuronal cultures

In order to study neuronal systems, I used cortex or hippocampal neurons obtained by microdissection from BL6 wild-type E16.5 mice, the DBN-KO E16.5 mice generated in the Eickholt lab, or P0-P1 Wistar rats. I established the long-term cultures (18-24 DIV) in the Eickholt lab from both mouse embryos and rat pups. In the following section, I describe the specific protocols needed to prepare and maintain neurons in culture.

1.6.2.1 Mouse primary neuronal cultures

Cortices or hippocampi were dissected from E16.5 C57BL/6 mice embryos. The dissected tissue was then dissociated in 0.5 mg/ml trypsin in HBSS for 15 minutes at 37°C, washed twice in HBSS buffer, washed once in Neurobasal (NB) medium supplemented with 1% GlutaMAX, 2% B27, 1% P/S, and 102.29 µM (1:100, and then 1:50 000 from stock solution) β-mercaptoethanol. Tissue was washed once in NB supplemented with 10% Horse Serum, and gently triturated in culture medium using a fire polished Pasteur pipette. Single cell suspension cells were plated on glass coverslips (Assistent) previously coated with Poly-Ornithine 1:50 (stock concentration 1.5 µg/µl). Cultures were maintained in NB supplemented with 1% GlutaMAX, 2% B27 and 1% P/S at 37°C and 5% CO_2. After 3 days, astrocyte conditioned medium (ACM) was diluted in growing medium to a final concentration of 2x. Half the medium was

replaced every medium change, once a week. Neurons were plated at a density of 50 000 cells/well in 24 well plates (TTP), 150 000 cells/well in 12-well plates, or 300 000 cells/well in 6-well plates (TTP).

1.6.2.2 Rat models

Cortices or hippocampi were dissected from Winstar rats postnatal stages (P0-P1), dissociated in papain (Worthington) according to the papain dissociation system kit protocol. 20 000 hippocampal cells were plated on 35 mm glass-bottom (MatTek Corporation) previously coated with 1:50 Poly-Ornithine (stock concentration 1.5 µg/µl). Two to four hours after plating the cells, 3 ml of the rat conditioned medium were pipetted in every dish.

1.6.2.2.1 Growing medium

Neurobasal medium supplemented with 1% GlutaMAX, 2% B27 and 1% P/S, and 102.29 µM (1:100 and then 1:50000 from stock solution) β-mercaptoethanol.

1.6.2.2.2 Generation of conditioned medium

Conditioned medium was required for all the types of neurons in order to maintain them in long term culture. For primary mouse neuronal cultures Astrocytes conditioned medium was produced as described in the following section. To culture primary rat neurons from postnatal rat animals, conditioned medium was used. To generate this medium cortical and glial conditioned mediums were produced as described in the next sections.

1.6.2.2.3 Astrocytes conditioned medium (ACM) for mouse primary cultures

Cortices were dissected from E16.5 C57BL/mice embryos, dissociated in 0.5 mg/ml trypsin diluted in HBSS for 15 min at 37°C, washed twice in HBSS, washed once in growing medium: Neurobasal medium supplemented with 1% GlutaMAX, 2% B27 and 1% P/S, and 102.29 µM (1:100 and then 1:50000 from stock solution) β-mercaptoethanol. Single cell suspension cells were plated on glass coverslips (Assistent) previously coated with 0.5% collage and grown in DMEM supplemented with 10% FCS and 1 % P/S until confluent. Then, astrocytes were washed once in 1x PBS and medium was replaced by Neurobasal (NB) medium supplemented with 1%

GlutaMAX, 2% B27 and 1% P/S, and 102.29 µM (1:100 and then 1:50000 from stock solution) β-mercaptoethanol. Medium replacement and collection were performed every 3 days.

1.6.2.2.4 Rat conditioned medium

This medium was prepared as follows: 80 % growing medium, 15% glial medium and 5% cortical medium.

1.6.2.2.5 Cortical conditioned medium for rat conditioned medium

In order to prepare cortical conditioned medium necessary for culturing P0-P1 rat neurons, cortices were dissected from Wistar rats postnatal stages (P0-P1) dissociated in papain (Worthington) according to the Papain dissociation system kit protocol. Single cell suspension cells were plated in T75 flasks previously coated with 1:50 poly-Ornithine (stock concentration 1.5 µg/µl) and grown in Neurobasal medium supplemented with 1% GlutaMAX, 2% B27 and 1% P/S, and 102.29 µM (1:100 and then 1:50000 from stock solution) β-mercaptoethanol. Medium was changed after two days and a week later, before collection, which was done every 3 days.

1.6.2.2.6 Glial conditioned medium

Cortices were dissected from Wistar rats postnatal stages (P0-P1) dissociated in papain according to the papain dissociation system kit protocol. Single cell suspension cells were platted in T75 flasks previously coated with 0.5% collagen and growth in Minimum Essential Medium (MEM) supplemented with 10% horse serum and 20% glucose and 1% P/S until confluent. Then, medium is replaced with NB medium supplemented with 1% GlutaMAX, 2% B27 and 1% P/S, and 102.29 µM (1:100 and then 1:50000 from stock solution) β-mercaptoethanol. Medium collection was performed every 3 days.

1.7 Treatments and cell transfection

In order to find regulatory inputs for DBN stability, cells were subjected to several treatments as described in the following section.

1.7.1 Transfection in multiple cell lines

SH-SY5Y, COS-7, N1E-115 or HEK293T cells were transfected 24 h after plating in 24 well (1.9cm^2) on cover slips, 12 well plates (3.8cm^2), or 6 well plates (9.5cm^2) using lipofectamine 2000 (Invitrogen), Opti-MEM as transfection reagent, and 1 µg, 1.5 µg, or 3 µg of plasmid, respectively. The transfection mix was prepared as suggested in the commercial Lipofectamine 2000 reagent protocol. Four hours after transfection the medium was replaced with fresh medium, and cells were incubated overnight at 37°C and 5% CO2 before cell fixation, cell lyses, or pulse labeling in pulse-chase experiments.

1.7.2 Oxidative stress induction

Stock concentrations of H_2O_2, paraquat or β-Amyloid Peptide (1-42) (Calbiochem) were prepared as follows. paraquat was dissolved in ddH_2O to a stock concentration of 500 µM. H_2O_2 was freshly dissolved in ddH_2O to a stock concentration of 97 µM. Aβ was dissolved in Hexafluoroisopropanol to a stock concentration of 60µM. 14 DIV cortical neurons were treated with different concentrations of H_2O_2, paraquat or Aβ for 24 h, and were then lysed for Western blot (6-well/12-well plates), or were fixed for immunocytochemistry (24-well plates).

1.7.3 Neuronal stimulation and network silencing

Neurons were treated with either 30 µM bicuculline to stimulate synaptic activity or TTX (1 µM) + APV (20 µM) to silence the network activity for the indicated time points.

1.8 Assays

Different classic assays such as SDS-page and western blot, as well as new assays, such as FUNCAT-PLA, were applied in this work. A detailed explanation of how these were performed is presented in this section.

1.8.1 SDS-PAGE and Western blotting (WB)

Neurons or cells were washed once with PBS and lysed in RIPA buffer supplemented with protease inhibitor and phosphatase inhibitors as specified in the consumables section. Equal amounts of protein were loaded in 8% acrylamide gels, transferred onto nitrocellulose membranes and blocked for 1 h in TBS supplemented with 1% Tween and 5% milk. Membranes were incubated 1 h in primary antibodies and washed three times for 5 min with TBS-Tween. They were then incubated for 1 h in secondary antibodies and washed three times for 5 min with TBS-Tween. Primary and secondary antibodies were prepared in TBS-Tween 5% milk.

1.8.1.1 Membrane development and imaging

ECL western blotting substrate for membrane development was applied for 1 minute and membranes were immediately developed with the system Fusion SL VILBER LOURMAT and digital images were captured for further analyses. Quantification of bands density was performed using ImageJ. The area of the band and the mean gray value were measured to obtain a relative density. For relative quantifications, measurements were normalized to loading control.

1.8.2 Lentiviral infection of DBN-KO neurons

Primary culture preparation was performed and 60 000 DBN-KO hippocampal neurons were grown on covers lips previously coated with 1:50 poly-O (stock concentration 1.5 µg/µl). Neurons were infected with 50 µl of YFP-DBN or YFP lentiviruses after 2 DIV and later fixed after 22 DIV. Description of the DBN-KO model generation and specifics about the virus are described in the following section.

5.1.1.1 DBN knockout mice

The DBN knockout (DBN-KO) mice line was developed in the Eickholt lab. The DBN knockout (DBN-KO) mice line was developed in the Eickholt lab. The Dbn1 mouse strain was used for the development of this mouse model from the embyonic stem cell clone. This clone, was obtained from KOMP Repository (www.komp.org) and the mouse model was generated at the Welcome Trust Sanger Institut (Skarnes, Rosen et.al.2011). The initial heterozygous mice holding a promoter-driven knockout allele (Dbn1tm1a(KOMP)Wtsi) were acquired from the KOMP Repository. Gene-trap cassette holding a constitutive null mutation was deleted after crossing with a FLP strain. Pre-conditional allele was validated by PCR and sequencing by Dr. Till Mack in the Eickholt Lab. This was followed by breading homozygote pre-conditional mice with a Cre strain (B6.C-Tg(CMV-cre)1Cgn/J, Jackson Laboratories) for the generation of homozygote null alleles and heterozygote null alleles. Genotyping with PCR was performed using the following primers:

Genotyping Primers (5'-3'):

F4: CGCCGGAACCGAAGTTCCTATT (forward primer for KO-PCR upstream of β-gal+ neo cassette)

F3: GAGGAGGTTAAAGGAGCAGTCTATCTTT (forward primer for WT-PCR end of exon 6)

RS1: AGGAATACTCAAGTTCCTGTCGGACC (reverse primer between exon 6 and exon 7)

5.1.1.2 YFP-virus

DBN-A wild-type-YFP and YFP lentiviruses with a synapsin promoter were generated by Dr. Till Mack (Eickholt Lab) and are based on pLenti6.3 backbone (Thermo Scientific).

1.8.3 Immunocytochemistry

Neurons or cells were fixed with 4% PFA, 4% sucrose or 4% paraformaldehyde (PFA), respectively for 20 min, washed three times with PBS, permeabilized for 15 min in 0.5%

triton in PBS-MC (PH7,4) and blocked for 1 h or overnight in 4% goat serum. Coverslips were incubated with primary antibodies for 1 h at room temperature, washed three times for 5 min with PBS, incubated with secondary antibodies for 1 h at room temperature and washed three times with PBS. Coverslips were incubated with Hoechst (1:50000 dilution) for 10 min and mounted using Mowiol. Primary and secondary antibodies were diluted in blocking solution. Antibodies were prepared in 4% goat serum as follows: Drebrin (mouse monoclonal [M2F6], GenTex) 1:200, α-tubulin (mouse monoclonal antibody, Sigma Aldrich) 1: 400, α–tubulin (rat monoclonal [YL1/2] Abcam) 1:50. Secondary antibodies anti-mouse alexa 568, anti-mouse alexa 488 and anti-rat alexa 568 (Invitrogen) were prepared in a dilution of 1:1000 in PBS 2% BSA, 1% goat serum and 1% Sodium azide.

1.8.4 Pulse-chase experiments in 293T cells

150 000 cells (HEK293-T) were plated on poly-ornithine coated 12-well plates and growth in DMEM medium supplemented with 10% FCS and 1% P/S for 24 h at 37°C and 5% CO_2. After 24 h the cells were transfected with Lipofectamine using 1.5 µg of plasmid DNA. Twenty four hours after transfection, cells were washed in pre-warmed methionine free DMEM medium supplemented with 10% FCS and 1% P/S. Cells were incubated for 1 h. Later, the medium was replaced by labeling medium: 1 mM azidohomoalanine (AHA) in methionine free DMEM medium supplemented with 10% FCS and 1% P/S. Cells were pulse-labeled for 1 h, washed once in complete medium and twice in PBS, and followed by cell lyses (no chase) or chase for: 24 h, 48 h and 72 h in complete medium before cell lyses. Cells were lysed in 150 µl of RIPA buffer supplemented with 1x protease inhibitor cocktail and 1x phosphatase inhibitors. Click-chemistry in the protein lysates was then performed.

1.8.5 Click-chemistry protein lysates

100 µl of cell lyses were collected and click-chemistry was performed using the Click-it Protein reaction buffer kit as suggested in the protocol provided. Cycloaddition was used with biotin-alkyne and precipitated protein was re-suspended in 1x Roti-Load sample buffer for western blot analyses. Labeled proteins were detected with Streptavidin-HRP (1:1500) and later stripped for 30 min at 45°C to further blot with anti-Flag 1:100,000. As loading control anti-α-Tubulin was used.

1.8.6 FUNCAT-PLA

Between 30 000-50 000 hippocampal rat neurons were plated on poly-ornithine coated 35 mm glass-bottom (MatTek Corporation) and growth in rat conditioned medium (see section 2.3.2.4). 18-21 DIV neurons were incubated for 2 h with Neurobasal A-Met free + 1% glutaMax, 2% B27 and 4 mM AHA, 40 µM Anisomycin (Aniso) or Methionine (Met). Conditioned medium for each plate was kept in the incubator during pulse-labeling to be re-used during the chase. After pulse-labeling with AHA or Met-control, cells were washed twice with PBS-MC (pH 7.4) and fixed with 4% PFA 4% Sucrose in PBS-MC (PH 7.4) (no chase) or chase in own medium for: 24 h or 68 h. Time points were coordinated to end at the same time. Fixed cells were permeabilized for 15 min with 0.5% triton in PBS-MC (pH 7.4), blocked for 1 h in 4% goat serum in PBS (pH 7.4) and washed twice with PBS pH 7.8 before click-chemistry.

Click-chemistry reaction for FUNCAT-PLA (1 reaction)

1 ml PBS, pH 7.8
1 µl of triazole ligand stock (Stock 200mM)
1 µl of freshly prepared TCEP (500mM)
0.5 µl biotin-alkyne (Stock 50mM)
1 µl $CuSO_4$ solution (200mM)

Cells were incubated in the click-chemistry reaction at room temperature overnight and then a second permeabilization step was performed in 15 min with 0.5% triton in PBS-MC (pH 7.4). Cells were washed twice with PBS-MC (pH 7.4) and blocked for 1h in 4 % goat serum in PBS (pH 7.4). Incubation with primary antibodies was followed and performed for 1.5 h at room temperature. Antibodies were prepared in blocking buffer at indicated dilutions (See table 1). DBN (mouse monoclonal [M2F6]) antibody was always used in these experiments.

1.8.7 High-resolution fluorescence in situ hybridization (Panomics probes)

These experiments were fully performed in the Schuman Lab. To do so, high-resolution fluorescence in situ hybridization probes were designed to detect DBN mRNA in rat neurons. Hippocampal rat neurons (21-24 DIV) were fixed with PFA-sucrose and

permeabilized before target hybridization. The FISH protocol was followed exactly as suggested in the Afimetrix kit manual (QuantiGene ViewRNA Cell Assay User Manual; P/N 1880).

The procedure consisted of three main steps:

- Fixing cells and hybridization (in this step the transcript-specific probe is applied).
- Amplification (in this step the signal is amplified).
- Antibody staining (MAP2 and phalloidin in this work).

1.8.8 Puromycilation (Puro)

For puromycilation, neurons or N1E-115 cells were incubated with 1 µM (for PLA) or 4 µM (for WB) puromycin or without puromycin as a control for 3 or 5 min (as indicated), in medium at 37 °C in an incubator with 5% CO2. After incubation, two fast washes with pre-warmed PBS-MC were performed and cells were either fixed for 20 min in PFA-sucrose or lysed in RIPA buffer for WB analyses. In neurons, the medium in which they were grown was always used for any drug treatments. As a protein synthesis inhibitor 40 µM anisomycin was applied 30 min to 1 h before puromycilation and in the presence of puromycin.

After fixation, cells were washed with PBS, permeabilized for 15 min with 0.5% triton in PBS-MC (pH 7.4), blocked for 1 h in 4% goat serum in PBS (pH 7.4) and followed by the proximity ligation assay as described in section 2.3.6 using the puromycin and rabbit polyclonal DBN (homemade; Eickholt Lab) antibodies for 1.5h at room temperature (see table 1 for antibody dilutions).

After cell lyses, samples were centrifuged, prepared as described in section 2.3.1, and analyzed with the puromycin antibody.

1.8.9 Proximity ligation assay (PLA)

This assay was applied for FUNCAT-PLA, Puro-PLA and PLA experiments modifying the antibodies as needed. This protocol was optimized following the directions of the Duolink *In Situ* manual and as described in the following section.

After primary antibody incubation, cells were washed three times for 5 min with PBS (pH 7.4) and incubated for 1 h at 37°C with freshly prepared PLA-probes (1:10) in a semi-wet chamber.

PLA probes (1 reaction = 80 µl)

8 µl PLA + (Probe Anti-Rabbit PLUS)
8 µl PLA – (Probe Anti-Mouse MINUS)
64 µl blocking buffer

After incubation with the PLA probes, cells were washed three times for 5 min with washing buffer A. Ligation was performed for 30 min at 37°C in a semi-wet chamber.

Ligation (1 reaction = 80 µl)

16 µl ligation-stock (PLA kit)
5 µl ligase
62 µl H_2O

After ligation, two washing steps with washing buffer A were performed, the amplification reaction was prepared and cells were incubated for 100 min at 37°C in this solution.

Amplification (1 reaction = 80 µl)

16 µl amplification-stock (PLA kit)
1 µl polymerase
63 µl H_2O

After amplification, two immediate washing steps with washing buffer B were performed followed by two of 10 min each, one with 0.01x washing buffer B and one with PBS. Finally, cells were incubated for 10 min with 4% PFA 4% sucrose in PBS for a second fixation step. The last step in this protocol is the staining of neurons with the MAP2 neuronal marker. For this purpose, cells were incubated in blocking solution overnight at 4°C and incubated with the MAP2 antibody for 1.5 h at room temperature. After three washing steps with PBS, cells were incubated with anti-guinea pig antibody

for 1h and further washed three times with PBS. Finally, nuclear staining was performed with Hoechst for 5 min and washed with PBS. Cells were maintained in PBS at 4°C until imaging.

1.9 Image-acquisition

In the Eickholt Lab, the images of cells were captured using a Confocal Laser Scanning Microscope Leica TCS SP8 using a 63x oil objective. Images were acquired with a resolution of 1024 x 1024 pixels through the entire sample as z-stacks size 0.5 µm. Laser intensities and gain were defined for every experiment and maintained without changes within an experiment.

In the Schuman Lab, the images were captured using a LSM780 confocal microscope (Zeiss) using a 40x oil objective. Images were acquired with a resolution of 1024 x 1024 pixels through the entire sample as z-stacks size 0.5 µm. Laser intensities and gain were defined for every experiment and maintained without changes within an experiment.

1.10 Analyses and statistical tests

1.10.1 Data normalization and calculations

To plot the data obtained from the pulse-chase experiments, we reasoned that at the time point 0 h chase, maximum protein labeling has been achieved. Therefore, we normalized the data considering AHA 0 h as 100%. In pulse chase experiments with 293T cells protein half-lives were calculated individually for every experiment using the exponential decay equation from the curves (0 h and 72 h chase) from multiple experiments ($n \geq 3$) and later mean values between half-lives were obtained. However, in pulse chase experiments in neurons the protein half-live for DBN was calculated using the exponential equation from the curve from three independent experiments.

Data was always normalized as percentage of control.

T-tests were applied in all cases and P-values were indicated on every figure. The standard error of the means (SEMs) were calculated and are represented in the error bars of the bar plots presented in the results section.

1.10.2 Image analyses

Five to ten images per condition were captured and processed for analysis in FIJI (Schindelin et al., 2012). Maximal projections were used for all quantitative analyses. All the images obtained from the FUNCAT-PLA, Puro-PLA and Panomics experiments were analyzed using our customize Plugin for PLA. The details for this plugin are explained in the results section X since this was part of the thesis work and the detailed script in the supplemental information section. Overall, PLA puncta and the area these occupied were quantified on a mask for a cell volume marker. In neurons: MAP2 and in N1E-115 cells: actin-stain. All the puncta not overlapping or in the close proximity with the respective cell volume marker were excluded from the analyses. Finally, PLA to cell volume marker ratios were calculated and experimental conditions were always normalized as percentage of control. The signal from a whole image was considered as the total or global signal in the case of further analyses to compare soma and dendrites.

1.10.3 Dendrites and soma PLA/Panomics analyses

A plugin to manually select the Soma in neurons was also developed for the analyses of this work (see supplemental figures for script). After selection of soma on a specific image, a subfolder was automatically created where the storage of soma pictures were kept. PLA analyses were later run on the specific folder and results were further analyzed in Excel. The following calculations were performed to quantify the signal along dendrites:

$$PLA_{global} - PLA_{soma} / MAP2_{global} - MAP2_{soma} = \text{Dendrites signal}$$

6 References

Ackermann, M., and Matus, A. (2003). Activity-induced targeting of profilin and stabilization of dendritic spine morphology. Nat. Neurosci. *6*, 1194–1200.

Aoki, C., Kojima, N., Saballauskas, N., and Al., E. (2009). Drebrin A Knockout Eliminates the Rapid Form of Homeostatic Synaptic Plasticity Excitatory synapses of Intac Adult Cerebral Cortex. J Comp Neurol. *517*, 105–121.

Ballif, B.A., Villén, J., Beausoleil, S.A., Schwartz, D., and Gygi, S.P. (2004). Phosphoproteomic analysis of the developing mouse brain. Mol. Cell. Proteomics MCP *3*, 1093–1101.

Beausoleil, S.A., Bakalarski, C.E., Elledge, S.J., Dephoure, N., Zhou, C., Ville, J., and Gygi, S.P. (2008). A quantitative atlas of mitotic phosphorylation ´. PNAS *105*.

Blenis, X.M. and J. (2009). Molecular mechanisms of mTOR-mediated translational control. Nat.Rev.Mol.Cell Biol. *10*, 307–318.

Briz, V., Hsu, Y.-T., Li, Y., Lee, E., Bi, X., and Baudry, M. (2013). Calpain-2-Mediated PTEN Degradation Contributes to BDNF-Induced Stimulation of Dendritic Protein Synthesis. J. Neurosci. *33*, 4317–4328.

Cajigas, I.J., Tushev, G., Will, T.J., Tom Dieck, S., Fuerst, N., and Schuman, E.M. (2012). The Local Transcriptome in the Synaptic Neuropil Revealed by Deep Sequencing and High-Resolution Imaging. Neuron *74*, 453–466.

Chew, C.S., Okamoto, C.T., Chen, X., and Thomas, R. (2005). Drebrin E2 is differentially expressed and phosphorylated in parietal cells in the gastric mucosa. Am. J. Physiol. Gastrointest. Liver Physiol. *289*, G320–G331.

Chimura, T., Launey, T., and Yoshida, N. (2015). Calpain-Mediated Degradation of Drebrin by Excitotoxicity In vitro and In vivo. PLoS One *10*, e0125119.

Cingolani, L.A., and Goda, Y. (2008). Actin in action: the interplay between the actin cytoskeleton and synaptic efficacy. Neuroscience *9*.

Cohen, L.D., Zuchman, R., Sorokina, O., Müller, A., Dieterich, D.C., Armstrong, J.D., Ziv, T., and Ziv, N.E. (2013). Metabolic Turnover of Synaptic Proteins: Kinetics, Interdependencies and Implications for Synaptic Maintenance. PLoS One *8*, e63191.

Costa-Mattioli, M., Sossin, W.S., Klann, E., and Sonenberg, N. (2009). Translational control of long-lasting synaptic plasticity and memory. Neuron *61*, 10–26.

Counts, S.E., He, B., Nadeem, M., Wuu, J., Scheff, S.W., and Mufson, E.J. (2012). Hippocampal drebrin loss in mild cognitive impairment. Neurodegener. Dis. *10*, 216–219.

Dieterich, D.C., Link, A.J., Graumann, J., Tirrell, D.A., and Schuman, E.M. (2006). Selective identification of newly synthesized proteins in mammalian cells using

bioorthogonal noncanonical amino acid tagging (BONCAT). Proc. Natl. Acad. Sci. U. S. A. *103*, 9482–9487.

Dieterich, D.C., Hodas, J.J.L., Gouzer, G., Shadrin, I.Y., Ngo, J.T., Triller, A., Tirrell, D. a, and Schuman, E.M. (2010). In situ visualization and dynamics of newly synthesized proteins in rat hippocampal neurons. Nat. Neurosci. *13*, 897–905.

Doherty, M.K., and Beynon, R.J. (2006). Protein turnover on the scale of the proteome. Expert Rev. Proteomics *3*, 97–110.

Doré, S., Takahashi, M., Ferris, C.D., Zakhary, R., Hester, L.D., Guastella, D., and Snyder, S.H. (1999). Bilirubin, formed by activation of heme oxygenase-2, protects neurons against oxidative stress injury. Proc. Natl. Acad. Sci. U. S. A. *96*, 2445–2450.

Engert, F., and Bonhoeffer, T. (1999). Dendritic spine changes associated with hippocampal long-term synaptic plasticity. Nature *399*, 66–70.

Garner, C.C., Tucker, R.P., and Matus, a (1988). Selective localization of messenger RNA for cytoskeletal protein MAP2 in dendrites. Nature *336*, 674–677.

Grintsevich E. Elena, et. al. (2010). Mapping of Drebrin Binding Site on F-Actin. J Mol Biol *398*, 542–554.

Guo, C., Zhang, Y.X., Wang, T., Zhong, M.L., Yang, Z.H., Hao, L.J., Chai, R., and Zhang, S. (2015). Intranasal deferoxamine attenuates synapse loss via up-regulating the P38/HIF-1?? pathway on the brain of APP/PS1 transgenic mice. Front. Aging Neurosci. *7*, 1–12.

Hamilton, A.M., Oh, W.C., Vega-ramirez, H., Stein, I.S., Hell, J.W., Patrick, G.N., and Zito, K. (2012). Activity-Dependent Growth of New Dendritic Spines Is Regulated by the Proteasome. Neuron *74*, 1023–1030.

Harigaya, Y., and Shoji, M. (1996). Disappearance of actin-binding protein, drebrin, from hippocampal synapses in alzheimer's disease. J. Neurosci. … *92*.

Hayashi, K., and Shirao, T. (1999). Change in the shape of dendritic spines caused by overexpression of drebrin in cultured cortical neurons. J. Neurosci. *19*, 3918–3925.

Hayashi, K., Suzuki, K., and Shirao, T. (1998). Rapid conversion of drebrin isoforms during synapse formation in primary culture of cortical neurons. Brain Res. Dev. Brain Res. *111*, 137–141.

Hu, C.D., Chinenov, Y., and Kerppola, T.K. (2002). Visualization of interactions among bZIP and Rel family proteins in living cells using bimolecular fluorescence complementation. Mol. Cell *9*, 789–798.

Ishikawa, R., Hayashin, K., Shiraon, T., Takagill, T., and Kohamas, K. (1994). Drebrin, a Development-associated Brain Protein from Rat embryo Causes the dissociation of Tropomysin from Actin Filaments. J. Biol. Chem. *269*, 29928–29933.

Ivanov, A., Esclapez, M., and Ferhat, L. (2009a). Role of drebrin A in dendritic spine plasticity and synaptic function. Am. J. Hum. Genet. *2*, 268–270.

Ivanov, A., Escalpez, M., Pellegrino, C., and Et.al (2009b). Drebrin A regulates dendritic spine plasticity and synaptic function in mature cultured hippocampal neurons. J. Cell Sci. *122*, 524–534.

Jares-Erijman, E. a, and Jovin, T.M. (2003). FRET imaging. Nat Biotechnol *21*, 1387–1395.

Jin, M., Tanaka, S., Sekino, Y., Ren, Y., Yamazaki, H., Kawai-Hirai, R., Kojima, N., and Shirao, T. (2002). A novel, brain-specific mouse drebrin: cDNA cloning, chromosomal mapping, genomic structure, expression, and functional characterization. Genomics *79*, 686–692.

Jung, G., Kim, E.J., Cicvaric, A., Sase, S., Gröger, M., Höger, H., Sialana, F.J., Berger, J., Monje, F.J., and Lubec, G. (2015). Drebrin depletion alters neurotransmitter receptor levels in protein complexes, dendritic spine morphogenesis and memory-related synaptic plasticity in the mouse hippocampus. J. Neurochem. *134*, 327–339.

Kang, H., Jia, L.Z., Suh, K.Y., Tang, L., and Schuman, E.M. (1996). Determinants of BDNF-induced hippocampal synaptic plasticity: role of the Trk B receptor and the kinetics of neurotrophin delivery. Learn. Mem. *3*, 188–196.

Klein, J.A., and Ackerman, S.L. (2003). Oxidative stress , cell cycle , and neurodegeneration. *111*, 785–793.

Kojima, N., Shirao, T., and Obata, K. (1993). Molecular cloning of a developmentally regulated brain protein, chicken drebrin A and its expression by alternative splicing of the drebrin gene. Mol. Brain Res. *19*, 101–114.

Kojima, N., Hanamura, K., Yamazaki, H., Ikeda, T., Itohara, S., and Shirao, T. (2010). Genetic disruption of the alternative splicing of drebrin gene impairs context-dependent fear learning in adulthood. Neuroscience *165*, 138–150.

Kojima, N., Yasuda, H., Hanamura, K., Ishizuka, Y., Sekino, Y., and Shirao, T. (2016). Drebrin A regulates hippocampal LTP and hippocampus-dependent fear learning in adult mice. Neuroscience *324*, 218–226.

Kreis, P., Hendricusdottir, R., Kay, L., Papageorgiou, I.E., van Diepen, M., Mack, T., Ryves, J., Harwood, A., Leslie, N.R., Kann, O., et al. (2013). Phosphorylation of the Actin Binding Protein Drebrin at S647 Is Regulated by Neuronal Activity and PTEN. PLoS One *8*, e71957.

Lee, M.-S., Jeong, M.-H., Lee, H.-W., Han, H.-J., Ko, A., Hewitt, S.M., Kim, J.-H., Chun, K.-H., Chung, J.-Y., Lee, C., et al. (2015). PI3K/AKT activation induces PTEN ubiquitination and destabilization accelerating tumourigenesis. Nat. Commun. *6*, 7769.

Lyford, G.L., Yamagata, K., Kaufmann, W.E., Barnes, C. a., Sanders, L.K., Copeland, N.G., Gilbert, D.J., Jenkins, N. a., Lanahan, A. a., and Worley, P.F. (1995). Arc, a growth factor and activity-regulated gene, encodes a novel cytoskeleton-associated protein that is enriched in neuronal dendrites. Neuron *14*, 433–445.

Mammoto, A., Sasaki, T., Asakura, T., Hotta, I., Imamura, H., Takahashi, K., Matsuura, Y., Shirao, T., and Takai, Y. (1998). Interactions of Drebrin and Gephyrin with Profilin 1. *89*, 86–89.

Martin, K.C., and Zukin, R.S. (2006). RNA trafficking and local protein synthesis in dendrites: an overview. J. Neurosci. *26*, 7131–7134.

Mizui, T., Takahashi, H., Sekino, Y., and Shirao, T. (2005). Overexpression of drebrin A in immature neurons induces the accumulation of F-actin and PSD-95 into dendritic filopodia, and the formation of large abnormal protrusions. Mol. Cell. Neurosci. *30*, 630–638.

Molina, H., Horn, D.M., Tang, N., Mathivanan, S., and Pandey, A. (2007). Global proteomic profiling of phosphopeptides using electron transfer dissociation tandem mass spectrometry. Database *104*, 2199–2204.

Olsen, J. V, Blagoev, B., Gnad, F., Macek, B., Kumar, C., Mortensen, P., and Mann, M. (2006). Global, In Vivo, and Site-Specific Phosphorylation Dynamics in Signaling Networks. Cell *127*, 635–648.

Ostroff, L.E., Fiala, J.C., Allwardt, B., and Harris, K.M. (2002). Polyribosomes redistribute from dendritic shafts into spines with enlarged synapses during LTP in developing rat hippocampal slices. Neuron *35*, 535–545.

Pilarski, R., Stephens, J. a., Noss, R., Fisher, J.L., and Prior, T.W. (2011). Predicting PTEN mutations: an evaluation of Cowden syndrome and Bannayan-Riley-Ruvalcaba syndrome clinical features. J. Med. Genet. *48*, 505–512.

Ramalingam, M., and Kim, S. (2011). Reactive oxygen/nitrogen species and their functional correlations in neurodegenerative diseases. J. Neural Transm.

Rush, J., Moritz, A., Lee, K.A., Guo, A., Goss, V.L., Spek, E.J., Zhang, H., Zha, X.M., Polakiewicz, R.D., and Comb, M.J. (2005). Immunoaffinity profiling of tyrosine phosphorylation in cancer cells. Nat. Biotechnol. *23*, 94–101.

Santini, E., Huynh, T.N., and Klann, E. (2014). Mechanisms of translation control underlying long-lasting synaptic plasticity and the consolidation of long-term memory (Elsevier Inc.).

Santini, E., Turner, K.L., Ramaraj, A.B., Murphy, M.P., Klann, E., and Kaphzan, H. (2015). Mitochondrial Superoxide Contributes to Hippocampal Synaptic Dysfunction and Memory Deficits in Angelman Syndrome Model Mice. J. Neurosci. *35*, 16213–16220.

Sasaki, Y., Hayashi, K., Shirao, T., Ishikawa, R., and Kohama, K. (1996). Inhibition by Drebrin of the Actin-Bundling Activity of Brain Fascin, a Protein Localized in Filopodia of Growth Cones. 980–988.

Schindelin, J., Arganda-Carreras, I., Frise, E., Kaynig, V., Longair, M., Pietzsch, T., Preibisch, S., Rueden, C., Saalfeld, S., Schmid, B., et al. (2012). Fiji: an open-source platform for biological-image analysis. Nat. Methods *9*, 676–682.

Schuman, E.M. (1999). mRNA trafficking and local protein synthesis at the synapse. Neuron *23*, 645–648.

Sekino, Y., Kojima, N., and Shirao, T. (2007). Role of actin cytoskeleton in dendritic spine morphogenesis. Neurochem. Int. *51*, 92–104.

Shim, K., and Lubec, G. (2002). Drebrin, a dendritic spine protein, is manifold decreased in brains of patients with Alzheimer's disease and Down syndrome. Neurosci. Lett. *324*, 209–212.

Shiraishi-Yamaguchi, Y., Sato, Y., Sakai, R., Mizutani, A., Knöpfel, T., Mori, N., Mikoshiba, K., and Furuichi, T. (2009). Interaction of Cupidin/Homer2 with two actin cytoskeletal regulators, Cdc42 small GTPase and Drebrin, in dendritic spines. BMC Neurosci. *10*.

Shirao, T., and Obata, K. (1985). Two acidic proteins associated with brain development in chick embryo. J. Neurochem. *44*, 1210–1216.

Shirao, T., Inoue, H.K., Kano, Y., and Obata, K. (1987). Localization of a developmentally regulated neuron-specific protein S54 in dendrites as revealed by immunoelectron microscopy. Brain Res. *413*, 374–378.

Söderberg, O., Mats, G., Jarvius, M., and Karin, R. (2006). Direct observation of individual endogenous protein complexes in situ by proximity ligation. Nat. Methods *3*, 995–1000.

Takahashi, H., Mizui, T., and Shirao, T. (2006). Down-regulation of drebrin A expression suppresses synaptic targeting of NMDA receptors in developing hippocampal neurones. J. Neurochem. *97*, 110–115.

Toda M. et.al. (1993). Molecular cloning of cDNA Encoding Human Drebrin E and Chromosomal Mapping of its Gene. 468–472.

Tom Dieck, S., Hanus, C., and Schuman, E.M. (2014). SnapShot: Local Protein Translation in Dendrites. Neuron *81*, 958–958.e1.

Tom Dieck, S., Kochen, L., Hanus, C., Heumüller, M., Bartnik, I., Nassim-Assir, B., Merk, K., Mosler, T., Garg, S., Bunse, S., et al. (2015). Direct visualization of newly synthesized target proteins in situ. Nat. Methods 1–7.

Tongiorgi, E., Righi, M., and Cattaneo, a (1997). Activity-dependent dendritic targeting of BDNF and TrkB mRNAs in hippocampal neurons. J. Neurosci. *17*, 9492–9505.

Vosseller, K., Hansen, K.C., Chalkley, R.J., Trinidad, J.C., Wells, L., Hart, G.W., and Burlingame, A.L. (2005). Quantitative analysis of both protein expression and serine/threonine post-translational modifications through stable isotope labeling with dithiothreitol. Proteomics 388–398.

Wang, X., Zaidi, A., Pal, R., Garrett, A.S., Braceras, R., Chen, X., Michaelis, M.L., and Michaelis, E.K. (2009). BMC Neuroscience. BMC Neurosci. *20*, 1–20.

Wollscheid, B., Eng, J.K., Li, X., Bodenmiller, B., Watts, J.D., Hood, L., and Aebersold, R. (2005). Quantitative phosphoproteome analysis using a dendrimer conjugation chemistry and tandem mass spectrometry. Nat. Methods *2*, 591–598.

Yi, J.J., and Ehlers, M.D. (2005). Ubiquitin and protein turnover in synapse function. Neuron *47*, 629–632.

Zheng, H., Hu, P., Quinn, D.F., and Wang, Y.K. (2005). Phosphotyrosine proteomic study of interferon alpha signaling pathway using a combination of immunoprecipitation and immobilized metal affinity chromatography. Mol. Cell. Proteomics MCP *4*, 721–730.

7 Supplemental information

7.1 Supplementary data

In this section I include the codes generated by Viktor Dinkel for the FIJI Plugin Script that I applied for the PLA data analyses. Three codes are shown: PLA analysis, PLA dendrites and PLA soma.

7.1.1 PLA analysis script

```
import ij.plugin.PlugIn;
import ij.IJ;
import ij.ImagePlus;
import ij.gui.GenericDialog;
import ij.process.ImageProcessor;
import ij.plugin.Duplicator;

import ij.plugin.filter.Analyzer;
import ij.measure.ResultsTable;
import java.io.File;
import ij.io.Opener;
import java.util.List;
import java.util.ArrayList;
import java.io.PrintWriter;
import java.io.FileWriter;

public class PLA_Analysis extends ImagePlus implements PlugIn {

     // STRING FOR OS
     public static String os_system = "";
     public static String os_slash = "";

    /////////// ---------- CONFIGURATION
    public static Double areaMaxValue = 9999999.0;    // AREA UPPER
BOUND FOR MAX PLA-SIZE
    public static Boolean fixedThreshold = true;// SET TO 0 IF YOU
WANT TO DEFINE IT AUTOMATICALLY, OTHERWISE YOUR FIXED VALUE WILL BE
USED
    public static Integer autoThreshold = 0;
    public static String map2ThresholdMethod;
    /////////// ----------------------------------------

    public static String version = "0.86";
    public static String path = "";
    public static String pathChannels;
    public static String pathAnalysis;
    public static ArrayList<String> imageFiles;
    public static ArrayList<String> plaResults;

     // Format of singleResults:
```

```
    public static Integer headerElements;
    public static ArrayList<String> csvHeader;
    public static String singleResults;
    public static String allResults;
    public static Integer plaThreshold;

    public static Double map2Area;
    public static Double plaArea;
     public static Double totalIntDen;
     public static Double maxIntDen;
     public static Double minIntDen;
    public static Double sumMAP2Area;
    public static Double sumPLAArea;
     public static Double sumIntDen;

    public static Integer countedAreas;
    public static Integer numAreas;

    public void run(String arg) {

    // Initialization

    imageFiles = new ArrayList<String>();
    plaResults = new ArrayList<String>();
    headerElements = 7;
    csvHeader = new ArrayList<String>();
    singleResults = "";
    allResults = "";
    plaThreshold = 70;
    map2Area = 0.0;
    plaArea = 0.0;
    sumMAP2Area = 0.0;
    sumPLAArea = 0.0;
    countedAreas = 0;
    numAreas = 0;
     totalIntDen = 0.0;
     maxIntDen = 0.0;
     minIntDen = 99999999.99;
     sumIntDen = 0.0;

    os_system = System.getProperty("os.name");
    if (os_system.contains("Mac"))
      os_slash = "/";
    else os_slash = "\\";

    IJ.log("-----------------[ Start PLA_Analysis V"+version+" ]----
-------------");
    IJ.log("System information: "+os_system+" separator:
"+os_slash);
    path = IJ.getDirectory("Choose Directory of Image File(s)");
    IJ.log("- Directory: "+path);

    // Ask for automatic/fixed MAP2-threshold
     GenericDialog gd_map = new GenericDialog("MAP2-Threshold");
```

```
     gd_map.addMessage("Do you want to define a fixed MAP2-threshold
for all files? \n\n\nSet the value to 0 if the threshold has to be
defined automatically for each image. ");
     gd_map.addNumericField("Threshold: ", autoThreshold, 0);
     gd_map.showDialog();
    if (gd_map.wasCanceled()) return;
    autoThreshold =
Math.max(0,Math.min((int)gd_map.getNextNumber(),254));
    if (autoThreshold == 0) {fixedThreshold = false;
map2ThresholdMethod = "Auto";}
    else {fixedThreshold = true; map2ThresholdMethod =
autoThreshold.toString();}

     // Ask for automatic/fixed MAP2-threshold
    GenericDialog gd_pla = new GenericDialog("PLA-Threshold");
    gd_pla.addMessage("Change the Number if you want a different
PLA-threshold for all files. Otherwise click OK.");
    gd_pla.addNumericField("Threshold: ", plaThreshold, 0);
    gd_pla.showDialog();
    if (gd_pla.wasCanceled()) return;
    plaThreshold = Math.max(0,
Math.min((int)gd_pla.getNextNumber(),254));

    final File folder = new File(path);
    imageFiles = listFilesForFolder(folder);
    createPaths(path);

    // Create the subfolders
     String imageName;

     IJ.log("---------------------- Start processing images");
     String HTMLString = "";
     for (int i=0; i<imageFiles.size(); i++){
          plaArea = 0.0;
          map2Area = 0.0;
               totalIntDen = 0.0;
               maxIntDen = 0.0;
               minIntDen = 99999999.99;

          imageName = imageFiles.get(i);
           if (csvHeader.size() < headerElements)
               csvHeader.add("imagename");
           singleResults += imageName+";";
           IJ.log("Image: "+imageName);
           processImage( imageName );
           measureImage( imageName );
           resetAll();

           if (i<imageFiles.size()-1)
           IJ.log("-----------------------------");

           sumMAP2Area += map2Area;
           sumPLAArea += plaArea;
               sumIntDen += (totalIntDen/countedAreas);

           HTMLString = makeHTML(i, imageName, false, HTMLString);
```

```
            allResults = allResults + singleResults+"\n";
            singleResults="";
            }
      makeHTML(0, "", true, HTMLString);
      writeCSS();
         writeCSV();

    System.gc();
      IJ.log("-----------------[ End PLA-Plugin ]-----------------");
      return;
    }

    public String convertToPNG(String imageName){
        String pathHTML = path+"pla"+os_slash+"HTML"+os_slash;
        //IJ.log(pathHTML);
        Boolean success = (new File(pathHTML)).mkdirs();
      if (!imageName.substring(imageName.length()-
4).toLowerCase().equals(".png"))
      {
      //ImagePlus imp = IJ.openImage(path+"\\"+imageName);
      ImagePlus imp = IJ.openImage(path+"/"+imageName);
      imageName = imageName.substring(0, imageName.length()-
4)+".png";
      IJ.saveAs(imp, "png", pathHTML+imageName);
      IJ.log("... converted to .png ");
      }
      return imageName;
    }

    public ArrayList<String> listFilesForFolder(final File folder) {
      ArrayList<String> dirFiles = new ArrayList<String>();
      ArrayList<String> fileFormats = new ArrayList<String>() {{
          add(".jpg");
          add(".tif");
          add(".png");
          add(".gif");
          add(".bmp");
        }};
        Integer k = 0;
          for (final File fileEntry : folder.listFiles()) {
              if (fileEntry.isDirectory()) {
                    //this is for recursive search of the directory
                  //listFilesForFolder(fileEntry);
                  //IJ.log("Skipped directory:
"+fileEntry.getName());
              } else {
                  String fileName = fileEntry.getName();

                  for (int i=0; i<fileFormats.size(); i++){
                      if (fileName.contains(fileFormats.get(i))){
                          // replace spaces
                        if (fileName.contains(" ")){
                                File newFile = new
File(path+fileName.replace(" ", "_"));
                                fileEntry.renameTo(newFile);
```

```
                                    fileName = fileName.replace(" ",
"_");
                                }

                            // convert the image into png-format
                            IJ.log("start converting file: "+fileName);
                            convertToPNG(fileName);

                            //if the image is not added for processing
                            if (!dirFiles.contains(fileName))
                                    {
                                        IJ.log("_"+k.toString()+".
Image-File: "+fileName);
                                        dirFiles.add(fileName);
                                    }
                                    k++;
                                    break;
                        }
                    }
                }
            }
      return dirFiles;
      }

    public void createPaths(String thispath){
      pathChannels = thispath +
"pla"+os_slash+"temp"+os_slash+"channels";
      pathAnalysis = thispath + "pla"+os_slash+"analysis";
      Boolean success = (new File(pathChannels)).mkdirs();
         Boolean success2 = (new File(pathAnalysis)).mkdirs();
    }

    public void processImage( String imageName ){
        splitChannels( imageName );
        maskMAP2(imageName);
        maskPLA();
        return;
    }

    public void measureImage( String imageName ){
        plaArea = measurePLA( imageName );
        map2Area = measureMAP2( imageName );
        return;
    }

    public void splitChannels( String imageName ){
        ImagePlus imp = IJ.openImage(path+imageName);
        IJ.run(imp, "Split Channels", "");

        IJ.log("SAVING CHANNELS AT: "+pathChannels);
        IJ.selectWindow(imageName+" (green)");
        IJ.saveAs("TIF", pathChannels+os_slash+"green.tif");

        IJ.selectWindow(imageName+" (blue)");
        IJ.saveAs("TIF", pathChannels+os_slash+"blue.tif");
```

```
        IJ.selectWindow(imageName+" (red)");
        IJ.saveAs("TIF", pathChannels+os_slash+"red.tif");

        IJ.run("Close All", "");
        return;
    }

    public void maskMAP2( String imageName ){
        IJ.log("MASKING MAP 2 :" +imageName);
        ImagePlus imp =
IJ.openImage(pathChannels+os_slash+"green.tif");
        imp.show();

        ImageProcessor ip = imp.getProcessor();
        Integer thisThreshold;
        if (!fixedThreshold){
            thisThreshold = ip.getAutoThreshold();}
        else{
            thisThreshold = autoThreshold;}
        if (csvHeader.size() < headerElements)
            csvHeader.add("map2-thr;pla-thr");
        singleResults += String.valueOf(thisThreshold)+";";
        singleResults += String.valueOf(plaThreshold)+";";
        IJ.log("- MAP2-Threshold (Mask):
"+thisThreshold.toString());

        IJ.setThreshold(imp, 0, thisThreshold);
        IJ.run("Threshold", "thresholded remaining black slice");

        IJ.run(imp, "Convert to Mask", "");
        IJ.run(imp, "Dilate", "");

        ImagePlus imp2 = new Duplicator().run(imp);

        IJ.saveAs("png",
pathAnalysis+os_slash+"DIL_MASK_"+imageName.replace(".tif","")+".png
");
        imp.close();
        imp2.show();
        return;
    }

    public void maskPLA(){
        ImagePlus imp =
IJ.openImage(pathChannels+os_slash+"red.tif");
        imp.show();

        IJ.setThreshold(imp, 0, plaThreshold);
        IJ.run("Threshold", "thresholded remaining black slice");

        IJ.run(imp, "Convert to Mask", "");
        IJ.run(imp, "Create Mask", "");

        imp.close();

        return;
```

```
    }

    public Double measurePLA(String imageName){
        //ImagePlus dilGreen =
IJ.openImage(pathAnalysis+"\\DIL_MASK_"+imageName+".jpg");
        //dilGreen.show();
        //String origTitle = dilGreen.getTitle();
        IJ.selectWindow("mask");
        IJ.run("Set Measurements...", "area mean integrated gray
redirect=DUP_green.tif decimal=3");
        IJ.run("Analyze Particles...", "size=0-Infinity
circularity=0.00-100.00 show display clear add in_situ");

        IJ.selectWindow("Results");

        ResultsTable rt = ResultsTable.getResultsTable();
        Integer numResults = rt.getCounter();
        Integer numColumns = rt.getLastColumn();
           IJ.log("- Amount of columns: "+numColumns.toString());
        Double area, mean, intDen, rawIntDen, totalArea;
        area=0.0; mean=0.0; intDen =0.0; rawIntDen=0.0;
totalArea=0.0;
           countedAreas = 0;
        numAreas = numResults;

        for (int i = 0; i<numResults; i++){
            area = rt.getValueAsDouble(0,i);
            mean = rt.getValueAsDouble(1,i);
                intDen = rt.getValueAsDouble(20,i);
                rawIntDen = rt.getValueAsDouble(25,i);

                //IJ.log("- IntDen "+intDen.toString());

            String addExcluded = "";
            if (area > areaMaxValue)
                addExcluded = " - TOO LARGE!!!";
            //IJ.log("A: "+String.valueOf(area)+addExcluded);
            //IJ.log("M: "+String.valueOf(mean));
            //IJ.log("---Area: "+String.valueOf(area)+" Mean:
"+String.valueOf(mean));
            if (mean>0.0 && area <= areaMaxValue){
                totalArea += area;
                countedAreas++;
                      totalIntDen += intDen;

                      if (intDen > maxIntDen) maxIntDen = intDen;
                      if (intDen < minIntDen) minIntDen = intDen;

            }
        }

        IJ.log("- PLA Area: "+String.valueOf(totalArea)+" (counted:
"+countedAreas.toString()+"/"+numResults.toString()+") intden:
"+intDen.toString()+" rawint: "+rawIntDen.toString());
        IJ.saveAs("Results",
pathAnalysis+os_slash+imageName+"_Results.csv"); // XLS OR CSV
```

```
           // just _Results.xls contains PLA area
        IJ.run("Close");

        IJ.selectWindow("mask");
        IJ.saveAs("tif",
path+os_slash+"pla"+os_slash+"temp"+os_slash+"red_mask.tif");
        Double ret;
        ret = totalArea;
        if (csvHeader.size() < headerElements)
            csvHeader.add("pla");
        singleResults += String.valueOf(ret).replace(".", ",")+";";

           if (csvHeader.size() < headerElements)
            csvHeader.add("min-pla-int;max-pla-int;mean-pla-
int;int/map2-ratio");

           double thisMeanIntDen = (totalIntDen/countedAreas);
           singleResults += String.valueOf(minIntDen).replace(".",
",")+";"+String.valueOf(maxIntDen).replace(".",
",")+";"+String.valueOf(thisMeanIntDen).replace(".", ",")+";";
     // String.format("%.2f",maxIntDen)

        return ret;
    }

    public Double measureMAP2(String imageName){
        ImagePlus imp =
IJ.openImage(pathChannels+os_slash+"green.tif");
        imp.show();

        ImageProcessor ip = imp.getProcessor();
        Integer thisThreshold;
        if (!fixedThreshold)
            {
            thisThreshold = ip.getAutoThreshold();
            autoThreshold = thisThreshold;
            }
        else{
            thisThreshold = autoThreshold;}

        IJ.setThreshold(imp, 0, thisThreshold);
        IJ.log("- MAP2-Threshold (Measure):
"+thisThreshold.toString());
        IJ.run("Threshold", "thresholded remaining black slice");
        IJ.run(imp, "Convert to Mask", "");
        IJ.run(imp, "Create Selection", "");
        IJ.run("Set Measurements...", "area mean gray redirect=None
decimal=3");
        IJ.run(imp, "Measure", "");
        IJ.run(imp, "Select None", "");
        imp.close();
        IJ.selectWindow("Results");

        ResultsTable rt = ResultsTable.getResultsTable();
        Double thisMap2Area = rt.getValueAsDouble(0,0);
```

```
        //IJ.log("- MAP2 Area: "+String.valueOf(thisMap2Area)+"
micron? = "+(String.valueOf(thisMap2Area)).contains("."));

        IJ.saveAs("Results",
pathAnalysis+os_slash+imageName+"_NeuronArea__Results.csv"); // XLS
OR CSV
 //_NeuronArea_Results.xls contains MAP2 Area
        IJ.run("Close");

        IJ.log("-- PLA/MAP2 - RATIO:
"+String.valueOf(plaArea/thisMap2Area)+"   * 100 =
"+String.valueOf((plaArea/thisMap2Area)*100));
        if (csvHeader.size() < headerElements)
            csvHeader.add("map2");
        singleResults +=
String.valueOf((totalIntDen/countedAreas)/thisMap2Area).replace(".",
",")+";"+String.valueOf(thisMap2Area).replace(".", ",")+";";
        if (csvHeader.size() < headerElements)
            csvHeader.add("pla/map2-ratio");
        singleResults +=
String.valueOf(plaArea/thisMap2Area).replace(".", ",")+";";
        Double ret = thisMap2Area;

        return ret;
    }

    public String makeHTML(Integer i, String imageName, Boolean
writeFileNow, String HTMLString){
     String pathHTML =
path+os_slash+"pla"+os_slash+"HTML"+os_slash+i.toString()+os_slash;
     Boolean success = (new File(pathHTML)).mkdirs();
        imageName = imageName.replace(".tif","");

        if (writeFileNow){
            // make new results file
                IJ.log("------------- SUMMARY -------------");
                Double meanPLA = sumPLAArea/imageFiles.size();
                Double meanMAP2 = sumMAP2Area/imageFiles.size();
                     Double meanIntDen =
sumIntDen/imageFiles.size();
                Double meanRatio = ((meanPLA/imageFiles.size()) /
(meanMAP2/imageFiles.size()))*100;
                IJ.log("SUM of Areas [PLA]
"+String.valueOf(sumPLAArea)+" / [MAP2]
"+String.valueOf(sumMAP2Area)+" =
"+String.valueOf(sumPLAArea/sumMAP2Area));
                IJ.log("MEAN Value [PLA] "+String.valueOf(meanPLA)+"
/ [MAP2] "+String.valueOf(meanMAP2)+" =
"+String.valueOf(meanRatio));

            String HTMLHeader = "<html><head><title>PLA-
Analysis</title><link href=\"../HTML/style.css\" rel=\"stylesheet\"
type=\"text/css\"></head><body><div
id=\"main_container\"><h1>Analysis of PLA</h1><div
class=\"content_left\"><p>MAP2-Threshold</p><p>PLA-
Threshold</p><p>Analyzed images</p><p>Mean-PLA</p><p>Mean-
```

```
MAP2</p><p>Mean-Ratio</p><p>Mean-Intensity</p></div><div
class=\"content_right\"><p>"+map2ThresholdMethod+"</p><p>"+plaThresh
old+"</p><p>"+imageFiles.size()+"</p><p>"+String.format("%.2f",
meanPLA)+"</p><p>"+String.format("%.2f",
meanMAP2)+"</p><p>"+String.format("%.2f",
meanRatio)+"%</p><p>"+String.format("%.2f", meanIntDen)+"</p><p><a
href=\"ALL_RESULTS.csv\" target=\"blank\"> >>
ALL_RESULTS.csv</a></p></div><div class=\"clear_float\"></div>";
            String fullHTML = HTMLHeader+HTMLString;
            try {
            PrintWriter writer = new
PrintWriter(pathAnalysis+os_slash+"results_summary.html", "UTF-8");
            writer.println(fullHTML);
            writer.close();
            }catch (Exception ex){
            }

            return HTMLString;
        }

        else {

            ImagePlus green =
IJ.openImage(pathChannels+os_slash+"green.tif");
            green.show();
            ImagePlus red =
IJ.openImage(pathChannels+os_slash+"red.tif");
            red.show();
            ImagePlus blue =
IJ.openImage(pathChannels+os_slash+"blue.tif");
            blue.show();

            IJ.run(green, "Merge Channels...", "c1=red.tif
c2=green.tif c3=blue.tif create");
            IJ.selectWindow("Composite");
            IJ.run("Split Channels", "");

            IJ.selectWindow("C1-Composite");
            IJ.saveAs("png", pathHTML+"red_orig.png");
            IJ.run("Close");
            IJ.selectWindow("C2-Composite");
            IJ.saveAs("png", pathHTML+"green_orig.png");
            IJ.run("Close");
            IJ.selectWindow("C3-Composite");
            IJ.saveAs("png", pathHTML+"blue_orig.png");
            IJ.run("Close");

            ImagePlus red_mask =
IJ.openImage(path+os_slash+"pla"+os_slash+"temp"+os_slash+"red_mask.
tif");
            red_mask.show();
            IJ.run(red_mask, "Invert", "");
            IJ.run(red_mask, "RGB Color", "");
            ImagePlus green_dil =
IJ.openImage(pathAnalysis+os_slash+"DIL_MASK_"+imageName+".png");
            green_dil.show();
```

```
            ImagePlus blue_orig =
IJ.openImage(pathHTML+"blue_orig.png");
            blue_orig.show();

            //IJ.log("HERE MERGE CHANNELS!");
            //IJ.selectWindow("red_mask.tif");
            //IJ.run("8-bit", "");

            Integer red_bitDepth = red_mask.getBitDepth();
            Integer green_bitDepth = green_dil.getBitDepth();
            Integer blue_bitDepth = blue_orig.getBitDepth();
            IJ.log("Bit-depths: "+red_bitDepth+" "+green_bitDepth+"
"+blue_bitDepth);
            if (( red_bitDepth != green_bitDepth ) || (red_bitDepth
!= green_bitDepth ) || ( green_bitDepth != blue_bitDepth )){
                IJ.run(red_mask, "RGB Color", "");
                IJ.run(green_dil, "RGB Color", "");
                IJ.run(blue_orig, "RGB Color", "");
            }

            IJ.run(green_dil, "Merge Channels...", "c1=red_mask.tif
c2=DIL_MASK_"+imageName+".png c3=blue_orig.png create");

            IJ.selectWindow("Composite");
            IJ.saveAs("png", pathHTML+"red_green_composite.png");
            IJ.run("Close");

            ImagePlus green2 =
IJ.openImage(pathChannels+os_slash+"green.tif");
            green2.show();
            IJ.run(green2, "Invert", "");
            IJ.saveAs("png", pathHTML+"green_inverted.png");
            IJ.run("Close");
            ImagePlus red2 =
IJ.openImage(pathChannels+os_slash+"red.tif");
            red2.show();
            IJ.run(red2, "Invert", "");
            IJ.saveAs("png", pathHTML+"red_inverted.png");
            IJ.run("Close");
            ImagePlus blue2 =
IJ.openImage(pathChannels+os_slash+"blue.tif");
            blue2.show();
            IJ.run(blue2, "Invert", "");
            IJ.saveAs("png", pathHTML+"blue_inverted.png");
            IJ.run("Close");

                // SAVE PLA MASK
                ImagePlus imp =
IJ.openImage(pathChannels+os_slash+"red.tif");
                imp.show();
                IJ.setThreshold(imp, 0, plaThreshold);
                IJ.run("Threshold", "thresholded remaining black
slice");
                IJ.run(imp, "Convert to Mask", "");
                IJ.run(imp, "Create Mask", "");
```

```
                IJ.saveAs("png",
pathAnalysis+os_slash+"PLA_MASK_"+imageName+".png");
                imp.close();
                IJ.run("Close");

            // append HTML-data to HTML-File
            HTMLString += "<div
class=\"results\"><h2>"+imageName+"</h2><div
class=\"upper_content_box\"><h3>Results</h3><div
class=\"content_left\"><p>MAP2 Area</p><p>MAP2-THR</p><p>PLA
Area</p><p>Ratio</p><p>Counted</p><p>Int/MAP2-Ratio</p></div><div
class=\"content_right\"><p>"+String.format("%.2f",
map2Area)+"</p><p>"+String.valueOf(autoThreshold)+"</p><p>"+String.f
ormat("%.2f", plaArea)+"</p><p>"+String.format("%.2f",
(plaArea/map2Area)*100)+"%</p><p>"+countedAreas.toString()+"/"+numAr
eas.toString()+"</p><p>"+String.format("%.4f",
(totalIntDen/countedAreas)/map2Area)+"</p></div></div><div
class=\"upper_content_box\"><h3>Original Image</h3><a
href=\"../HTML/"+imageName+".png\" target=\"blank\"><img
src=\"../HTML/"+imageName+".png\" /></a></div><div
class=\"upper_content_box\"><h3>Dilated mask</h3><a
href=\"DIL_MASK_"+imageName+".png\" target=\"blank\"><img
src=\"DIL_MASK_"+imageName+".png\" /></a></div><div
class=\"clear_float\"></div><h4>Channels</h4><div
class=\"lower_content_box\">    <a
href=\"../HTML/"+i.toString()+"/red_orig.png\" target=\"blank\"><img
src=\"../HTML/"+i.toString()+"/red_orig.png\" /></a>    <a
href=\"../HTML/"+i.toString()+"/red_inverted.png\"
target=\"blank\"><img
src=\"../HTML/"+i.toString()+"/red_inverted.png\" /></a></div>
<div class=\"lower_content_box\"><a
href=\"PLA_MASK_"+imageName+".png\" target=\"blank\"><img
src=\"PLA_MASK_"+imageName+".png\" /></a> <b>PLA Mask</b><br
/><br /> <b>Intensity</b><br /> min:
"+String.format("%.2f",minIntDen)+"<br /> max:
"+String.format("%.2f",maxIntDen)+"<br /> &empty;:
"+String.format("%.2f", (totalIntDen/countedAreas))+"</div>     <div
class=\"lower_content_box\">    <a
href=\"../HTML/"+i.toString()+"/green_orig.png\"
target=\"blank\"><img
src=\"../HTML/"+i.toString()+"/green_orig.png\" /></a>    <a
href=\"../HTML/"+i.toString()+"/green_inverted.png\"
target=\"blank\"><img
src=\"../HTML/"+i.toString()+"/green_inverted.png\"
/></a></div></div><div class=\"clear_float\"></div>";
            //countedAreas.toString()+"/"+numAreas.toString()
            if (csvHeader.size() < headerElements)
                csvHeader.add("counted_areas;total_areas");
            singleResults +=
String.valueOf(countedAreas.toString())+";";
            singleResults +=
String.valueOf(numAreas.toString())+";";
            if (i == imageFiles.size()-1){
                HTMLString+="</div></body></html>";
                }
            }
```

```
    return HTMLString;
    }

    public void writeCSS(){
        String pathCSS =
path+os_slash+"pla"+os_slash+"HTML"+os_slash;
        String cssString = "@font-face {font-family: 'Dosis';font-
style: normal;font-weight: 400;src: local('Dosis Regular'),
local('Dosis-Regular'),
url(http://themes.googleusercontent.com/static/fonts/dosis/v2/xIAtSa
glM8LZOYdGmG1JqQ.woff) format('woff');} body, div, h1, h2, h3, h4,
h5, h6, p, ul, ol, li, dl, dt, dd, img, form, fieldset, input,
textarea, blockquote {margin: 0; padding: 0; border: 0;} body {font:
15px 'Dosis', sans-serif; text-transform: uppercase; }
#main_container {position:relative;margin:0px auto;width: 820px;}
.results{position:relative;background-color: white;margin-
top:40px;margin-left:20px;padding-left:10px;width:
800px;border:0px;border-top: 1px solid grey;}
.upper_content_box{position:relative;float:left;background-
color:white;margin-right:10px;margin-
top:0px;height:260px;width:250px;} .results .upper_content_box
img{width:248px;height:248px;border: 1px solid grey;}
.lower_content_box{position:relative;background-
color:white;float:left;margin-right:10px;margin-
bottom:10px;height:122px;width:250px;} .results h4{color:red;}
.results .lower_content_box img{position:relative;float:left;margin-
left:2px;width:120px;height:120px;border: 1px solid grey;}
.clear_float{clear:both;} .content_left{float:left;background-
color:white;padding-top:20px;} .content_right{float:left;margin-
left:10px;background-color:white;padding-top:20px;} h2{color:grey;}
.content_left p{margin-bottom:10px;text-align:right;font-size:20px;}
.content_right p{margin-bottom:10px;text-align:left;font-size:20px;}
.results .upper_content_box img:hover {border-color:blue;} .results
.lower_content_box img:hover {border-color:blue;} a:link { text-
decoration:none; } a:visited { text-decoration:none;  } a:hover {
text-decoration:none; } a:active { text-decoration:none;  } a:focus
{ text-decoration:none;  }";

        try {
            PrintWriter writer = new
PrintWriter(pathCSS+"style.css", "UTF-8");
            writer.println(cssString);
            writer.close();
        }catch (Exception ex){
        }
    }

    public void writeCSV(){
        String pathCSV =
path+os_slash+"pla"+os_slash+"analysis"+os_slash;
        try {
            PrintWriter writer = new
PrintWriter(pathCSV+"ALL_RESULTS.csv", "UTF-8");
            String headerString = "";
```

```
            for (int k = 0; k<csvHeader.size(); k++){
                headerString = headerString + csvHeader.get(k)+";";
                }
            writer.println(headerString);
            writer.println(allResults);

            writer.close();
        }catch (Exception ex){
        }
    }

    public void resetAll(){
      IJ.run("Close All", "");
      IJ.selectWindow("ROI Manager");
      IJ.run("Close");
         return;
    }
}
```

7.1.2 PLA dendrites

```
import ij.plugin.PlugIn;
import ij.IJ;
import ij.ImagePlus;
import ij.gui.GenericDialog;
import ij.gui.WaitForUserDialog;
import ij.io.OpenDialog;
import ij.WindowManager;
import java.io.File;
import ij.measure.Calibration;

public class PLA_Dendrites extends ImagePlus implements PlugIn {

     // STRING FOR OS
     public static String os_system = "";
     public static String os_slash = "";

     public static String version = "0.85";

     public void run(String arg) {
          IJ.log("-----------------[ Start PLA_Dendrites
V"+version+" ]-----------------");

           os_system = System.getProperty("os.name");
          if (os_system.contains("Mac"))
            os_slash = "/";
          else os_slash = "\\";

           OpenDialog od = new OpenDialog("Select imagefile");
           ImagePlus imp = IJ.openImage(od.getPath());

           String path =
od.getPath().substring(0,od.getPath().length()-
imp.getTitle().length());
```

```
            String imageName = imp.getTitle();
            IJ.log("img: "+imageName+" path: "+path);

            // GET MEASUREMENTS (PIXLE/MICRONS)
            Calibration cal = imp.getCalibration();
            double x = cal.pixelWidth;
            double y = cal.pixelHeight;

            IJ.run(imp, "Select All", "");
         Integer oldWidth = (int)imp.getRoi().getFloatWidth();
            Integer oldHeight = (int)imp.getRoi().getFloatHeight();
         double distance = oldHeight/(oldHeight*x);

         IJ.run(imp, "Select None", "");
            IJ.log("Measurements: "+x+" x "+y+" | "+oldWidth+" x
"+oldHeight+" = "+(oldHeight*x)+" => distance:
"+oldHeight/(oldHeight*x));

            IJ.setTool("polyline");
            imp.show();
            new WaitForUserDialog("Selection required", "1. Track the
dendrite with left clicks.\n\n2. Place your last selection with
right click. \n\n3. Press the OK button to continue").show();
            IJ.run("Straighten...",
"title=straightened_"+imp.getTitle()+" line=20");
            imp.close();
            ImagePlus imp2 = WindowManager.getCurrentImage();
            IJ.log("img2: "+imp2.getTitle());

            String fullpath = createPaths(path);
            IJ.run(imp2, "Set Scale...", "distance="+distance+"
known=1 pixel=1 unit=micron");
            IJ.saveAs(imp2, "Tiff",
fullpath+os_slash+imp2.getTitle());
            imp2.close();

            //IJ.run("Close All", "");
         System.gc();
            return;

      }

      public String createPaths(String path){
            String fullpath = path+os_slash+"Straightened"+os_slash;
            Boolean success = (new File(fullpath)).mkdirs();
            return fullpath;
     }

}
```

7.1.3 PLA Soma script

```
import ij.plugin.PlugIn;
import ij.IJ;
```

```
import ij.ImagePlus;
import ij.gui.GenericDialog;
import ij.gui.WaitForUserDialog;
import ij.io.OpenDialog;
import ij.WindowManager;
import ij.measure.Calibration;
import java.io.File;

public class PLA_Soma extends ImagePlus implements PlugIn {

     // STRING FOR OS
     public static String os_system = "";
     public static String os_slash = "";

     public static String version = "0.85";

     public void run(String arg) {
          IJ.log("-----------------[ Start PLA_Soma V"+version+" ]-
----------------");

           os_system = System.getProperty("os.name");
          if (os_system.contains("Mac"))
            os_slash = "/";
          else os_slash = "\\";

           OpenDialog od = new OpenDialog("Select imagefile");
           ImagePlus imp = IJ.openImage(od.getPath());

           String path =
od.getPath().substring(0,od.getPath().length()-
imp.getTitle().length());
           String imageName = imp.getTitle();
           IJ.log("img: "+imageName+" path: "+path);

           // GET MEASUREMENTS (PIXLE/MICRONS)
           Calibration cal = imp.getCalibration();
           double x = cal.pixelWidth;
           double y = cal.pixelHeight;

        IJ.run(imp, "Select All", "");
        Integer oldWidth = (int)imp.getRoi().getFloatWidth();
           Integer oldHeight = (int)imp.getRoi().getFloatHeight();
        double distance = oldHeight/(oldHeight*x);

        IJ.run(imp, "Select None", "");
           IJ.log("Measurements: "+x+" x "+y+" | "+oldWidth+" x
"+oldHeight+" = "+(oldHeight*x)+" => distance:
"+oldHeight/(oldHeight*x));

        // IJ.run(imp, "Set Scale...", "distance=5.5494 known=1
pixel=1 unit=micron");

           IJ.setTool("brush");
           imp.show();
           new WaitForUserDialog("Selection required", "1. Hold the
left mouse button down and drag the brush over the soma.\n\n2. Areas
```

```
can be erased by clicking with the brush tool outside the marked
area and drag it on the zone which shall be removed. \n\n3. Press
the OK button to continue").show();
           IJ.run("Copy", "");

           Integer newWidth = (int)imp.getRoi().getFloatWidth();
           Integer newHeight = (int)imp.getRoi().getFloatHeight();

           // Add 1/3 of height and width to the borders to make
sure that the cell mass is less than the background
           newHeight += 2*(int)(newHeight/3);
           newWidth  += 2*(int)(newWidth/3);

           Integer bitDepth = imp.getBitDepth();
           IJ.log("NewFile: "+newWidth+" x "+newHeight+" bitD:
"+bitDepth);
           imp.close();
           ImagePlus imp2 = IJ.createImage("brushed_"+imageName,
bitDepth+"-bit black", newWidth, newHeight, 1);
           IJ.run(imp2, "Paste", "");
           IJ.run(imp2, "Select None", "");
           imp2.show();
           String fullpath = createPaths(path);
        IJ.run(imp2, "Set Scale...", "distance="+distance+" known=1
pixel=1 unit=micron");
           IJ.saveAs(imp2, "Tiff",
fullpath+os_slash+imp2.getTitle());

           //IJ.run("Close All", "");
        System.gc();
           return;

     }

     public String createPaths(String path){
           String fullpath = path+os_slash+"Brushed"+os_slash;
           Boolean success = (new File(fullpath)).mkdirs();
           return fullpath;
    }

}
```

8 Collaborations and technical support

For this thesis work the contribution of different people was necessary. Viktor Dinkel developed the plugin for PLA analyses, Dr. Till Mack generated the flag-tagged DBN-E constructs and performed the mutagenesis for DBN_{S601A}-flag and DBN_{S601D}-flag. Moreover, he produced the virus constructs, virus particles and coordinated the generation of the DBN-KO mouse model. In the Schuman Lab (Max Planck Institute for Brain Research, Frankfurt am Main) Dr. Susanne Tom Dieck helped me with the planning of the first FUNCAT-PLA experiments. In parallel with me, Ina Bartnik performed the first FUNCAT-PLA experiments for DBN. Lisa Kochen designed the image analyses sequence (Image J) for the analyses of PLA and shared it with me. Susanne Tom Dieck, Ina Bartnik and Lisa Kochen occasionally helped with the microscopy imaging of FUNCAT-PLA and panomics experiments and Susanne Tom Dieck performed one of the three panomics experiments. Kristin Lehman and Kerstin Schlawe did most of the preparation for the primary cultures. Beate Diemar performed some of my western blots.

9 Acknowledgments

My PhD has been an adventure and what an adventure. There have been ups and downs but overall a lot of learning. Permanent and non-stop learning. Perhaps that is the part that I find most exciting about doing scientific research. There is so much to know and so much to explore. During this adventure of learning many people contributed in the process and I would like to acknowledge some of them.

I start by thanking Prof. Britta Eickholt. There are many reasons I am grateful to her. First of all, I thank Britta for inviting me to work in her lab and to provide me with a very interesting, challenging and fun project. Second of all, I thank her for her dedicated supervision during my PhD. I feel particularly grateful to her for fully supporting me when I wanted to go to conferences and specially that one time when I met Prof. Erin Schuman. I still remember the first time during my PhD that I went to a scientific meeting and how much I had to fight to pursue Britta to let me go. Several times she came back to me saying: -Eugenia it is too soon!-. But finally, on that day I suggested I could go to this PhD meeting in the MPI in Göttingen she said: -Yes, I'll support that one!-. So there I went and it was absolutely fruitful. After that meeting, our collaboration with the Schuman Lab started. I thank Britta, for the support and the freedom I received from her, concerning my trips to Frankfurt. Last, I thank her for the orientation in the writing of this thesis.

All the work I did during my PhD would have not been possible without the support, orientation and scientific discussions with George, Till, Paloma, Kai, Patricia, Steffi, Mayur, Julia, Sandra, Annika and Willem. I also thank them for making of our group a very pleasant place to be, especially during those times of cake eating, summers of gin and tonics and long nights of beer drinking. That was fun!

I thank our technicians Beate, Kerstin and Kristin, their work was really important in the development of my work in the lab. From teaching German to learning together how to perform new protocols and so on.

I am very thankful to Prof. Erin Schuman. I thank her for opening me the doors to her lab. I thank her for listening, reading, supporting and caring. Having met her makes me very happy and keeps me going in this adventure. She is an inspiration and a motivation to go on.

I thank Susu, Ina and Lisa for all the support when it came to making experiments with them and the Mexican, French and other parties they organized when I was there in Frankfurt. That was not only a very productive time but also a very fun one. I thank in general all the Schuman Lab and the team in the MPI for supporting me and always make me feel welcome. I thank Anne-Sophie for hosting me when I visited Frankfurt the last times and for discussing science with me. It is not always easy to have deep and interesting discussions but with Anne-Sophie, this is possible.

I thank Viktor Dinkel for developing the plugin with me and for teaching me how to teach.

I am grateful to Prof. Rojas for proof-reading and guiding me in the writing of this thesis. I also thank him for all the support he gave me for starting my collaboration with Viktor. He is a motivation to keep on studying and trying hard to stay in academia: learning, teaching and sharing. Gracias Rojas!

I thank my friends for listening to all my complaints and providing advice and support…always!

I thank my entirely family for all the support. For the support every day of my life and every day during my PhD. My father's support… I have no words to thank for that one.

The rest of my family, when I started this adventure they helped me to make it happen. I don't forget.

Finally, I am deeply thankful to my partner, my best friend, my favorite person, the father of our future daughter and my husband. Erik's help has been perhaps the most important one during this adventure. I am really lucky to have such a life partner. He has listed to my science stories probably every day since the last four years and our scientific discussions, although sometimes ending in fights the outcome was always positive. Thank you B.

10 Selbständigkeitserklärung

Ich, Eugenia Rojas Puente, erkläre, dass ich die vorgelegte Dissertation mit dem Thema „Turnover and localization of the actin binding protein Drebrin in Neurons“ selbst verfasst und keine anderen als die angegebenen Quellen und Hilfsmittel benutzt, ohne die unzulässige Hilfe Dritter verfasst und auch in Teilen keine Kopien anderer Arbeiten dargestellt habe.“

Datum Unterschrift